Dissertation

submitted to the

Combined Faculty of Natural Sciences and Mathematics

of the Ruperto Carola University Heidelberg, Germany

for the degree of

Doctor of Natural Sciences

Presented by

M.Sc. Simone Borgoni

born in: Torino, Italy

Oral-examination: 17.01.2020

Time-resolved profiling reveals ATF3 as a novel mediator of endocrine resistance in breast cancer

Referees: Prof. Dr. Stefan Wiemann

Prof. Dr. Frank Lyko

Declaration of Authorship

I hereby declare that the work presented in this thesis was carried out between September 2015 and September 2019 under the supervision of Prof. Dr. Stefan Wiemann in the group of Molecular Genome Analysis at the German Cancer Research Center (Heidelberg, Germany).

If not stated otherwise and mentioned in the text, the experiments described have been designed and performed by myself and the data obtained has not been presented as part of a university examination.

Heidelberg, _____

Simone Borgoni

Table of content

List of Figures

List of Tables

Summary

Breast cancer is one of the leading causes of death for women worldwide. Patients whose tumors express Estrogen Receptor α (ERα) account for ~70% of cases, and can be treated with targeted endocrine therapy. Endocrine therapy abrogates estrogen (E2) mediated tumor growth either by blocking the ER itself (tamoxifen, fulvestrant) or by inhibiting the enzyme responsible for E2 production (aromatase inhibitors). However, around 40% of the patients eventually relapse due to resistance development. While several advancements have been made and second-line treatments are available for relapsing patients, resistance remains an urgent clinical problem that needs to be addressed. To investigate the mechanisms underlying development of resistance to endocrine therapies, I utilized various strategies to tackle two different aspects. To identify novel drivers of resistance, I developed new resistant cell lines and investigated the early phases of the resistance process with a combination of high throughput techniques. The analysis revealed ATF3 as a putative regulator of the response to therapy and of the rewiring of cells' central processes. The role of ATF3 was validated *in vitro* modulating its expression through knockout, knockdown and overexpression. ATF3 was identified to be essential in controlling proliferation, cell cycle and apoptosis rate of the cells under treatment through the regulation of MAPK/AKT signaling pathways. Its role was confirmed *in vivo* in a xenograft mouse model and the high expression levels were verified in patient datasets, adding clinical relevance to the findings. The second aspect I investigated was the relevance of clonality in endocrine therapy resistance. To do this, I used a cellular barcoding approach to track single cells during resistance development against tamoxifen and E2 deprivation *in vitro*. The analysis of the barcodes complexity in resistant clones revealed cell line-specific and treatment-specific mechanisms of resistance development. The distinct barcodes composition also reflected different signaling pathways activities that indicate specific paths to resistance for the independent replicates. Overall this study elucidates key features of endocrine resistance both through the identification of ATF3 as a novel mediator of endocrine resistance and through the dissection of the mechanisms underlying the selection/adaptation of independent replicates to the endocrine treatments.

Zusammenfassung

Brustkrebs ist eine der führenden Todesursachen bei Frauen weltweit. Patientinnen deren Tumore den Östrogenrezeptor α (ERα) exprimieren machen ~70 % aller Fälle aus und können mittels gezielter endokriner Therapie behandelt werden. Die endokrine Therapie unterbindet das Östrogen- (E2) abhängige Tumorwachstum entweder durch Blockierung des ER (Tamoxifen, Fulvestrant) oder durch die Inhibierung des Enzyms, welches für die E2-Produktion verantwortlich ist (Aromatase-Inhibitoren). Nichtsdestotrotz rezidivieren ungefähr 40 % der Patientinnen letztendlich aufgrund einer Resistenzentwicklung. Obwohl einige Fortschritte gemacht wurden und Zweitlinientherapien für rezidivierende Patientinnen verfügbar sind, bleibt die Resistenz ein dringliches klinisches Problem, das adressiert werden muss. Um diejenigen Mechanismen, die der Resistenzentwicklung gegenüber endokrinen Behandlungen zugrunde liegen, zu untersuchen, verwendete ich verschiedene Strategien um zwei unterschiedliche Aspekte anzugehen. Um neuartige Treiber der Resistenz zu identifizieren, entwickelte ich neue resistente Zelllinien und untersuchte die frühen Phasen des Resistenzprozesses durch eine Kombination von Hochdurchsatztechniken. Die Analyse enthüllte ATF3 als vermutlichen Regulator der Therapieantwort und der Neuvernetzung der zentralen zellulären Prozesse. Die Rolle von ATF3 wurde *in vitro* durch Modulation der Genexpression mittels Knockout, Knockdown und Überexpression validiert. ATF3 wurde als essenziell für die Kontrolle von Proliferation, der Zellzyklus- und Apoptose-Rate der Zellen unter Behandlung durch Regulation der MAPK/AKT Signalwege identifiziert. Seine Rolle wurde *in vivo* in einem Xenograft-Mausmodell bestätigt und die hohen Expressionslevel in Patientinnendatensätzen verifiziert, was den Ergebnissen klinische Relevanz hinzufügte. Der zweite Aspekt, den ich untersuchte, war die Relevanz von Klonalität in der endokrinen Therapieresistenz. Dazu verwendete ich einen zellulären Barcoding-Ansatz um einzelne Zellen während der Resistenzentwicklung gegen Tamoxifen und E2-Entzug *in vitro* zu verfolgen. Die Analyse der Barcode-Komplexität in resistenten Klonen enthüllte Zelllinien-spezifische und Behandlungs-spezifische Mechanismen der Resistenzentwicklung. Die verschiedenen Barcode-Zusammensetzungen spiegelten auch unterschiedliche Signalwegaktivitäten wider, die auf

spezifische Wege zur Resistenz in den unabhängigen Replikaten hinweisen. Insgesamt klärt diese Studie Schlüsselmerkmale der endokrinen Resistenz sowohl durch die Identifikation von ATF3 als neuartigen Treiber der endokrinen Resistenz als auch durch die Zergliederung von Mechanismen, die der Selektion/Adaption von unabhängigen Replikaten gegenüber endokrinen Behandlungen unterliegen, auf.

1. Introduction

1.1. Breast Cancer

Cancer is one of the main public health concerns worldwide, estimated to have 18.1 million of new cases and 9.6 million cancer deaths, being the second leading cause of death globally after cardiovascular diseases ("WHO | Cancer" 2019; Bray et al. 2018). Breast cancer is the most diagnosed type of cancers among women, accounting for 25-30% of all new cancer diagnosis, and the second-leading cause of death after lung cancer (Siegel, Miller, and Jemal 2019).

Since breast cancer is a highly heterogeneous disease, a generalized therapeutic approach cannot be successfully applied in the clinic. For this reason, many studies have focused on this issue trying to stratify patients to find therapeutic subtypes that would benefit from specific treatments.

1.1.1 Histopathological classification

Breast cancer can be histologically divided in ductal carcinoma in situ (DCIS) or invasive carcinoma (IDC) with the latter accounting for the majority of the cases (Vuong et al. 2014). IDC is subdivided in more than 20 subtypes, with the not defined subtype, the invasive carcinoma not otherwise specified (IDC NOS) being the most abundant, accounting for 50-80% of all breast cancers (Weigelt et al. 2008). The other subtypes are characterized by special features and include the invasive lobular, tubular, mucinous, metaplastic, neuroendocrine, medullary and apocrine carcinomas (Vuong et al. 2014). The histological grading of the tumors is done based on specific guidelines, which consider the proportion of tubule formation, the degree of nuclear pleomorphism and the mitotic count (Elston and Ellis 1991).

The scoring grades of breast tumors can range from 1 to 3, with 1 being the most differentiated. High-grade cancers tend to recur more and metastasize early, while low-grade

tumors have a better clinical outcome. Pathologically, breast tumors are staged based on the TNM guidelines that consider the tumor size(T), the status of the lymphnodes (N) and the spread to distant sites (M) (Giuliano, Edge, and Hortobagyi 2018).

1.1.2 Molecular subtypes

In order to stratify patients based on the clinical outcome and therapeutic strategies, breast cancers have been subdivided based on the expression of specific genes. Specifically, breast cancer can be classified using intrinsic or clinical subtypes. The intrinsic subtyping is based on gene expression profiling, with classifiers that divide the breast cancers in Luminal A (LA), Luminal B (LB), Her2-enrichded (HER2+), basal-like (Basal) and normal-like (Normal) (Table 1) (Perou et al. 2000). These classifiers are using an intrinsic list of genes to subdivide the tumors in these five classes (Sørlie et al. 2001; Hu et al. 2006; Parker et al. 2009). However, in the last years, the normal like subtype is less used as highly similar to the LA (Raj-Kumar et al. 2019).

The clinical sub-typing is instead based on immunohistochemistry (IHC) for estrogen receptor (ER), progesterone receptor (PR) HER2 receptor (HER2) and Ki-67. These markers are regularly used in the clinic and they are the only accepted stratification method for treatment decision making (Inwald et al. 2015). Based on the IHC markers the tumors are divided in LA (ER+/HER2−/Ki67−), LB (ER+/HER2−/Ki67+ or ER+/HER2+), HER2 (ER−/PR−/HER2+), Triple negative (TN; ER−/PR−/HER2−) (Goldhirsch et al. 2013).

Since the two classification methods do not completely overlap, new assays and gene sets are proposed regularly to try to improve the consistency of subtypes definition in breast cancer (Milioli et al. 2016; Raj-Kumar et al. 2019). As a notable example, a recent clustering analysis based on genomic and transcriptomic analysis of 2000 breast cancer proposed a 10 subgroups classification to further stratifies the intrinsic subtypes, with well characterized genomic features and distinct clinical outcome (Table 1) (Curtis et al. 2012).

Table 1: Molecular subtypes of breast cancer (Modified from Vuong et al. 2014)

Intrinsic subtypes by gene expression profiling	Histological types	Histological grade	ER status by IHC	HER2 status by IHC/ ISH	Ki67 by IHC	Key molecular features	Predominant integrated cluster association
Luminal A	IC-NST, classic lobular, tubular, cribriform, mucinous, neuroendocrine	1–2	ER+	HER2−	Low	*PIK3CA* mutations, *MAP3K*1 mutations, *ESR1* high expression, *XBP1* high expression, *GATA3* mutations, *FOXA1* mutations, quiet genomes; gain of 1q, 8q, loss of 8p, 16q	Int cluster 2, Int cluster 3, Int cluster 4, Int cluster 7, Int cluster 8
Luminal B	IC-NST, micropapillary	2–3	ER+/ −	HER2 −/+	High	*TP53* mutations, *PIK3CA* mutations, *Cyclin D1* amplification, *MDM2* amplification, *ATM* loss, enhanced genomic instability, focal amplifications (e.g. 8p12, 11q13)	Int cluster 1, Int cluster 2, Int cluster 6, Int cluster 9
HER2	IC-NST, apocrine, pleomorphic lobular	2–3	ER+/ −	HER2+	High	*HER2* amplification, *TP53* mutations, *PIK3CA* mutations, *FGFR4* high expression, *EGFR* high expression, APOBEC mutations, *Cyclin D1* amplification, high genomic instability	Int cluster 5
Basal-like	IC-NST, medullary, metaplastic, adenoid cystic, secretory	3	ER−	HER2−	High	*TP53* mutations, *RB1* loss, *BRCA1* loss, high expression of DNA repair proteins, *FOXM1* activation, high genomic instability, focal amplifications (e.g., 8q24)	Int cluster 4, Int cluster 10

+ positive, − negative, +/− mostly positive, −/+ mostly negative, *ER* oestrogen receptor, *HER2* human epidermal growth factor receptor 2, *IC-NST* invasive carcinoma no special type, *IHC* immunohistochemistry, *ISH* in situ hybridisation

1.1.3 Luminal

Luminal tumors are the most abundant subtype, accounting for around 70% of all breast cancers. They are characterized by the expression of hormone receptors for estrogen alpha (ERα) and/or progesterone (PR). Their expression profiles are similar to the luminal epithelial cells of the normal breast, with high expression of ER related genes and lower expression of proliferation related genes. Indeed, tumors belonging to the luminal subtype are generally having lower grade and slower growth compared to other subtypes. Luminal tumors can be further subdivided into luminal A and luminal B that account for 50% and 20% of all breast cancer respectively. Histologically, luminal A tumors are ER+ and/or PR+, HER2- and express low levels of Ki67, while luminal B can either be ER+ and/or PR+ and HER2+ with low Ki67, or ER+ and/or PR+ and HER2- with high Ki67 (Dai et al. 2015).

Luminal A tumors are characterized by a low-grade, a high differentiation and slow proliferation. In comparison, luminal B tumors are showing higher grade and a poor differentiation with a high proliferation rate as reflected by the high levels of ki67. Luminal A cancers key molecular features include the high expression of ER-related genes as *ESR1*, *FOXA1*, *XBP1* and high mutations rate in *PIK3CA* (45%), *MAP3K1* (13%) and *GATA3* (14%) (Cancer Genome Atlas Network 2012). Luminal B subtype has high expression of proliferative genes *MYC* and *FOXM1*, higher genomic instability with mutation in *PIK3CA* (29%) and *TP53* (29%) and amplification in *CCND1* and *MDM2* (Cancer Genome Atlas Network 2012).

Given the high expression of ER and the dependency on estrogen for the growth, luminal patients are commonly treated with endocrine therapy and the availability of targeted therapies for luminal cancers make them the ones with the most favorable prognosis. Luminal A tumors are highly responsive to this treatment with low response rate to traditional chemotherapy. On the other hand, luminal B tumors have a minor benefit from endocrine therapy treatment alone and a better response to chemotherapy, particularly in neoadjuvant setting (Ades et al. 2014)

1.1.4 HER2-enriched

HER2-enriched (HER2+) subtype is characterized by the amplification and/or overexpression of the HER2, the lack of expression of hormone receptors ER and PR and high levels of ki67. Clinically they are identified by IHC or fluorescent in situ hybridization (FISH) (Dai et al. 2015). Other molecular features include mutations in *TP53* (72%) and *PIK3CA* (39%) and high molecular instability. HER2+ breast cancer includes around 15% of all breast cancers and is associated with a more aggressive clinical course compared to the luminal subtype (Cancer Genome Atlas Network 2012). HER2 is a member of the epidermal growth factor receptors and following dimerization can activate a variety of signaling pathway leading to uncontrolled cell growth. The use of monoclonal antibodies directed against HER2, namely pertuzumab and trastuzumab, are highly effective in the treatment of this subtype (Swain et al. 2015).

Particularly their use in combination with chemotherapy is standard practice for patients with this disease. One of the major clinical problems related to the use of these antibodies is the arise of resistance and to tackle this problem this antibodies have been conjugated with cytotoxic components as emtansine (DM-1) to increase the response rate in second line therapy (Bartsch and Bergen 2018).

1.1.5 Triple negative / Basal

Triple negative breast cancer (TNBC) is identified by the lack of expression of ER, PR and Her2 and a high level of ki67 and accounts for around 15% of all breast cancers. This histologically-define subtype mostly overlap the intrinsic classification of basal-like tumors (Vuong et al. 2014). The triple negative tumors are highly undifferentiated and aggressive having the worst prognosis among the different breast cancer subtypes. Molecular features include germline and/or somatic *BRCA1* and *BRCA2* mutations, the overexpression of cytokeratin CK 5/6 and CK14 typical of the basal compartment of the normal breast, as well as high mutation in TP53 and genomic instability (Cancer Genome Atlas Network 2012).

They usually present as grade 3 tumors with high heterogeneity and this has led to particular effort to try to substratify this group of patients. One classification divided TNBC in this subtype into 6 sub-subtypes, 2 basal-like (BL1 and BL2), 1 immunomodulatory (IM), 1 mesenchymal (M), 1 mesenchymal stem-like (MSL) and 1 luminal androgen receptor (LAR) subtype(Lehmann et al. 2011). This classification was later refined to include only 4 sub-subtypes, namely BL1, BL2, M and LAR (Lehmann, Jovanovi, et al., 2016). Independently of the classification, TNBC remain highly aggressive mainly due to the lack of targeted therapies that are instead available for the Luminal and Her2-enriched subtypes. Clinically they are treated mostly with anthracycline, platinum or taxane-based chemotherapy, but the overall survival remains the lowest (Foulkes, Smith, and Reis-Filho 2010).

1.1.6 Endocrine therapy

The standard treatment for breast cancer patients involves surgery and/or radiotherapy. Depending on the subtype of breast cancer, patients may undergo additional treatments which include chemotherapy or targeted therapy, like endocrine therapy or monoclonal antibodies. These treatments can be administered in neo-adjuvant setting, to shrink the tumor before surgery, or adjuvant setting, as a long-term maintenance treatment and to hit potential metastasis.

Endocrine therapy is the most used treatment for hormone receptor positive breast cancers (Liedtke and Kolberg 2016). It consists in different drugs that act by abrogating the estrogen induced ER activation. Antiestrogens can be divided in Selective ER modulators (SERMs), like tamoxifen, that act by competitively inhibiting the estrogen binding to ERα, and selective ER downregulators (SERDs), like fulvestrant, which bind the ER and lead to its degradation. Another class of agents used for endocrine therapy are the aromatase inhibitors (AIs), like letrozole, that block the enzymes involved in the synthesis of estrogen (Traboulsi et al. 2017).

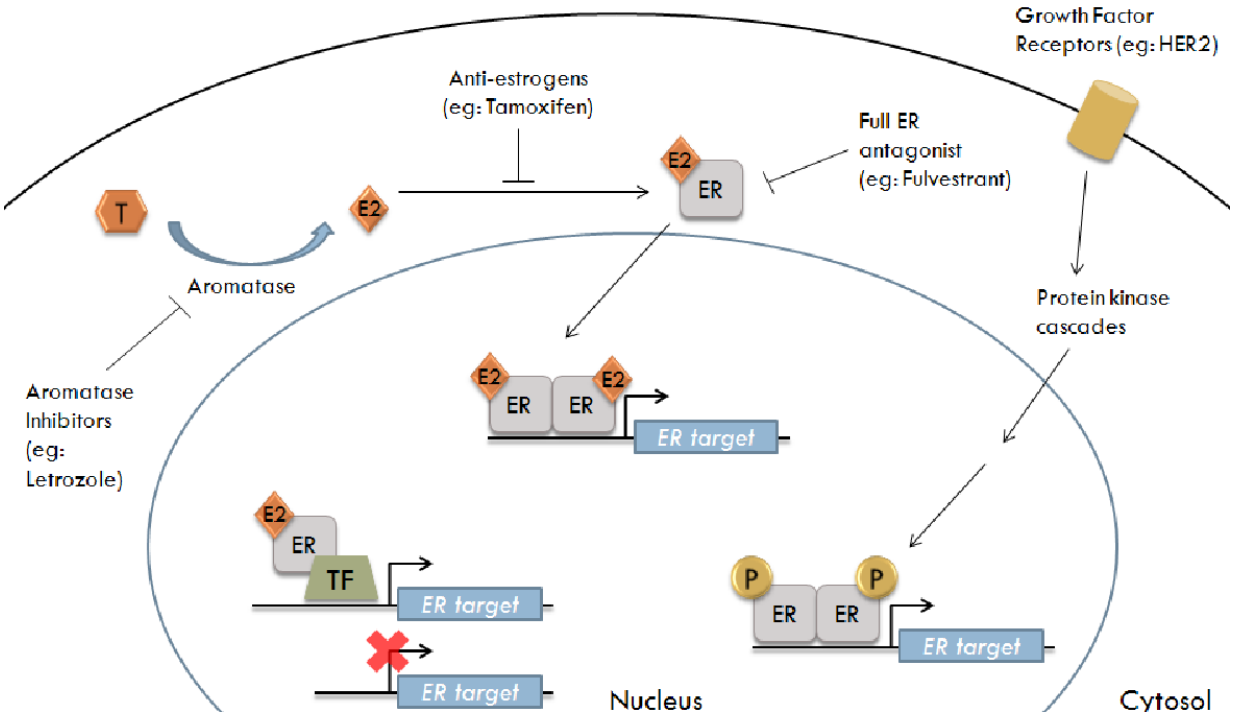

Figure 1: Mechanism of action of endocrine therapy (Chan, Petrossian, and Chen 2016)

1.1.7 SERMs - Tamoxifen

SERMs are the first antiestrogen drugs used for the treatment of breast cancer. They are a class of nonsteroidal compounds that function as ligands for ER. Tamoxifen was the first to be approved by FDA in 1970 and it has been used since as adjuvant treatment for ER+ primary breast cancer of all stages, proved to effectively decrease the mortality rate (Smith 2014). Even though many tamoxifen-analogues of have been developed and tested to try to reduce side effects and increase efficacy (tamofitoremifene, droloxifene, idoxifene, raloxifene, arzoxifene, lasofoxifene, basedoxifene), tamoxifen is still the most effective and most used in the clinic (Arnott et al. 2014). It is routinely delivered as a 5-year long treatment after surgery and recent trials suggest that a even longer treatment period of 10 years might have even higher efficacy in reducing relapse and mortality rates (Davies et al. 2013).

Even though tamoxifen has an antagonist activity in breast cancer cells, it has a estrogenic-like effect in the bones and uterus, thus being associate with an increased risk of endometrial cancer (Da Vies, Syne and Nicholson, 1979). Tamoxifen treatment is mostly used for pre-menopausal patients, where the ovaries activity prevents the use of AIs. This is mainly because the ovaries are the main source of estrogen for pre-menopausal women and exposure to AIs would induce an increase in gonadotrophin secretion, that in turn would increase the production of more estrogen in the ovaries, having the opposite effect (Scharl and Salterberg 2016).

1.1.8 SERDs - Fulvestrant

To minimize agonist activity of SERMs and tackle resistance, a new class of antiestrogens was developed. This group of drugs includes steroidal compounds of which the most used is fulvestrant. Fulvestrant is a "pure" ER antagonist, with a binding affinity to the receptor 100 times higher than tamoxifen. Additionally the binding induce the rapid degradation of the receptor, thus decreasing even further the ability of ER to activate gene transcription (Boér 2017). Fulvestrant is routinely used as a second line therapy for postmenopausal women after

resistance to first line endocrine therapy (tamoxifen or AIs). Recent trials however proved the efficacy of fulvestrant also as first line, alone or in combination with AIs (Robertson et al. 2016). More studies are needed to prove if fulvestrant is an effective and tolerable alternative to standard first line endocrine therapy and which patients might benefit mostly from its direct administration.

1.1.9 Aromatase inhibitors

Aromatase inhibitors (AIs) act by inhibiting aromatase, an enzyme that belongs to the cytochrome p450 superfamily and catalyze the aromatization of androstenedione to estrone and testosterone to estradiol (Mantas et al. 2016). There are three generations of AIs based on the year of development and they are further classified in type 1 and type 2. Type 1 inhibitors are steroidal analogues of androstenedione that irreversibly bind to aromatase while type 2 inhibitors are non-steroidal and bind reversibly to the heme group of the aromatase. The third generation AIs have been developed in 1990 and are the only ones regularly used in clinic. They include both type 1 (anatrozole and letrozole) and type 2 inhibitors (examestane) (Wood, Smith, and Dowsett 2003).

As stated before AIs are can only be used to treat postmenopausal women and they are the treatment of choice for these patients both in first and second line therapy. However, given the efficacy, recent studies are proposing the implementation of ovarian suppression of ablation and AIs administration also for premenopausal women (Rugo et al. 2016). Additionally several trials have proven the enhanced efficacy of AIs when used in combination with other drugs as CDK4/6 inhibitors or mTOR inhibitors and these regiment are now being considered for clinical application in second and third line setting (Flaum and Gradishar 2018).

1.1.10 Resistance to endocrine therapy

Despite the clear benefit of endocrine therapy for patients with ER+ breast cancer, resistance to the treatment is a critical clinical issue that involves a large number of patients. Several studies have shown that recurrence to endocrine therapies occurs in approximately 10-15% of patients within 5 year (Dowsett et al. 2010). This numbers rises to 30% after 15 years from the therapy administration, and eventually up to 40-50% of the patients will relapse (Cynthia X. Ma 2009; EBCTCG 2005). Resistance can occur due to several factors and this adds complexity to the difficult task to identify drivers of this phenomena to target in the clinic (Figure 2) (Dixon 2014; Murphy and Dickler 2016).

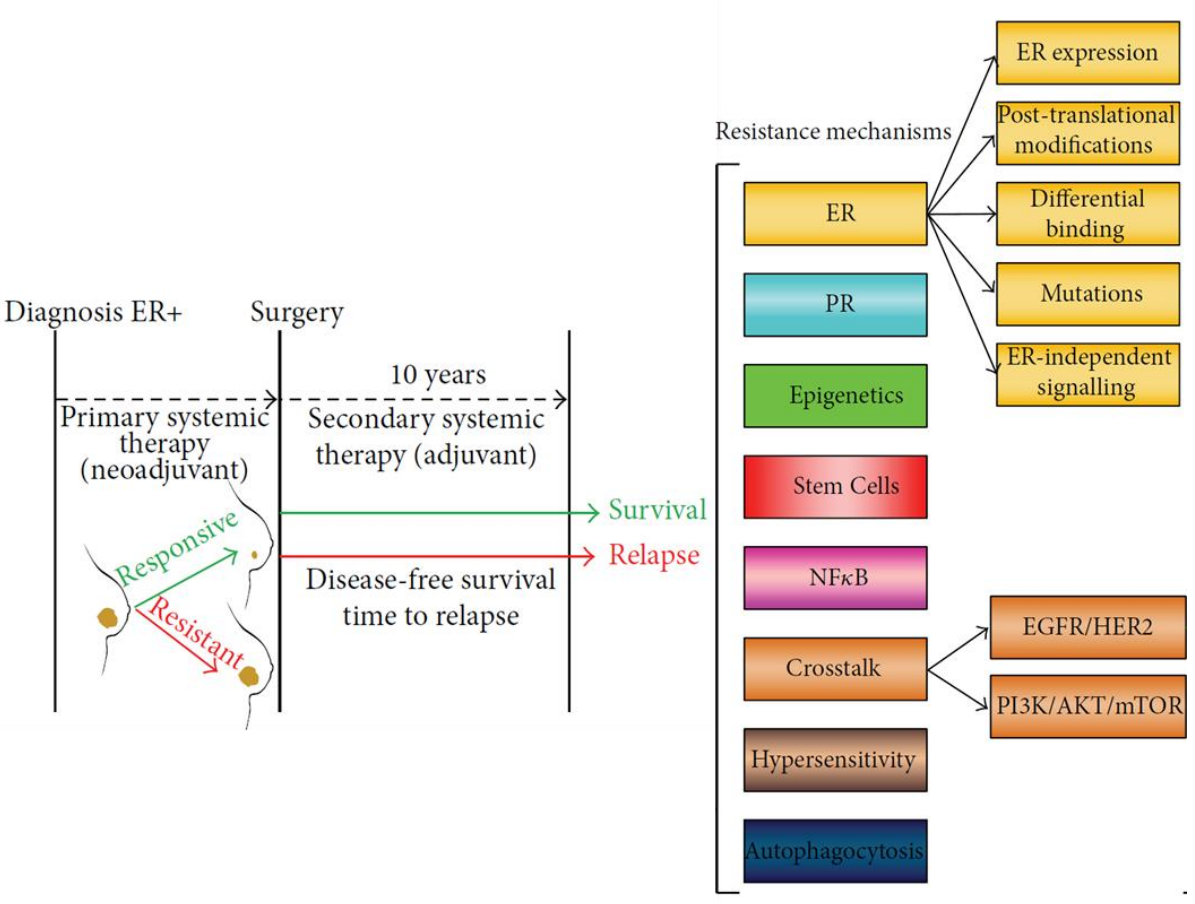

Figure 2: Mechanisms of endocrine therapy resistance (Modified from Dixon JM, 2014)

1.1.10.1 Hormone receptors status and modifications

Estrogen Receptor (ER) is the target molecule of endocrine therapy and many alterations in its expression or activity have been proved to be involved in resistance development. These can be summarized in:

- *ESR1* mutations: activating mutations on *ESR1* gene are mostly found in the ligand binding domain and are responsible for its activation even in absence of a ligand. They are occurring in about 11-39% of relapsing patients and the mutations are generally not present in the primary tumors, identifying this as a mechanism of acquired resistance (Reinert et al. 2017). Highly reported alterations on *ESR1* are Y537S and D538G that are having an occurrence rate of 13% and 21% respectively and have been associated with shorter overall survival (Chandarlapaty et al. 2016; Merenbakh-Lamin et al. 2013).
- Tumor heterogeneity and ER expression: the IHC classification of a tumor considers it ER+ if more than 1% of the cells in the tumor are stained. This makes some tumors (or parts of it) not responsive to this specific treatment that may not be the appropriate therapy choice for this patients in the first place (Harbeck and Rody 2012).
- ER post-translational modifications: ER can be modified by a number of post-translational modifications (phosphorylation, acetylation, sumoylation) that can influence the activity, stability and binding of ER to target genes even in absence of a ligand (Heo 2019).
- Differential ER binding: ER can selectively bind to specific Estrogen Responsive Elements (EREs) in open chromatin regions, helped and directed in this by FOXA1 and other factors. Reports have shown that the activities of these co-factors can adjuvate ER binding in tamoxifen-resistant tumors (Ross-Innes et al. 2012)
- ERα-independent signaling: ER+ tumor treated with endocrine therapy can lose their ER expression (15-20%) and rely for their proliferation on ERα independent mechanisms. These involve, among others, the activity of additional estrogen-regulated receptors, like estrogen receptor β (ERβ) and estrogen-related receptor γ (ERRγ) (Heckler et al. 2014; Speirs et al. 1999).

ER is not the only receptor that is screened with IHC for the classification of patients. PR, an hormone receptor for progesterone, is indeed expressed in many ER+ tumors, but some patients are ER+/PR- and this has been shown to affect prognosis and response to therapy (Díaz Flaqué et al. 2013).

1.1.10.2 Crosstalk with other growth signaling pathways

Receptor tyrosine kinases (RTKs) are some of the main mediators of growth signaling in the cells and many of these growth factor receptors, like EGFR, HER2, HER3, FGFR1 and IGFR1, are associated with endocrine resistance (Murphy and Dickler 2016). Their activation and further signal propagation is estrogen independent as it is induced by receptor specific ligands as EGF, FGF or IGF. These receptors converge downstream in the PI3K/AKT/mTOR and ERK/MEK pathways, thus promoting estrogen-independent proliferation. However they can also phosphorylate and activate the ERα itself, thus overcoming the efficacy of endocrine therapies (Schiff et al. 2004).

Overexpression of growth factor receptor is not the only mechanism by which these pathways can be activated. As mentioned before, PIK3CA is the most common mutation in breast cancer (40%) and in general mutation in the proteins involved in PI3K pathway are found in approximately 70% of breast cancer (Fu, Osborne, and Schiff 2013). Activating mutations in positive regulators of the pathway (PIK3CA, PIK3CB, AKT1, AKT2) or inhibiting mutation in negative regulators, like PTEN, could then promote both ER-dependent and ER-independent transcriptional activation and proliferation (Miller, Balko, and Arteaga 2011). Another pathway involved in proliferation and survival is the NFκB pathway and its crosstalk with the ER receptor has been deeply investigated in literature (Pradhan et al. 2010; Nettles et al. 2008). Alteration of this pathway have been reported in *in vitro* models of resistance and further studies are needed to clarify its role in this phenomena (Yde et al. 2012).

1.1.10.3 Cell-cycle dysregulation

The deregulation of key cell cycle checkpoints and survival proteins are other contributors to the loss of response to endocrine therapy. *CDK4/6* and *CCND1* regulate the transition from G1 to S phase via phosphorylation of RB1 and are important in highly proliferative cancer cells (Weinberg 1995). Several studies showed the aberrant expression of cell-cycle related molecules like cyclin-D1, c-MYC, RB1 and p21 in resistant tumors (Dixon 2014). The cyclin-D1 dependent escape from senescence is one of the most common resistance associated events and can be caused by amplifications or mutations of CDK4, CDK6, cyclin-D1 or other related proteins (p16, p21) (Cancer Genome Atlas Network 2012). This has been shown to play an active role particularly in ER positive breast cancer as CCND1 is a direct target gene of ER and novel CDK4/CDK6 inhibitor are tested in the clinics with promising results (Pernas et al. 2018).

1.1.10.4 Epigenetic regulation

While many studies proved that genetics might have a role in therapy resistance, recent publications reported that epigenetic might have a major role in the acquisition of resistance to endocrine therapies. This role is exploited both at the DNA methylation level, with activation of oncogenes and silencing of tumor suppressor genes, and at the histone modification level, with changes in chromatin accessibility. DNA methylation exerts its role in resistance both by targeting the ER itself, by inducing promoter methylation, and genome wide, by changing the methylation levels of EREs (Stone et al. 2015; Martínez-Galán et al. 2014). At the same time, histone modifications and genome-wide rearrangement of chromatin have been identified as a common phenomenon in endocrine resistance (Patten et al. 2018; Abdel-Hafiz 2017).

1.1.10.5 Other resistance mechanisms

Several other resistance mechanisms have been described in literature. Additional pathway have been reported to play a role in resistance development, including Notch and Wnt (Nguyen et al. 2015; Riggins et al. 2007). Particularly, their involvement in the maintenance of a population of cancer stem cells (CSCs) is important in keeping a subset of cells insensitive to the drug, thus promoting resistance (Piva et al. 2014; Lombardo et al. 2014). Other cellular processes, like metabolism, autophagy and epithelial-to-mesenchymal transition (EMT) have been proven play a role in resistance to endocrine therapy, even though their role remains poorly understood and further studies are needed to shed light in their involvement in the resistance process (Nguyen et al. 2015; Samaddar et al. 2008; Hiscox et al. 2006).

There are also treatment-specific aspects to take into account. An example related to tamoxifen involves the status of the enzyme involved in its conversion to the active metabolite 4-hydroxy-tamoxifen is the cytochrome P450 2D6. Patients lacking for this enzyme have been reported to be insensitive to tamoxifen treatment and other therapeutic options should be considered (Hoskins, Carey, and McLeod 2009). At the same time, regarding aromatase inhibitors, studies have shown that even if they deplete the tissues from estrogen, low levels remains and cells can develop hypersensitivity to this residual hormone levels, thus still activating ER-related pathways (Sikora et al. 2012).

Overall resistance to endocrine therapy is complex and mediated by numerous cellular processes and pathways. Understanding the reasons and the driving mechanisms behind resistance development is essential to develop new clinical strategies to tackle resistance.

1.1.11 Treatment of endocrine resistant breast cancer

After the failure of first line endocrine therapy, recurrent ER+ breast cancer can be treated with alternative strategies to target growth and survival pathways responsible for the relapse (Figure 3). As mentioned before, one of the therapeutic options is to use SERDs like fulvestrant to block

and degrade the ER. Fulvestrant can be use both in monotherapy or in combination either with other endocrine therapies or with approved drugs for advanced breast cancer, as CDK4/6 inhibitors, mTOR inhibitors and PI3K inhibitors (Sammons, Kornblum, and Blackwell 2019). While the administration of fulvestrant alone is already beneficial for patients, with increased progression free survival (PFS) up to 6 months, its administration in combinatorial therapies showed better results in recent clinical trials, therefore opening the possibilities for more effective second line treatments (Schmid et al. 2018; Cristofanilli et al. 2016; Di Leo et al. 2018).

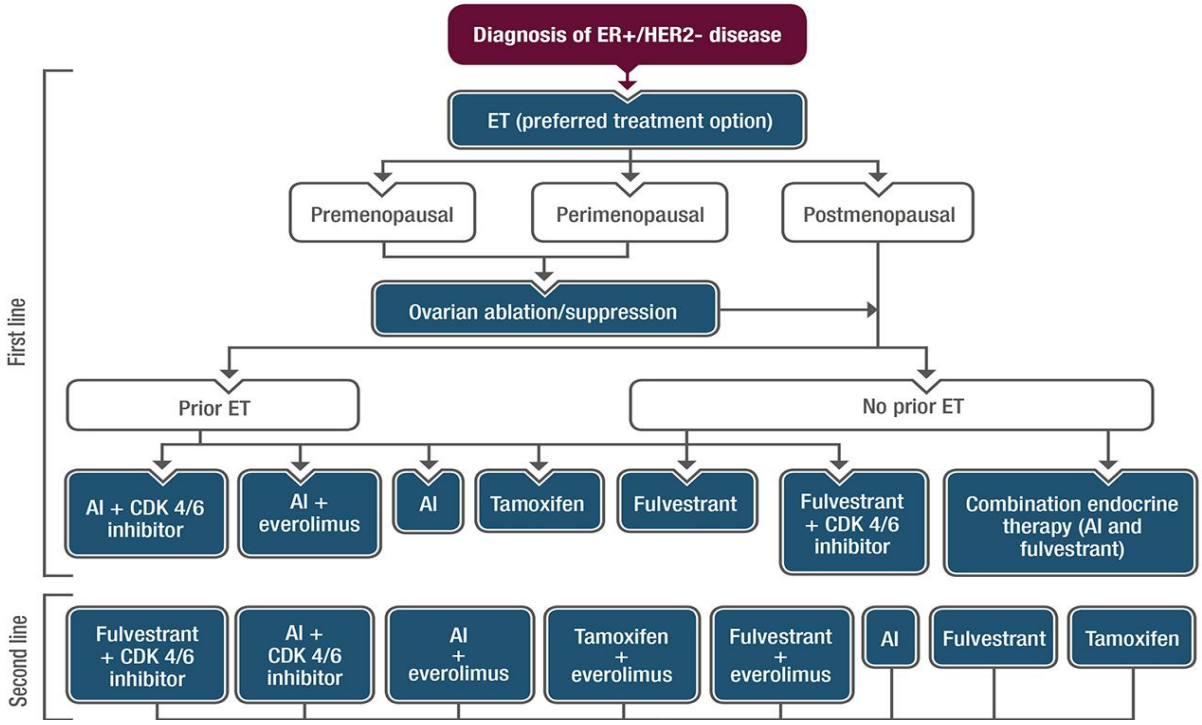

Figure 3: Treatment of ER+ breast cancer (Modified from Cardoso *et al.*, 2018)

CDK4/6 inhibitors are small molecules that interfere with the G1-S phase transition during cell cycle by blocking CDK4 and CDK6 phosphorylation of Rb. Three different inhibitors are currently used in clinic trials to treat luminal breast cancer: palbociclib, ribociclib and abemaciclib (Cortés et al. 2017). They have been tested both as first and second line therapies in combination with standard endocrine therapies showing a consistent increase PFS (Vidula and Rugo 2016).

Inhibitors for mTOR and PIK3 are also being used in clinical trials in combination with endocrine therapy, given the importance of this pathway in the resistance process (Steelman et al. 2016). Rapamycin was the first mTOR inhibitor discovered and new derivatives of this drug are now tested in the clinic, as tensirolimus, everolimus and deforolimus. Several clinical trial using these inhibitors in combination with different endocrine therapies are under way and results show improved PFS and overall survival (Rotundo et al. 2016). PI3K inhibitors act upstream of mTOR and they are currently tested in clinical trials in combination with fulvestrant for second line therapy (Alpelisib, Buparsilib, Pictisilib). Initial results show promising effects, with a particular high efficiency in patients harboring mutations in PI3KCA (AlFakeeh and Brezden-Masley 2018). Additionally studies are on-going to test the efficacy of the combination of both CDK4/6 and mTOR or PI3K inhibitors as second line treatment with AIs or fulvestrant (D'Souza, Spicer, and Lu 2018).

Other therapeutic strategies currently tested are the combination of standard endocrine therapy with HDAC inhibitors (vorinostat and entinostat) or immunotherapy (anti-PD-1 and anti-PD-L1 antibodies) but further studies are needed to prove their efficacy (D'Souza, Spicer, and Lu 2018).

1.2. Tumor heterogeneity

Cancer is a heterogeneous disease. Heterogeneity does not only refers to the differences between patients having the same tumor (inter-tumor heterogeneity) but also to variation inside the tumor itself (intra-tumor heterogeneity) (Stanta and Bonin 2018). Indeed, at a specific time, tumors include different cells in terms of genetics, epigenetics or transient gene expression and this closely affects cancer progression and resistance to therapy. To explain this heterogeneity two general models have been described in literature:

- Clonal evolution: genetic and epigenetic changes occur in individual cells through time, giving them selective advantage. These clones can therefore out-grow others becoming the dominant population in the tumor (Nowell 1976).

- Cancer stem cell: the growth and progression of tumors is driven by a subset of stem cells called cancer stem cells (CSCs). This cells are responsible for the initiation and maintenance of the tumors suggesting a hierarchical organization of tumor evolution (Lapidot et al. 1994; Reya et al. 2001)

Even if the two models propose different interpretations of tumor heterogeneity, they are not mutually exclusive and it has been proved that they can both contribute to tumor progression. Indeed genetic and epigenetic events can affect both CSCs and daughter cells, giving rise to sub-clones with phenotypic advantages (Figure 4) (J. Wang, Ma, and Cooper 2013).

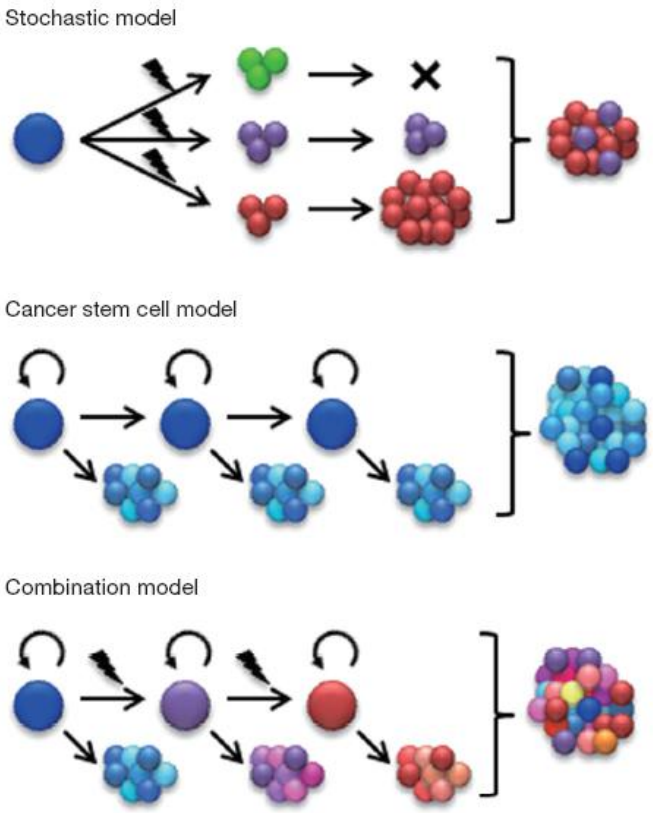

Figure 4: Models of tumor heterogeneity (Modified from Wang, Ma and Cooper, 2013)

This heterogeneity is reflected in the spatial localization of specific cell in a tumor. Recent techniques allowed the deep molecular characterization of spatial heterogeneity confirming the

unequal distribution of molecular alterations across primary tumors in different types of cancer (Dagogo-Jack and Shaw 2018). This proves the limitation of biopsies and bulk analysis for therapy decision as important alterations might be masked based on the approach used. An additional layer to add to the heterogeneity of a tumor is the temporal heterogeneity. This can be caused both by the natural accumulation of mutation over time or by external factor. Indeed, several studies proved that therapy administration can change the molecular profile of tumors (Murugaesu et al. 2015; TCGA 2008).

1.2.1 Role of tumor heterogeneity in drug resistance

The heterogeneity of cancer cells, which can have different grade of sensitivity to therapies, is one of the main drivers of resistance development. This can be proven by the fact that many patients, after an initial response to drugs like chemotherapeutic agents or targeted therapies, relapse and are resistant if treated with the same compound (Garraway and Jänne 2012). There are two main reasons that can explain this phenomenon:

- Resistant clones: presence in the tumor population of resistant clones to the therapy applied. While an initial response to the therapy is seen as the majority of sensitive cells die, the growth of the pre-resistant clone give rise to a relapse resistant to the same treatment (Dagogo-Jack and Shaw 2018). In several studies has been shown that low-frequency alteration in pre-treatment tumors are selected and identified as the reason of the development of the resistance (Shaw et al. 2016; Yu et al. 2014). Additionally, evidence from *in vitro* barcoding experiments showed expansion of pre-existing resistant population to targeted therapies (Bhang et al. 2015; Hinohara et al. 2018).
- Adaptation of “persister” clones: some clones in the bulk population survive the initial drug treatment and acquire additional alterations that later on confer resistance to the therapy. It has been described that these “persister” cells enter a long quiescent phase with no proliferation, during which a fraction of the initial population can gain the ability to expand (Hata et al. 2016; Ramirez et al. 2016). Some studies identified this "persister"

state to be transient and stochastic and mainly driven by epigenetic regulation rather than genetic mutations (Sharma et al. 2010; Shaffer et al. 2017).

Due to this complexity in the tumor population, the characterization of tumors cells in time is essential to understand the dynamics of clones and choose the appropriate therapeutic regimen. Nowadays, the common practice in clinic is to make treatment decision based exclusively on pre-treatment biopsies, therefore limiting the information on a snapshot of the tumor. However, as it has been shown that therapy itself can cause the selective pressure to induce specific clonal selection, longitudinal sampling is needed also during therapy administration and even more after relapse. Additionally, the identification of clonal alterations is essential to implement combinatorial treatment that can have adjuvant role to standard therapy (Dagogo-Jack and Shaw 2018).

1.2.2 Clonal heterogeneity in breast cancer

Breast cancers are not homogeneous population of cells and as such the single cells in the tumor have different characteristics and response to the drugs. A clear example in ER+ breast cancer is the expression of the estrogen receptor. IHC analysis shows that ER expression levels can range from 1 to 100 % and this can impact the response to endocrine therapies as ER negative cells would not be affected by the treatment (Iwamoto et al. 2012; Groenendijk et al. 2019). The advent of next generation techniques allowed for a deeper analysis of clonality both in terms of genetics and epigenetics. Multi-regional DNA sequencing has revealed the presence of a high-level subclonal diversity both in primary and relapsing tumors. While no specific temporal genetic pattern was revealed, some subclonal mutation detectable before chemotherapeutic treatment were found enriched in the relapsing tumor, proving the selection of resistant clones (Yates et al. 2015). Single cell resolution techniques added further resolution in the analysis of resistance. Indeed an *in vivo* study in TNBC patients revealed the presence of pre-existing clones with genetic characteristic that are selected after chemotherapy administration, while the expression profiles are acquired in response to the drug (Kim et al.

2018). In contrast a recent *in vitro* study in MCF7 revealed that pre-existent clones with specific expression profiles are selected during chemotherapy administration (Prieto-Vila et al. 2019).

In the context of endocrine therapy, only few studies tried to address the role of clonality in resistance. A barcoding approach used in vitro to track single clones of MCF7 during tamoxifen and fulvestrant resistance development revealed a selection of specific pre-existing clones. The resistant clones were described to arise from around 1% of the initial population and specific genetic variants were associated with the clonal selection (Hinohara et al. 2018). A different study approached the issue of clonality in the tumors mapping the epigenetic status of tumors with ChIP, with a focus on the role of enhancers in tumor heterogeneity. Their results show that the administration of the therapy itself drives the selection of non-genetically defined clones (Patten et al. 2018). Thus, the understanding of the role of clonal heterogeneity in breast cancer and its impact on endocrine therapy administration is still evolving. More studies are needed to establish the role of epigenetic and genetics in the selection or adaptation of resistant clones and define the exact mechanism that drives selection for specific drugs.

2. Aims of the study

Resistance to endocrine therapy in breast cancer is an urgent clinical problem that affects around 40% of all patients treated with this therapy. To address this question in an *in vitro* setting, researchers developed cellular models of endocrine therapy resistance. In literature, the strategy to identify the mechanisms of resistance development and novel targets involved in the process has focused on the differences between resistant and sensitive cells. Even though some progresses have been made and new targeted drug are now available to treat resistant breast cancer, mortality rate for these patients remains high. Additionally there is a lack of understanding of the role of clonality in the tumors and how the initial heterogeneity might affect treatment outcome. The aim of this PhD thesis was to address these issues related to the mechanisms of endocrine therapy resistance development with two different approaches:

1) Time-resolved profiling of resistance development for identification of novel drivers:
    a. Generation of cell lines resistant to tamoxifen treatment and to estrogen deprivation
    b. Profiling of the cell lines during resistance development to identify the timing of changes in gene expression, methylation and acetylation
    c. Identification of target genes driving early stages of resistant development
    d. Validation of the role of a selected target in resistance-associated phenotypes *in vitro* with knock-down, knock-out and over-expression approaches
    e. Investigation of the mechanisms by which the candidate gene regulates resistance
    f. Confirmation of the role of the selected target *in vivo* in a xenograft model
    g. Correlation of the in vitro generated data to patients' datasets to add clinical relevance to the findings.

2) Barcoding of cell lines to investigate the role of clonality, selection and stochasticity in endocrine therapy resistance:
    a. Generation of barcoded cell lines and induction of resistance

b. Sequencing of barcodes to identify the mechanism of resistant clones selection
c. Comparison between treatments (tamoxifen and estrogen deprivation) and cell lines (MCF7 and T47D)
d. Correlation of barcode composition to pathway activation analysis

3. Materials and Methods

3.1. Materials

3.1.1 Instruments

Aushon 2470 contact printer	Aushon / Quanterix
Bacterial Incubator (37°)	Memmert
Bacterial shaking Incubator (37°)	INFORS HT
Bioanalyzer	Agilent
Biohit Proline multichannel pipette	Sartorius
Bioruptor Plus sonication device	Diagenode
Cell culture hood HERA Safe	Thermo Fisher Scientific
Cell culture incubators	Heraeus Binder
Centrifuges	Eppendorf AG Heraeus Hettich
DNA gel apparatus	Renner
Flow Cytometer FACS Calibur	Becton Dickinson
Fluorescent microscope Axiovert 40 CFL	Carl Zeiss
Freezer (-20°)	Liebherr
Freezer (-80°)	Sanyo
Fridge (+4°)	Liebher
Gel documentation system	Herolab
Glomax explorer plate reader	Promega
Light Microscope	Hund Wetzlar
LSM 800 Confocal Microscope	Carl Zeiss
Magnetic Stand	Thermo Fisher Scientific

Molecular Devices Microscope IXM XLS	Molecular Devices
Nanodrop ND-1000 spectrophotometer	Thermo Fisher Scientific
Neubauer chamber	BRAND
Odyssey Infrared Imaging System	Li-Cor Biosciences
Pipetboy acu pipette	INTEGRA Biosciences
Pipetman pipette	Gilson
Power Supply GPS 200/400	Pharmacia LKB
Protein Gel Apparatus MiniProtean II	Bio-Rad
Qubit Fluorometric Quantification	Thermo Fisher Scientific
SW41 Ti Rotor and Tubes	Beckman Coulter
Sequence Detection System ABI 7900HT	Applied Biosystems
Quantstudio 5 Real-Time PCR System	Thermo Fisher Scientific
Thermocycler	Applied Biosystems
Thermomixer	Eppendorf AG
Titramax 100 rocking platform	Heidolph
Trans-Blot turbo Transfer	Bio-Rad
Vacusafe	INTEGRA Biosciences
Vortex mixer	NeoLab
Water Bath	Julabo

3.1.2 Chemicals and Reagents

7-Aminoactinomycin D (7-AAD)	BD Biosciences
Anisomycin	Biomol
Bromodeoxyuridine (BrdU)	BD Biosciences
BSA	Sigma-Aldrich
β-estradiol	Sigma-Aldrich
cOmplete Mini Protease Inhibitor	Roche Diagnostics

Cocktail	
Charcoal Stripped Fetal Bovine Serum	Sigma-Aldrich
Dynabeads Protein A	Thermo Fischer Scientific
Dynabeads Protein G	Thermo Fischer Scientific
DMSO	Sigma-Aldrich
DMEM medium	Gibco
EDTA	Sigma-Aldrich
EGTA	Sigma-Aldrich
Ethanol	Sigma-Aldrich
Fast Green FCF	Carl Roth
Fetal Bovine Serum	Gibco
Formaldehyde solution 37%	Sigma-Aldrich
Glycerol	Sigma-Aldrich
Glycin	Sigma-Aldrich
Hepes	Sigma-Aldrich
Hoechst 33258	Sigma-Aldrich
IGEPAL	Sigma-Aldrich
Isopropanol	Greiner Bio-One International
KOH	Sigma-Aldrich
LiCl	Sigma-Aldrich
Lipofectamine RNAiMAX	Thermo Fischer Scientific
Lipofectamin CRISPRMAX Cas 9	Thermo Fischer Scientific
L-glutamine, 200mM	Gibco
Methanol	Greiner Bio-One International
M-PER mammalian protein extraction reagent	Thermo Fischer Scientific
NaCl	VWR International
Na-deoxycholate	Sigma-Aldrich

NaOH	Sigma-Aldrich
N-lauroylsarcosine	Sigma-Aldrich
non-DEPC treated nuclease-free water	Thermo Fisher Scientific
Opti-MEM medium	Gibco
PBS	Gibco
Paraformaldehyde 16%	Thermo Fisher Scientific
PhosSTOP Phosphatase Inhibitor Cocktail	Roche Diagnostics
Protein Marker Precision Plus Protein Dual Color	BioRad
Penicillin/Streptomycin	Gibco
Proteinase K	Sigma-Aldrich
RIPA Lysis and Extraction buffer	Thermo Fisher Scientific
RNAiMax	Invitrogen
Rockland Blocking Buffer	Rockland Immunochemicals Inc.
Roti-Load 1, 4x sample loading buffer	Carl Roth
SDS	Carl Roth
siRNAs	Dharmacon, Thermo Fisher Scientific
Sodium pyruvate, 100mM	Gibco
SPRIselect beads	Beckman Coulter
TITANIUM Taq DNA Polymerase	Takara Bio
NaF	Sigma-Aldrich
Na2VO4	Bernd Kraft
TaqMan Fast Universal PCR Master Mix (2x)	Applied Biosystems
TGFß2 Recombinant Protein	R&D Systems
Trypsin EDTA Solution (0.25%)	Gibco
Tris HCl	Sigma-Aldrich
Tris-base	Sigma-Aldrich

Triton X-100	Sigma-Aldrich
Tween 20	Sigma-Aldrich
T-PER tissue protein extraction reagent	Thermo Fischer Scientific
(Z)-4-Hydroxytamoxifen ≥98%	Sigma-Aldrich

3.1.3 Assay Kits

Annexin V: PE Apoptosis Detection Kit	BD Bioscience
BCA Protein Assay Kit	Thermo Fisher Scientific
cDNA Synthesis Kit	Thermo Fisher Scientific
CellTiter-Glo Luminescent assay	Promega
Cytofix/Cytoperm	BD Biosciences
DNeasy Blood & Tissue kit	Qiagen
DuoSet Ancillary Reagent Kit 2	R&D Systems
Human TGF-beta 2 DuoSet ELISA	R&D Systems
Infimium MethylationEPIC BeadChip	Illumina
Qubit dsDNA HS Assay Kit	Thermo Fisher Scientific
Rnase free Dnase Set	Qiagen
RNeasy Mini kit	Qiagen
qPCR MasterMix (RT-QP2X-03+NR)	Eurogentec
RevertAid™ H Minus First Strand cDNA synthesis kit	Thermo Fisher Scientific
Wizard SV Gel and PCR Clean-up System	Promega

3.1.4 Consumables

Micro centrifuge tubes (1,5 and 2ml)	Eppendorf AG
Petri dishes (100 and 150mm)	Techno Plastic Products (TPP)
Conical tubes (15 and 50ml)	Becton Dickinson

Multi-well plates (6, 12, 24, 48 wells)	Thermo Fisher Scientific
96-well plate transparent	Becton Dickinson
96-well plate black	Greiner Bio-One International GmbH
96-well plate white	PerkinElmer
96-well Clear V-Bottom Deep Well Plate	Corning
Adhesive Plate Seal	Thermo Fisher Scientific
AMICON® Ultra-4 filtration units	Merck Millipore
BioCoat Matrigel Invasion Chambers	Corning
Cell Culture Flasks, T-25, T-75, T-175	Techno Plastic Products (TPP)
Cell Scraper	Corning
Cry vials 1.8mL	Thermo Fisher Scientific
FACS tubes	Corning
Filter tips, 10µL, 20µL, 200µL, 1000µL	Neptune
Matrigel Invasion Chambers	Corning
Mini-PROTEAN TGX Precast Gels	BioRad
Oncyte Nitrocellulose Film-Slide	Grace Bio-Labs
Optical 384 wells plates for Taqman	Applied Biosystems
PCR strips	Steinbrenner Laborsysteme GmbH
PVDF membrane Immobilon-P	Merck Millipore
Qubit Assay tubes	Thermo Fisher Scientific
Reservoirs 50ml	Corning
Round-Bottom polypropylene tubes 5ml	Thermo Fisher Scientific
Serological pipettes 2.5mL, 5mL, 10mL, 25mL, 50ml	Becton Dickinson
Stainless steel beads 5ml	Qiagen
Trans-well system (8.0µm pore size)	Corning
Tips for micropipettes	Starlab
Trans-Blot Turbo mini PVDF Transfer Kit	BioRad

3.1.5 Software

Easeq	http://easeq.net
Flowjo v10	Becton Dickinson
GenePix Pro v7.0	Molecular Devices
GraphPad Prism v5	GraphPad Software, Inc.
Image J	NIH
Inkscape	Software Freedom Conservancy, Inc.
Molecular Devices Analysis Software	Molecular Devices
Odyssey v2.1	LI-COR
QuantStudio Design and Analysis	Agilent Technologies
Roche UPL Design Center	Roche Diagnostics
SDS v2.2	Applied Biosystems
Tinn-R	Rgui Team

3.1.6 Databases and datasets

Ensembl (release 91)	EMBL-EBI
Human GRCh37/hg19	UCSC Genome browser
MSigDB	Broad Institute
GSE111563	Geo DataSets
GSE80077	Geo DataSets
GSE20181	Geo DataSets
GSE55374	Geo DataSets
GSE10281	Geo DataSets
GSE59515	Geo DataSets

3.1.7 Buffers and solutions

ChIP			
Lysis Buffers (1/2/3)	50mM Hepes-KOH 150mM NaCl 1mM EDTA 10% Glycerol 0.5% IGEPAL 0.25% Triton X-100 1x Protease Inhibitor Cocktail	10mM Tris-HCl 200mM NaCl 1mM EDTA 0.5mM EGTA 1x Protease Inhibitor Cocktail	10mM Tris-HCl 100nM NaCl 1mM EDTA 0.5mM EGTA 0.1% Na-Deoxycholate 0.5% N-lauroylsarcosine 1x Protease Inhibitor Cocktail
Elution Buffer	50mM Tris-HCl 10mM EDTA 1% SDS		
TE Buffer	M-PER lysis buffer 1x Complete Mini Protease Inhibitor Cocktail 1x PhosSTOP Phosphatase Inhibitor Cocktail		
Washing buffer	PBS with 0.5% BSA		
ELISA			
Blocking buffer	PBS with 1% BSA		
Washing buffer	PBS with 0.25% Tween 20		
RPPA and WB			
Blocking buffer	1:1 Rockland blocking buffer: TBS 1 mM Na_3VO_4 10 mM NaF		
FCF staining solution	0.005% Fast Green FCF 10% Acetic acid 30% Ethanol		
FCF destaining	10% Acetic acid,		

solution	30% Ethanol
Protein Lysis buffer	M-PER lysis buffer 1x Complete Mini Protease Inhibitor Cocktail 1x PhosSTOP Phosphatase Inhibitor Cocktail
6x SDS buffer	10% Glycerol 4% SDS 10 mM DTT 125 mM Tris–HCl pH 6.8
SDS running buffer	192 mM glycine 25 mM Tris 0.1% SDS
10X TBS	1.37M NaCl, 200mM Tris, pH 7.6
1X TBST	0.1% Tween 20 in 1x TBS
Transfer buffer	20% Trans-BlotR Turbo™ 5x Transfer Buffer 20% EtOH 60% H2O

3.1.8 Antibodies

PRIMARY ANTIBODIES			
Target	**Antibody ID**	**Company**	**Species**
4E-BP1	CST 9644	Cell Signaling	rabbit
AKT	CST 9272	Cell Signaling	rabbit
ATF3	ab207434	Abcam	rabbit
β-Actin	Actin- Clone4	MP Biomedicals	mouse
β-Catenin	CST 9562	Cell Signaling	rabbit
CSNK2B	sc 12739	Santa Cruz	mouse
c-RAF	CST 9422	Cell Signaling	rabbit

CSNK1A1	CST 2655	Cell Signaling	rabbit
CSNK1E	CST 12448	Cell Signaling	rabbit
CTNNBIP1	ab 129011	Abcam	rabbit
Dishevelled 3	ab 76081	Abcam	rabbit
DKK1	WH0022943M1	Sigma	mouse
EGFR	CST 2232	Cell Signalling	rabbit
ERBB2	MS-730	Thermo scientific	mouse
ERBB4	ab76303	Abcam	rabbit
ERK1	RnD AF1575	R&D	rabbit
FAK	CST 3285	Cell Signaling	rabbit
GAB1	CST 3232	Cell Signaling	rabbit
GRB2	CST 3972	Cell Signaling	rabbit
GSK-3alpha	CST 9338	Cell Signaling	rabbit
GSK-3beta	CST 9315	Cell Signaling	rabbit
ERBB3	CST 12708	Cell Signaling	rabbit
JNK1	CST3708	Cell signalling	mouse
LKB1	CST 3050	Cell Signaling	rabbit
LRP5	CST 5731	Cell Signaling	rabbit
MEK1	BD 610122	BD Biosciences	mouse
MSK1	AF2518	R&D	goat
MSK2	CST 3679	Cell Signaling	rabbit
mTOR	CST 2972	Cell Signaling	rabbit
NF-kappaB p65	CST 8242	Cell Signaling	rabbit
p38 MAPK	CST9212	Cell Signaling	rabbit
P44/42	CST9102	Cell Signaling	rabbit
p70 s6 kinase	CST 2708	Cell Signaling	rabbit
PAK1	CST 2602	Cell Signaling	rabbit
PAK2	ab76293	Abcam	rabbit

PDK1	CST3062	Cell Signaling	rabbit
Phospho-4E-BP1_Thr37_Thr46	CST 2855	Cell Signaling	rabbit
Phospho-Akt_Ser473	CST 9271	Cell Signaling	rabbit
Phospho-beta-Catenin_Ser675	CST 9567	Cell Signaling	rabbit
Phospho-c-Jun_Ser73	CST 9164	Cell Signaling	rabbit
Phospho-c-Raf_Ser259	CST 9421	Cell Signaling	rabbit
Phospho-eIF4B _Ser406	CST 5399	Cell Signaling	rabbit
Phospho-GSK-3beta_Ser9	CST 9323	Cell Signaling	rabbit
Phospho-JNK Thr183_Tyr185	CST 4668	Cell Signaling	rabbit
Phospholipase C gamma	ab 41433	Abcam	mouse
Phospho-LKB1_Ser428	CST 3482	Cell Signaling	rabbit
Phospho-MEK1_Ser298	CST 9128	Cell Signaling	rabbit
Phospho-NF-kappaB p65_Ser536	CST 3033	Cell Signaling	rabbit
Phospho-p38 MAPK_Thr180-Tyr182	CST 9215	Cell Signaling	rabbit
Phospho-p44/42 MAPK_ERK1-2_Thr202-Tyr204	CST 4370	Cell Signaling	rabbit
Phospho-p70 S6 Kinase_Thr389	CST 9234	Cell Signaling	rabbit
Phospho-p90RSK_Ser380	CST 9341	Cell Signaling	rabbit
Phospho-PDK1_Ser241	CST 3061	Cell Signaling	rabbit
Phospho-PLCgamma1_Ser1248	CST 4510	Cell Signaling	rabbit
Phospho-PRAS40_Thr246	CST 2997	Cell Signaling	rabbit
Phospho-PTEN_Ser380_Thr382-383	ab 109454	Abcam	rabbit
Phospho-S6 Ribosomal Protein_Ser235-236	CST 4858	Cell Signaling	rabbit
Phospho-Src Family_Tyr416	CST 2101	Cell Signaling	rabbit
PI3 Kinase p110 beta	ab 32569	Abcam	rabbit

PI3 Kinase p110alpha	CST 4249	Cell Signaling	rabbit
PI3 Kinase p85 alpha	ab 40755	Abcam	rabbit
PKCdelta	CST 9616	Cell Signaling	rabbit
PRAS40	CST 2691	Cell Signaling	rabbit
RSK1	CST 8408	Cell Signalling	rabbit
S6 Ribosomal Protein	CST 2217	Cell Signaling	rabbit
SOS	CST 12409	Cell Signalling	rabbit
SRC	CST 2123	Cell Signaling	rabbit
SECONDARY ANTIBODIES			
F(ab')2-Goat anti-Rabbit IgG (H+L) Cross-Adsorbed Secondary Antibody, Alexa Fluor 680	A21077	Thermo Fisher Scientific	
F(ab')2-Goat anti-Mouse IgG (H+L) Secondary Antibody, Alexa Fluor 680	A21059	Thermo Fisher Scientific	
Rabbit anti-Goat IgG (H+L) Cross-Adsorbed Secondary Antibody, Alexa Fluor 680	A21088	Thermo Fisher Scientific	

3.1.9 siRNAs

siRNA	Annotation	Target Sequence
ON-TARGETplus control siRNA	siCTRL	UGGUUUACAUGUCGACUAA
		UGGUUUACAUGUUGUGUGA
		UGGUUUACAUGUUUUCCUA
		UGGUUUACAUGUUUUCUGA
ON-TARGETplus TGFB2 siRNA	siTGFB2	GGAUUGAGCUAUAUCAGAU
		CUGCGUGUCCCAAGAUUUA
		GAUGCGGCCUAUUGCUUUA
		GAGCAUGCCCGUAUUUAUG

ON-TARGETplus ATF3 siRNA	siATF3	GGUUUGCCAUCCAGAACAA
		CAGUGGUGUUUGAGGAUUU
		GCGACGAGAAAGAAAUAAG
		AGACGGAGUGCCUGCAGAA

3.1.10 PCR Primers

Gene	Primer Left	Primer Right	Probe
ATF3	TTTGCCATCCAGAACAAGC	CATCTTCTTCAGGGGCTACCT	53
ACTB	ATTGGCAATGAGCGGTTC	GGATGCCACAGGACTCCA	11
RPS6KA5	GAAATGGATCCCACTTATTCTCC	CAACAAAGGAATAGCCCTGAA	43
DUSP1	CGAGGCCATTGACTCATAGA	CTGGCAGTGGACAAACACC	65
DUSP10	TGAATGTGCGAGTCCATAGC	TGGCAATTCAAGAAGAACTCAA	22
JUN	CCAAAGGATAGTGCGATGTTT	CTGTCCCTCTCCACTGCAAC	19
TGFB2	CCAAAGGGTACAATGCCAAC	CAGATGCTTCTGGATTTATGG	67
BAMBI	CGCCACTCCAGCTACATCTT	CACAGTAGCATCGAATTTCACC	71
ERBB2	GGGGAAACCTGGAACTCACCT	AGCGATGAGCACGTAGCC	4

3.1.11 sgRNAs

Gene	Annotation	Sequence
ATF3	KO1	AAAGUGCCGAAACAAGAAGA
ATF3	KO2	AGAAGGCACUCACUUUCUGC

3.2. Methods

3.2.1 Cell Culture

3.2.1.1 Cell cultivation

All parental breast cancer cells were obtained from ATCC. MCF7-TAMR (tamoxifen resistant) and MCF7-LTED (Long-Term Estrogen Deprived) were kindly provided by Dr. Luca Magnani form Imperial College London (ICL). Cell lines were regularly sent for cell line authentication to Multiplexion GmbH and tested for mycoplasma contamination. The cell lines were cultured in the respective media (Table 2) and incubated at 37°C with 5% CO_2 in a humidified atmosphere. Cells were passaged when they reached 80% confluency under aseptic conditions in a laminar air-flow hood.

Table 2: Cell lines

Cell line	Source	Characteristics	Growth media
MCF7	ATCC HTB-22	Luminal A breast cancer cell line	DMEM + 10% FBS + 1% P/S + 10^{-8}M 17-ß-estradiol (E2)
T47D	ATCC HTB-133		
MCF7-T	Dr. Luca Magnani, ICL	Resistant to 100nM TAM	DMEM + 10% FBS + 1% P/S + 100nM TAM (TAM)
T47D-T	Derived from T47D		
MCF7-L	Dr. Luca Magnani, ICL	Resistant to long-term estrogen deprivation	DMEM - phenol red + 10% charcoal stripped FBS + 1% P/S + 1% Glutamine + 1% Sodium Pyruvate
T47D-L	Derived from T47D		
MCF7 ATF3-KO1	Derived from MCF7	ATF3 Crispr-Cas9 KO	DMEM + 10% FBS + 1% P/S + 10^{-8}M 17-ß-estradiol (E2)
MCF7 ATF3-KO2			
MCF7 Empty	Derived from MCF7	pLX304 – empty	DMEM + 10% FBS + 1% P/S + 10^{-8}M 17-ß-estradiol + Blasticidin S
MCF7 ATF3 OE		pLX304 – ATF3	
T47D Empty	Derived from T47D	pLX304 – empty	
T47D ATF3 OE		pLX304 – ATF3	
MCF7-T shSCR	Derived from MCF7-T	pLKO.1 - Scramble	DMEM + 10% FBS + 1%

			P/S + 100nM tamoxifen (TAM) + Puromycin
MCF7-T shATF3_1		pLKO.1 - TRCN0000013570	
MCF7-T shATF3_2		pLKO.1 - TRCN0000013572	
T47D-T shSCR	Derived from T47D-T	pLKO.1 - Scramble	
T47D -T shATF3_1		pLKO.1 - TRCN0000013570	
T47D -T shATF3_2		pLKO.1 - TRCN0000013572	
MCF7-L shSCR	Derived from MCF7-L	pLKO.1 - Scramble	DMEM - phenol red + 10% charcoal stripped FBS + 1% P/S + 1% Glutamine + 1% Sodium Pyruvate + Puromycin
MCF7-L shATF3_1		pLKO.1 - TRCN0000013570	
MCF7-L shATF3_2		pLKO.1 - TRCN0000013572	
T47D-L shSCR	Derived from T47D-L	pLKO.1 - Scramble	
T47D -L shATF3_1		pLKO.1 - TRCN0000013570	
T47D -L shATF3_2		pLKO.1 - TRCN0000013572	
MCF7 barcoded	Derived from MCF7	ClonTracer barcoding Library	DMEM + 10% FBS + 1% P/S + 10^{-8}M 17-ß-estradiol + Puromycin
T47D barcoded	Derived from T47D		

Briefly, cells were washed with PBS and incubated with 0.25% trypsin-EDTA at 37^{o}C. Once the cells detached, full growth medium was added to neutralize the trypsin. The cells were counted using a Neubauer cell counting chamber and seeded in the appropriate cell number for further

expansion or experiments (Table 3). Parental cells were used for experiments up to passage number 25.

Table 3: Cells plating conditions

Cell line	Culture conditions	Experimental conditions
All cell lines	25 cm^2 flasks: $5x10^5$ cells 75 cm^2 flasks / 10cm dishes: $1x10^6$ cells 150 cm^2 flasks / 15cm dishes: $2x10^6$ cells	6 wells: $1x10^5$ cells 12 wells: $5x10^4$ cells 24 wells: $2,5x10^4$ cells 96 wells: $5x10^2$ cells

Frozen cell stocks were generated by centrifuging cells at 1200 rpm and re-suspending cell pellets in full growth medium supplemented with 10% FBS and 10% DMSO. Cells were aliquoted in 1.5ml cryo-vials and cooled down in isopropanol bath at -80°C for short term storage and then transferred to liquid nitrogen containers for long term storage.

Frozen vials of cells were recovered by thawing in a 37°C water bath and the cell suspension was centrifuged at 1200 rpm to remove the remaining DMSO. Cells were then seeded in a dish or flask and allowed to attach overnight before changing the media.

3.2.1.2 Generation of resistant cell lines

Parental sensitive T47D were cultured for 1 year in the presence of 100nM tamoxifen or in estrogen deprivation to obtain T47D-TAMR and T47D-LTED respectively. The cells were passaged when they reached 80% confluency or reseeded in a new dish if they were not reaching confluency for more than 4 weeks. In this case, the medium was changed every week to ensure availability of nutrient. Two independent resistance acquisitions were performed in parallel therefore generating two replicates of resistant cell lines.

3.2.1.3 Generation stable cell lines

Stable cell lines were generated in the Stable isogenic cell line core facility at the DKFZ. Briefly, HEK293FT cells were co-transfected with the lentiviral constructs (pLX-304 vector with/without ATF3 ORF, pLKO.1 with shSCR/shATF3 or pRSI9-U6 with the ClonTracer library) and 2nd generation viral packaging plasmids VSV.G (Addgene #14888) and psPAX2 (Addgene #12260). 48h after transfection, virus containing supernatant was removed and cleared by centrifugation (5min/500g). MCF7 and T47D cells were transduced with lentiviral particles at 70% confluency in the presence of 10 µg/ml polybrene. For the ClonTracer library (Addgene #67267) transduction, an MOI (Multiplicity Of Infection) of 0.05 was used to ensure the delifery of a single barcode per cell. Considering that the number of cell receiving a viral particle follows a Poisson distribution, with an MOI of 0.05 there will be:

$P(1) = 0.05e^{-0.05}$	0.0475 cells infected with 1 barcode
$P(>1) = 1 - e^{-0.05}(0.05 + 1)$	0.001 cells infected with more than 1 barcode
$P(0) = e^{-0.05}$	0.951 cells not infected

24h after transduction virus containing medium was replaced with selection medium for the respective constructs in S2 lab conditions and cells were provided by the core facility and transferred to S1 lab conditions. Transduced cells were selected with the specific antibiotic (puromycin or blasticidin) and kept constantly in the selection medium.

3.2.1.4 siRNA transfections

Cells were seeded as stated before. Transfections were performed the day after seeding with RNAiMax® according to manufacturer's instructions. siRNAs were used at a final concentration of 30nM. Before the siRNA transfection, the medium was changed to growth media without P/S. Following the volumes indicated in **Errore. L'origine riferimento non è stata trovata.** a pre-

mix of RNAiMax and Opti-MEM was prepared, and siRNAs were diluted in Opti-MEM. The siRNA and RNAiMax pre-mix were mixed, incubated for 5min and then added to the cells. Cells were then incubated in 37^{o} C, 5% CO_2 humidified atmosphere for different time points depending on the assay being performed.

Table 4: Volumes of reagents used for siRNA transfections

Plate Format	P/S-free medium	Lipofectamine RNAiMAX	Opti-MEM	siRNA	Opti-MEM	siRNA mix added
6-well	960	5	115	18	102	240
12-well	480	2,5	57,5	9	51	120
24-well	240	1,25	28,75	4,5	25,5	60
96-well	80	0,416	9,583	1,5	8,5	20

3.2.1.5 Crispr/Cas9 transfections

ATF3 knockout clones were generated with CRISPR/Cas9 technology using two sgRNAs targeting exon 4 of the ATF3 gene. Cells were seeded at 60% confluency and were transfected the following day according to manufacturer's instructions with Lipofectamin CRISPRMAX Cas9 transfection reagent. After 3 days the cells were detached and seeded in a 96-well plate at a dilution of 0.8 cells/well to obtain single clones. The media was changed every week to ensure availability of nutrient and the single-cell derived clones were moved to bigger wells when confluent. When the clones had reached a 6 well plate format they were screened for the presence of the editing both at the DNA level with Sanger sequencing and at the protein level with Western Blot.

3.2.2 Analysis of RNA expression

3.2.2.1 RNA isolation and reverse transcription

mRNA was isolated and purified using the "RNeasy Mini" Kit from Qiagen according to manufacturer's instructions and the RNA was eluted in 80µl of nuclease free water. RNA concentration was measured with NanoDrop-ND 1000. 500ng of RNA was used to synthesize the cDNA using the RevertAid H Minus First Strand Reverse Transcription Kit. RNA was mixed with 1 µl of Oligo(dT) primer to a volume of 12 ul. After 5 minutes incubation at 70°C, 4 µl of 5x Reaction Buffer, 1 µl of RiboLock Ribonuclease Inhibitor, 2 µl of dNTP mix (10 mM) and 1 µl of RevertAid H Minus-MuIV Reverse Transcriptase, were added to the RNA. The cDNA was synthesised using following PCR programme:

5 min - 37°C

60 min - 42°C

10 min - 70°C

3.2.2.2 Quantitative RT PCR

The cDNA was diluted to 2 ng/ µl with nuclease free water and 5 µl were used for the Taqman RT-PCR assay. For each sample the master mix for one gene included 5,5 µl of primaQUANT real-time PCR Master Mix, 0.11µl of forward primer, 0.11µl reverse primer, 0.11µl Taqman probe and 0,17 µl water. 6µl of the mix was pipetted with 5 µl of cDNA into 384 well plates in triplicates. The plate layout was prepared on the SDS or QuantStudio software and the following qPCR program was used:

2 min - 50°C

15 min - 95°C

15 sec - 95°C 60 sec - 60°C	45 cycles

The data were analysed using the SDS or QuantStudio software with the ΔΔCt method. The Ct values were normalized to housekeeping gene *ACTB*.

3.2.2.3 RNA sequencing

RNA sequencing (RNA-seq) was performed using HiSeq 4000 Paired-End 100 base pair in the Genomics and Proteomics Core Facility at the DKFZ. Data analysis was performed by Maryam Soleimani and Dr. Perry Moerland from the University of Amsterdam (UvA). Briefly, raw sequencing data were subjected to quality control using FastQC and trimmed using Trimmomatic (v0.32). Reads were aligned to the human reference genome (hg38) using HISAT2 (v2.0.4). Gene level counts were obtained using HTSeq (v0.6.1) and the human GTF from Ensembl (release 85). Statistical analyses were performed using the edgeR and limma R/Bioconductor packages. Genes with more than 5 counts in 1 or more samples were retained. Count data were transformed to log2-counts per million (logCPM) with a prior count of 3 and normalized by applying the trimmed mean of M-values method.

Gene-wise linear models were fitted with coefficients for each combination of treatment (+E2, +TAM, -E2) and time point and a coefficient to correct for systematic differences between the two biological replicates. For both LTED and TAM treated samples, contrasts were made between each individual time point t and the WT cell line, that is, $(-E2_t)$ – $untreated_0$ and $(+TAM_t)$ – $untreated_0$, respectively. Differential expression was assessed using empirical Bayes moderated statistics with an intensity-dependent trend fitted to the prior variances. Resulting p-values were corrected for multiple testing using the Benjamini-Hochberg false discovery rate (FDR). Genes that changed in at least one time point compared to E2 were selected based on their moderated F-statistics and corresponding FDR<0.1 (-E2) or FDR<0.25 (+TAM). Additional gene annotation was retrieved from Ensembl (release 91) using the biomaRt R/Bioconductor package.

3.2.3 Analysis of protein expression

3.2.3.1 Protein extraction and quantification

Before harvesting the proteins cells were washed once with cold PBS. The amount of lysis buffer added was based on the plate size (40 µl for 6well plates, 100 µl for 100 mm dishes) and

the cells were detached using a cell scraper. Cells were incubated on ice with the lysis buffer for 30 min, vortexing them every 10 min and proteins were separated by centrifuging the samples at 13000 rpm for 10 min. Lysates were stored at -80^{o}C or used directly.

Protein concentrations were determined using the BCA Protein Assay Kit according to manufacturer's instructions. Briefly, BSA standards of different concentrations were prepared by diluting BSA in PBS. 25µl of each standard and 5µl of each sample was pipetted into a 96-well microplate in duplicates. The BCA reagent was prepared freshly by mixing Reagent A and Reagent be in a 50:1 ratio. 200µl of the mix was then added to each well of the microplate. The plate was protected from light and incubated at 37^{o}C for 40 min. After the incubation the absorbance at 562nm was measured with the Glomax explorer plate reader.

Based on the BSA standard, a standard curve was prepared and protein concentrations of the samples were calculated from this curve.

3.2.3.2 Western Blot

Samples were prepared for gel electrophoresis by mixing the lysates with 4x RotiLoad in a 1:4 dilution and water to obtain 30 µg as a final protein amount. The samples were then heated at 95^{o}C for 5min to denature the proteins. In the meantime the Mini-PROTEAN TGX Precast Gels were loaded into the MiniProtean gel apparatus filled with 1x running buffer. After the removal of the comb, the gel were loaded with 3 µl molecular weight marker and 15, 20 or 50 µl of sample based on the gel size (15, 12 or 10 wells respectively). Electrophoresis was performed at 145V for 60min.

After protein separation via SDS-PAGE, the proteins were transferred to a PVDF membrane using the Trans-BlotR Turbo Transfer System accordance to manufacturer's instruction. The membrane was then blocked for 2h at RT with Rockland blocking buffer and subsequently incubated with a target specific primary antibody diluted in blocking buffer ON at 4°C on a rocking platform. The membrane was washed 3x 10 min in TBST followed by a 1h incubation with Alexa Flour 680 conjugated secondary antibody. After washing again for 3x 10 min in TBST,

the membrane was scanned at an excitation wavelength of 685 nm and a resolution of 84 µm using the Odyssey Infrared Imaging System.

3.2.3.3 Reverse Phase Protein Array

The lysates were adjusted to a total protein concentration of 2 µg/µl. Samples were mixed with 6x SDS Buffer and denatured at 95°C for 5min. The lysates were then pipetted into 348-well plates and centrifuged for 2min at 1200 rpm. As internal controls a dilution series of cell line pools were created using 4 different samples starting from a concentration of 2.5 µg/µl. All samples were printed as technical triplicates on Oncyte Avid Nitrocellulose Film-Slides using an Aushon 2470 contact printer equipped with 185 µm solid pins. These pins allow to spot 1.6nl of sample per spot, with an average spot diameter of 250µm. The humidity during the printing run was kept constant at 80%. Slides were stored after the print run at -20°C. After spotting the slides were blocked for 2h at RT with filtered Rockland blocking buffer.

After blocking, the slides were incubated with target-specific primary antibodies at 4°C ON. Representative subarrays were incubated without primary antibody and served as "blank" control. After incubation the slides were washed 3 x 10 min with TBST and subsequently incubated with Alexa Fluor® 680 F(ab')2 fragments of goat anti-mouse IgG or anti-rabbit IgG in 1:12000 dilution for 1h at RT in the dark. Slides were again washed 3 x 10 min with TBST followed by two final washing steps with ultra-pure water for 5min. The slides were then air dried. The last slide of each spotting plate was stained using Fast Green FCF protein dye for total protein quantification to be used for normalization. All the slides were scanned with an excitation wavelength of 685nm and a resolution of 21 µm with the Odyssey® Infrared Imaging System and the resulting TIFF images (16 bit) were used for further analysis.

Signal intensities of individual spots were quantified using GenePixPro 7.0 software. The acquired TIFF image of each slide and gene pix array list file obtained from the Aushon spotter's software was matched into a gpr file. A visual inspection of each spot was performed manually and slides without uniform background signal were excluded from further analysis. RPPA raw

data preprocessing and quality control were performed using the *RPPanalyzer* R-package (Mannsperger et al. 2010). The raw signal intensities of the control samples were plotted against the respective total protein concentration. Only antibodies showing a linear correlation between target signal intensity and protein concentration were used for further analysis. Next, target signals were normalized to the total protein amount per spot via FCF control. After median calculation of technical replicates, normalized target signal intensities were plotted against the signal intensities obtained by incubation of secondary antibody controls (blank signal) and only antibodies with a clear signal above blank levels were kept for the further analysis.

3.2.3.4 ELISA

Enzyme linked immunosorbent assay (ELISA) was used to detect and quantify TGFB2 in the supernatant of the cells after perturbations. To this end, Human TGF-beta 2 DuoSet ELISA kit was used according to the manufacturer's instructions. Briefly, a 96-well plate was coated with the capture antibody diluted in PBS to its working concentration and incubated ON. The plate was then washed with the wash solution and 200 µl of blocking buffer were added to each well and the plate was incubated for 2 hours. TGFB2, secreted by the cells in an inactive form, was activated by pH change, adding 25 µl of 1N HCl to 125 µl of sample, incubating for 10 minutes and increasing the pH again with 1,2 N NaOH/0,5 M HEPES. Subsequently, the plate was washed again and 100 µl of the serial standard dilution and all samples were added in duplicate and incubated at RT for 2 hours. For the detection, the wells were washed and incubated with a biotinylated detection antibody for 2 hours at RT followed by Streptavidin-HRP incubation for 20 min at RT. The plate was washed again and Substrate Solution, consisting of 1:1 mixture of Colour Reagent A (H2O2) and Colour Reagent B (Tetramethylbenzidine), was added to each well, followed by another 20 min incubation at RT. Addition of 50 µl of Stop Solution (2 N H2SO4) stopped the catalytic reaction and the light absorbance at 450 nm was measured with the Glomax Explorer Plate Reader. An additional measurement at 560 nm was performed to correct optical imperfections. For the analysis the results of measurement at 560 nm were

subtracted from those at 450 nm. The obtained values were used for the calculation of TGFB2 amount in the media from the standard curve formula. The standard curve was always set in a way that $R2 > 0.97$. All results were normalized to the RNA amount quantified via NanoDrop ND-1000 Spectrophotometer and then to the respective control.

3.2.4 Analysis of epigenetic profile

3.2.4.1 Chromatin Immunoprecipitation

Cells were harvested by trypsinization and cross-linked with 1% formaldehyde diluted in growth media for 10 min at RT. To stop the reaction 520 µl of 2.5M Glycine was added to a final concentration of 0.15 M. The cells were incubated for 5 min at RT and pelleted by centrifugation at 1200 rpm for 5 min at 4°C. Cells were then washed twice with cold PBS followed by centrifugation and the pellets were stored at -80°C until further processing.

10 µl magnetic beads were pre-washed 3x with 1ml washing buffer and re-suspended in 350 µl of washing buffer with 2µg of antibody for each ChIP. The mix was then incubated for 6 hours rotating at 4°C. In the meantime the cells were lysed with three lysis buffers. Each time the pellet was re-suspended, incubated 10min at 4°C and centrifuged at 2000 rmp 5 min. At the last step the cells were re-suspended in 300 µl of lysis buffer 3 and sonicated in the Bioruptor for 10min with 30 second on/off cycles. After sonication 30 µl 10% Triton X-100 were added and the cells were spun down 10 min at 4°C at 13000 rpm. For ChIP-seq application 15 µl were kept for input, 5 µl to run on a SDS-PAGE gel to check for fragmentation efficiency and the rest was added to 800 µl lysis buffer 3, 90 µl 10% Triton X-100 and incubated with the beads. For ChIP-PCR application DNA was quantified with the nanodrop and 25 ug of DNA was used for each condition. 5 µl of DNA was run on a SDS-PAGE gel to check for fragmentation efficiency. Before incubation the beads were washed to remove unbound antibody and re-suspended in 100 µl lysis buffer 3 for each ChIP. Both the chromatin sample were incubated ON rotating at 4°C. Samples for the gel run were de-crosslinked ON at 65°C with 100 µl of elution buffer. DNA was extracted with Phenol-Chloroform and precipitated with NaCl. DNA was then re-suspended in

water and loaded in a 1% agarose gel at 70V for 40 minutes. Successful chromatin fragmentation was examined under UV light (Figure 5 a)

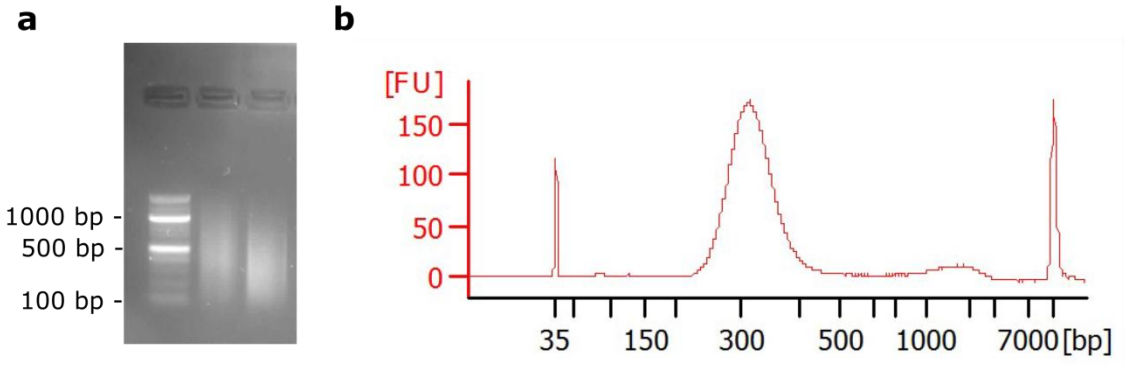

Figure 5: Validation of ChIP sonication and size selection
(**a**) Agarose gel validation of sonication efficacy. 1st lane: 100bp ladder, 2nd lane: sonicated DNA from MCF7, 3rd lane: sonicated DNA from T47D. (**b**) Example of the size selection validation with Agilent Bioanalyzer after library preparation

After ON incubation, chromatin samples were washed with 3x 300 µl RIPA and 2x 300 µl TE buffer before proceeding to de-crosslink as mentioned above. After ON incubation the beads were captured and the supernatant was incubated for 30 min at 37°C with RNAse followed by 1 hour at 55°C with Proteinase K. To purify the product SPRIselect beads were used according to manufacturer's instructions. For Chip-seq samples were measured with the Qubit dsDNA HS Assay Kit according to manufacturer´s instructions. Before construction of ChIP-seq libraries, enrichment of the immunoprecipitated sample was ascertained using positive and negative controls with ChIP-qPCR. To prepare the libraries for sequencing the NEBNext Ultra DNA Library Prep Kit was used according to manufacturer's instructions. The size distribution was evaluated on the Agilent Bioanalyzer with the High sensitivity DNA kit (Figure 5 b). Samples were then multiplexed and run on the Next Seq500 75 SR in the BRC Genomic Facility of Imperial College London. Bioinformatics pre-processing and peak calling was performed by Giacomo Corleone from ICL as previously described (Patten et al. 2018). For ChIP-qPCR purified samples were diluted 1:4 in water and a quantitative RT PCR was performed as described in the previous chapter.

3.2.5 Analysis of barcode composition

3.2.5.1 PCR amplification and sequencing

DNA was extracted using the DNeasy Blood & Tissue kit according to manufacturer's instructions. PCR was used to amplify the barcode sequence and introduce Illumina adaptors and index sequences for multiplexing (Bhang et al. 2015). The primers used are reported in Table **5**. Two parallel reactions with 2,5 µg of genomic DNA were used as a template to ensure sufficient template coverage. For each sample the master mix included 5 µl of 10X Titanium Taq PCR buffer, 1 µl of forward primer, 1 µl reverse primer, 1 µl 50X dNTP (10nM), 1 µl 50X Titanium Taq DNA polymeraseand, 2 µl DMSO and water to a volume of 50 µl. The following PCR amplification program was used:

5 min - 95°C

30 sec - 95°C 15 sec - 69°C 9 sec - 72°C	30 cycles

7 min - 72°C

The PCR products were cleaned with the Wizard SV Gel and PCR Clean-up System and the final concentration and size was evaluated with the Bioanalyzer. 10 samples were multiplexed for each lane and sequenced using HiSeq 2000 V4 Single-read 50 base pair in the Genomics and Proteomics Core Facility at the DKFZ using the custom sequencing primer TCTACACACTGACTGC-AGTCTGAGTCTGACAG

Table 5: Barcoding PCR and sequencing primers

PCR Forward Primer	AATGATACGGCGACCACCGAGATCTACACACTGACTGCAGTCTGAGTCTGACAG
PCR Reverse Primer 1	CAAGCAGAAGACGGCATACGAGATACGATCGTGAGTGACTGGAGTTCAGACGTGTGCTCTT CCGATCTCTAGCACTAGCATAGAGTGCGTAGCT
PCR Reverse Primer 2	CAAGCAGAAGACGGCATACGAGATCTAGATCGTGGTGACTGGAGTTCAGACGTGTGCTCTT CCGATCTCTAGCACTAGCATAGAGTGCGTAGCT

PCR Reverse Primer 3	CAAGCAGAAGACGGCATACGAGATGACTCGATCAGTGACTGGAGTTCAGACGTGTGCTCTT CCGATCTCTAGCACTAGCATAGAGTGCGTAGCT
PCR Reverse Primer 4	CAAGCAGAAGACGGCATACGAGATTGACTAGCTCGTGACTGGAGTTCAGACGTGTGCTCTT CCGATCTCTAGCACTAGCATAGAGTGCGTAGCT
PCR Reverse Primer 5	CAAGCAGAAGACGGCATACGAGATATGCTCAGCAGTGACTGGAGTTCAGACGTGTGCTCTT CCGATCTCTAGCACTAGCATAGAGTGCGTAGCT
PCR Reverse Primer 6	CAAGCAGAAGACGGCATACGAGATCGATCTGCATGTGACTGGAGTTCAGACGTGTGCTCTT CCGATCTCTAGCACTAGCATAGAGTGCGTAGCT
PCR Reverse Primer 7	CAAGCAGAAGACGGCATACGAGATGATAGCTGACGTGACTGGAGTTCAGACGTGTGCTCTT CCGATCTCTAGCACTAGCATAGAGTGCGTAGCT
PCR Reverse Primer 8	CAAGCAGAAGACGGCATACGAGATAGTACGCATGGTGACTGGAGTTCAGACGTGTGCTCTT CCGATCTCTAGCACTAGCATAGAGTGCGTAGCT
PCR Reverse Primer 9	CAAGCAGAAGACGGCATACGAGATGTATCACGACGTGACTGGAGTTCAGACGTGTGCTCTT CCGATCTCTAGCACTAGCATAGAGTGCGTAGCT
PCR Reverse Primer 10	CAAGCAGAAGACGGCATACGAGATTCGCAGTACTGTGACTGGAGTTCAGACGTGTGCTCTT CCGATCTCTAGCACTAGCATAGAGTGCGTAGCT

3.2.5.2 Barcode-composition analysis

The bioinformatics analysis was performed by Dr. Luca Penso Dolfin (DKFZ). FASTQ files were reformatted using *fastq_quality_converter* from the package *fastx_toolkit*, using the following parameters: -n -Q 33. The resulting files were filtered for a minimum average read quality of 30 and a minimum quality of 10 at any position. Reads were subsequently checked for concordance with the expected barcode pattern ([AT][GC])x15, and counts of each barcode sequence were calculated in each sample separately. Tab delimited files containing barcode count information were used as input for the clustering algorithm *starcode* (Zorita, Cuscó, and Filion 2015) which was used to group together highly similar barcode sequences based on specific distance criteria. Specifically, *starcode* was run using parameters -s -d 1 -r 40 -i input_file -o output_file --print-clusters --seq-id. This lead to the generation of sequence groups (clusters) consisting of a consensus with frequency at least 40 times higher than any secondary sequence, and an edit distance equal to 1. These clusters were further modified using in-house python scripts, allowing only secondary sequences with a frequency <10 to be included in a

cluster. The calculation of barcode enrichment was performed using a combination of bash programming and in-house python scripts. Specifically, the average representation (% of frequency) of each barcode across all INITIAL samples was calculated first, considering each cell line separately. The cell line specific threshold to identify barcode enrichment was defined as the highest mean percentage observed in the INITIAL samples (MCF7: 0.001232; T47D: 0.003869). Figures were generated in Rstudio v3.6.0 using the package ggplot2.

3.2.6 Functional assays

3.2.6.1 Analysis of cell proliferation by Hoechst staining

Cell growth under different conditions (siRNA, treatment media) was analyzed with the molecular devices microscope IXM XLS. Cells were seeded in clear-bottomed 96 well black plates and they were transfected with siRNA or treated with treatment media. At different time points DNA was stained with fluorescent intercalating dye Hoechst-33258 (1:5000 dilution in growth media) for 45min. The plates were imaged and all nuclei within a certain size and intensity and were detected and counted by the Molecular Devices Software. For the cells transduced with the ClonTracer library that express RFP, the plates were scanned every day for 7 days. All the cells showing red fluorescence with a pre-determined minimum intensity were detected and counted by the Molecular Devices Software.

3.2.6.2 Cell Titer Glo Assay

Cell titer Glo assay from Promega was used to assess cell viability through detection of ATP in cells as a measurement of their metabolic activity. The assay was performed according to manufacturer's instructions. Briefly, the kit's reagents were mixed and added to the wells of a 96 well black plate. The incubation with the reagents resulted in the lysis of the cells which released ATP. The plate was placed on a shaker for 1 min to help the lysis. Luciferin, catalyzed in the assay by UtraGlo Luciferase, and the ATP generated oxyluciferin, which was detected via

luminescence measurement using the Glomax Explorer Plate Reader 10 minutes after incubation with the reagents.

3.2.6.3 Transwell assays

24 well plate format BioCoat Matrigel Invasion Chambers were thawed and 500 µl DMEM without FBS was added to pre-hydrate the matrix for 2 hours in the incubator at 37°C. After the rehydration the media was removed and $2x10^5$ cells were seeded on the upper chamber in 200 µl of media without FBS. As chemoattractant 500 µl DMEM supplemented with 20% FBS was used in the lower chamber. Invasion assays were stopped after 72 hours incubation at 37°C. Cells were swiped off the top off the upper chambers with a cotton swab and the lower chambers were by fixed with 4% PFA for 10 min. Transwell inserts were then moved to a new 24 wells plate and stained with crystal violet for 40 min. After staining the inserts were washed in water to remove the staining in excess and let dry on the bench ON. For quantification the transwells were either eluted with 10% acetic acid and quantified with the Glomax Explorer Plate Reader measuring the absorbance at 590nm or imaged with the Zeiss LSM 800 microscope. Images were exported and analyzed on Image J software using a macro built by Dr. Damir Krunic (Light Microscopy Core Facility, DKFZ).

3.2.6.4 Analysis of apoptosis by AnnexinV/PI staining

Apoptosis rate of cells in different conditions (siRNA, treatment media) was assessed with the Annexin/PI kit and analyzed with Flow Cytometry (FACS) according to manufacturer's instructions. $2,5x10^4$ cells were seeded in a 24 well plate and were transfected with siRNA or treated with treatment media. After 4 days the supernatant and the cells were collected in a 96- deep well plate and centrifuged at 1200 rpm for 5 min. The supernatant was discarded and the pellet was washed once with 500 µl PBS. After discarding the washing buffer each sample was re-suspended in 100 µl of Annexin Binding Buffer (10x diluted with water) with 4 µl FITC Annexin V and 4 µl PI and incubated for 15 min at RT in the dark. After incubation the samples

were transferred to round-bottom tubes on ice and analyzed with the Flow Cytometer FACS Calibur. The cells were analyzed by gating on the physical parameters, forward scatter (FSC) and side scatter (SSC) and then selecting the positive cells based on the signal intensities in the FL1 channel for Annexin V and FL2 channel for PI. Analysis was performed with FlowJo v10.

3.2.6.5 Analysis of cell cycle by BrdU/7-AAD staining

Cell cycle distribution of cells in different conditions (siRNA, treatment media) was assessed with Bromodeoxyuridin (BrdU) and 7-Aminoactinomycin D (7-AAD) staining and analyzed with FACS. $5x10^4$ cells were seeded in a 12 well plate and were transfected with siRNA or treated with treatment media. After 4 days the cells were starved by changing the media to DMEM without FBS for 16 hours to synchronize the cell cycle distribution. After starvation the cells were incubated for 2 h with BrdU diluted to 10 µM in full growth media. Following the BrdU pulsing the cells were collected in a 96- deep well plate and centrifuged at 1200 rpm for 5 min. The supernatant was discarded and the pellets were washed and permeabilized with 700 µl Perm/Wash buffer (10x diluted with water). After centrifugation the supernatant was discarded and 250 µl Cytofix/Cytoperm buffer was added and incubated for 20 min at RT to fix the cells. The cells were washed as before and DNase was added and incubated for 1 hour at 37°C to expose the BrdU. After a new wash each sample was incubated with 10 µl FITC-anti BrdU antibody diluted in 50 µl PBS for 20 min at RT in the dark. Following the incubation, a new wash was performed and each sample was incubated with 4 µl 7-AAD diluted in 150 µl PBS. Cells were incubated 1hour in the dark, transferred to round-bottom tubes on ice and analyzed with the Flow Cytometer FACS Calibur. The cells were analyzed by gating on the physical parameters, forward scatter (FSC) and side scatter (SSC) and then gating the populations based on the signal intensities in the FL1 channel for BrdU and FL3 channel for 7-AAD. Analysis was performed with FlowJo v10.

3.2.7 In vivo experiments

The mouse experiments were performed in the DKFZ animal facility by the group of Dr. Müller-Decker under the animal experiment project number G272-16 using 4 weeks-old female NSG mice. All mice were injected with a 21-day release estrogen pellet (0.25 mg/pellet) in the neck under isoflurane anesthesia. After 7 days the mice were randomized and injected in the mammary fat pad (MFP) with 2.5 million cells (see Table 6 for the groups) in a 1:1 dilution with matrigel. 14 days after MFP injection the treatment pellets were injected in the neck under isoflurane anesthesia as reported in Table 6. Pellets were replaced every 60 days until mice were sacrificed. Mice were sacrificed when the tumor reached 1 cm of diameter in one of the dimensions, if they presented health problems or more than 20% weight loss or if they reached the planned end point of the experiment (120 days of treatment, 2 pellets). Due to health issues, one mouse from the Group 1 and one mouse from Group 2 were sacrificed and their results were excluded from further analysis. Additionally, in one mouse from Group 7 the tumor did not engraft and this mouse has been excluded from further analysis as well.

Table 6: Conditions used for the *in vivo* experiment

Group	Number of mice	Cell line	Treatment pellet	Pellet dosage (60 days release)
1	6	MCF7- WT	Estrogen	0,72 mg/pellet
2	6	MCF7 ATF3 KO1	Estrogen	0,72 mg/pellet
3	6	MCF7 ATF3 KO2	Estrogen	0,72 mg/pellet
4	6	MCF7- WT	tamoxifen	5 mg/pellet
5	6	MCF7 ATF3 KO1	tamoxifen	5 mg/pellet
6	6	MCF7 ATF3 KO2	tamoxifen	5 mg/pellet
7	6	MCF7- WT	letrozole	1,66 mg/pellet

8	6	MCF7 ATF3 KO1	letrozole	1,66 mg/pellet
9	6	MCF7 ATF3 KO2	letrozole	1,66 mg/pellet

3.2.8 Statistical Analysis and graphical illustration

Unless otherwise mentioned, data are presented as mean of biological replicates ± SEM and statistical analyses were performed by unpaired two-tailed Student's t-test using GraphPad Prism Software. p-values <0.05 were considered statistically significant and p-values <0.05, <0.01 and <0.001 are indicated with one, two and three asterisks, respectively. All graphs were generated using the GraphPad Prism Software, R or EaSeq and illustrated via Inkscape v 0.91

4. Results

4.1. Part I: Time-resolved profiling of resistance development for identification of novel drivers

4.1.1 Generation of resistant T47D cells

To investigate *in vitro* the endocrine therapy resistance process I choose T47D, a luminal A cell line widely used as model of ER+ breast cancer. The generation of the resistant cell lines was done by cultivating two independent replicates of T47D for 1 year either with 100 nM tamoxifen (TAM) or in estrogen (E2) deprived media (Figure 5a). The resistance development process was performed in collaboration with another PhD student in the lab, Emre Sofyali. To assess the resistance development, cells were tested for their proliferative and invasive capabilities at different stages of the process. Cells treated with TAM showed increased viability as early as 5 months from the start of the treatment compared to sensitive cells (Figure 5b). This increased viability was not limited to the dose used to chronically treat the cells (100nM), but even to concentration 10 times higher.

When comparing the proliferation rate of the cells under treatment, TAM treated cells were able to sustain a slow growth starting from month 5, even if slower that the parental cells (Figure 5c, left panel). Their proliferation speed continued to increase during the time of resistance development eventually matching with the one of the sensitive cells (Figure 5c, middle and right panel). In comparison, the cells deprived from estrogen remained in a non-proliferative state for most of the resistance development, increasing their proliferative rate only after 1 year of chronic treatment (Figure 5c). Even so, these cells remained slower than their sensitive counterpart.

Finally, as resistance phenotype is often associated with an increase in the invasive potential, the cells were tested in a transwell assay. Surprisingly, even though they were stuck in a non-

proliferative state, the E2 deprived cells showed a significant increase in invasion compared the sensitive T47D (Figure 5d). However, no difference was observed for the TAM treated cells.

This data collectively indicate that resistance to both TAM and E2 deprivation was successfully induced in these cells.

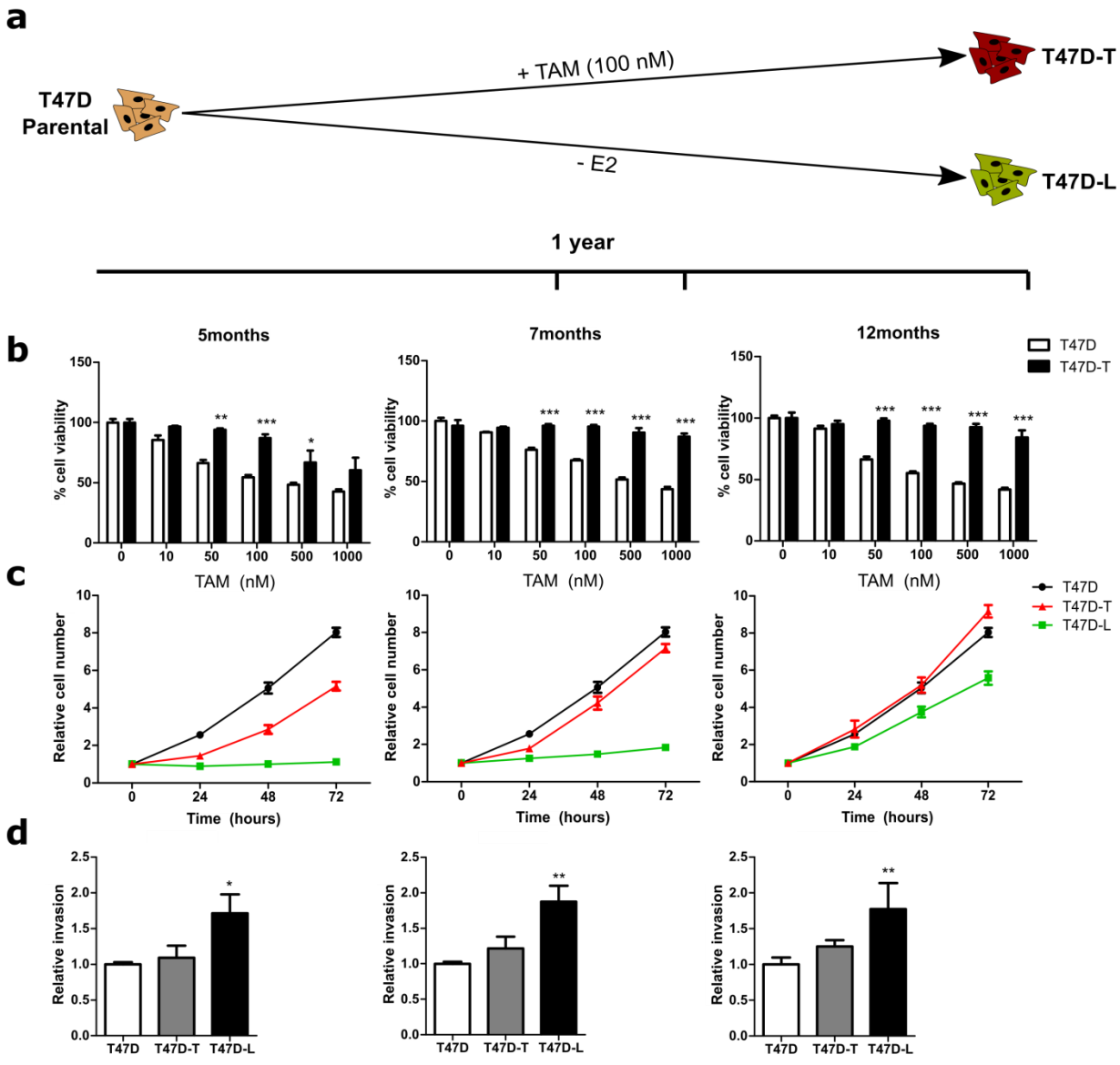

Figure 6: Generation and characterization of resistance development in T47D
(**a**) Schematic representation of resistance development during 1 year of treatment with 100nM TAM (T47D-T) or E2 deprivation (T47D-L). Three time points (5, 7 and 12 months) were chosen to investigate resistance development (**b**) Viability of cells treated for 72h with increasing doses of

TAM. Assay measurement performed with CellTiterGlo at indicated time points. (**c**) Proliferation assay measured as nuclei count at indicated time points. (**d**) 72h transwell invasion assay measured at indicated time points. All values are represented as relative values normalized to the control. For viability and nuclei count assays values are represented as mean + SD of 6 technical replicates, for invasion of 3 technical replicates. *** p-value <0.001, ** p-value <0.01, * p-value <0.05

4.1.2 Characterization of resistant MCF7 cells

To be able to confirm the results obtained with the T47D cell line, we choose another luminal A cell line model, MCF7 and its resistant counterparts to TAM and E2 deprivation, which were kindly provided by Dr. Luca Magnani from Imperial College London (Nguyen et al. 2015). This cell line model has been developed as stated for T47D, with 1 year chronic treatment, therefore being a perfect control to generalize results in a second cell line (Figure 6a). However, these cells were available only at the endpoint of resistance induction, namely taken after 1 year of cultivation under selective pressure.

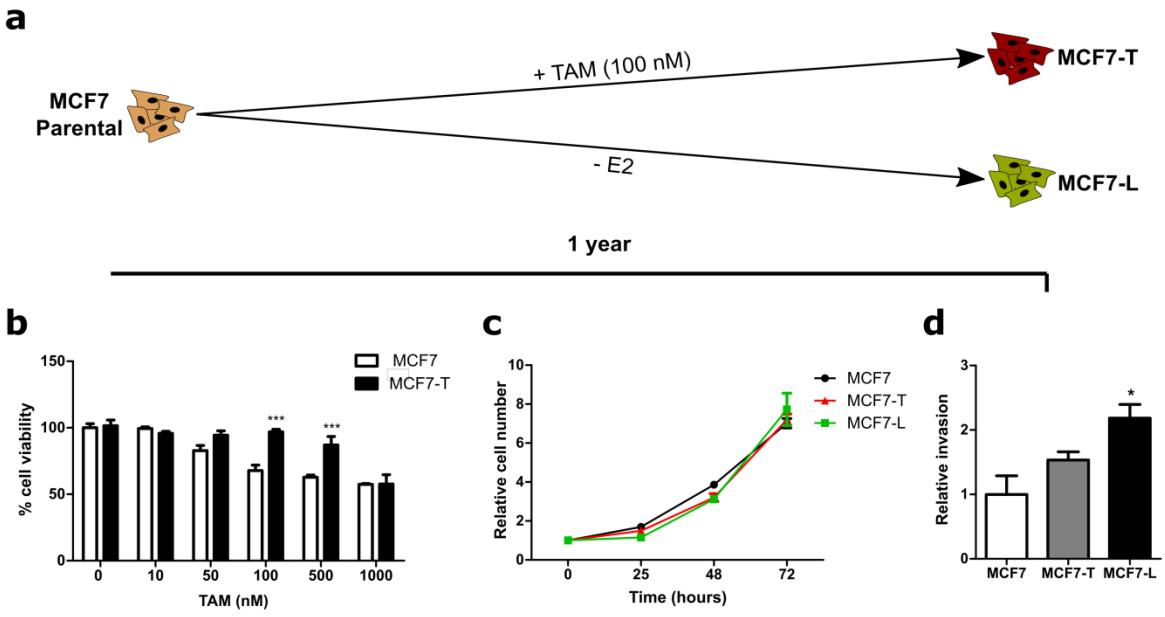

Figure 7: Characterization of resistant MCF7
(**a**) Schematic representation of resistance development performed in ICL for 1 year with 100nM TAM (MCF7-T) or E2 deprivation (MCF7-L). (**b**) Viability of cells treated for 72h with increasing doses of TAM. Assay measurement performed with CellTiterGlo. (**c**) Proliferation assay measured

as nuclei count at indicated time points. (**d**) 72h transwell invasion assay. All values are represented as relative values normalized to the control. Data are represented as mean + SEM. For viability and nuclei count assays n=2 (with 6 technical replicates), for invasion n=3 (with 3 technical replicates). *** p-value <0.001, ** p-value <0.01, * p-value <0.05

To confirm their resistance phenotype the cells were tested for their viability under TAM treatment, proliferation and invasive capabilities. Indeed the MCF7-T showed increase viability under 100 and 500 nM TAM treatment compared to the sensitive MCF7 (Figure 6b). At the same time, all the cell lines had similar proliferative capabilities in their respective media (Figure 6c). Finally, cells were tested for their invasive potential in a transwell assay. In line with the results obtained with the T47D cell line system, MCF7-L showed a significantly increased invasion compared to MCF7 and MCF7-T (Figure 6d).

The results obtained in the MCF7 cell line model thus confirm the phenotypes observed with resistant T47D and corroborate previously published data.

4.1.3 Profiling of resistance development in T47D

Several studies have investigated the differences between endocrine resistant and sensitive cells, but the understanding of the drivers of this phenomena remains limited. For this reason a time-resolved analysis of the early phases of resistance development is essential to identify genes responsible for this process. To address this I performed RNA-seq profiling of the cells during the resistance development at months 1, 2, 5 and 7. The RNA-seq results have been processed and analyzed by Maryam Soleimani and Perry Moerland (University of Amsterdam, UvA). Gene selected for downstream analysis were determined based on a set cut-off on the adjusted p-value on the changes in gene expression during time for each treatment independently. This selection resulted in 1477 genes for TAM treated and 1163 genes for E2 deprived cells. To investigate genes' behavior over time we utilized a clustering approach in order to group together genes with similar temporal expression patterns (Figure 8 a-b) (McDowell et al. 2018). The clusters were then investigated for enrichment of specific

pathways. An example is reported for Cluster 1 and 8 of the E2 deprived cells. Cluster 1, containing genes upregulated upon stress was enriched of MAPK signaling pathway, while cluster 8, containing genes downregulated upon stress, presented an enrichment for Cell cycle and DNA replications pathways (Table 7). This is in concordance with the behavior of the cells that are stuck in cell cycle progression, while activating MAPK pathways, responsible for several cellular processes, including survival.

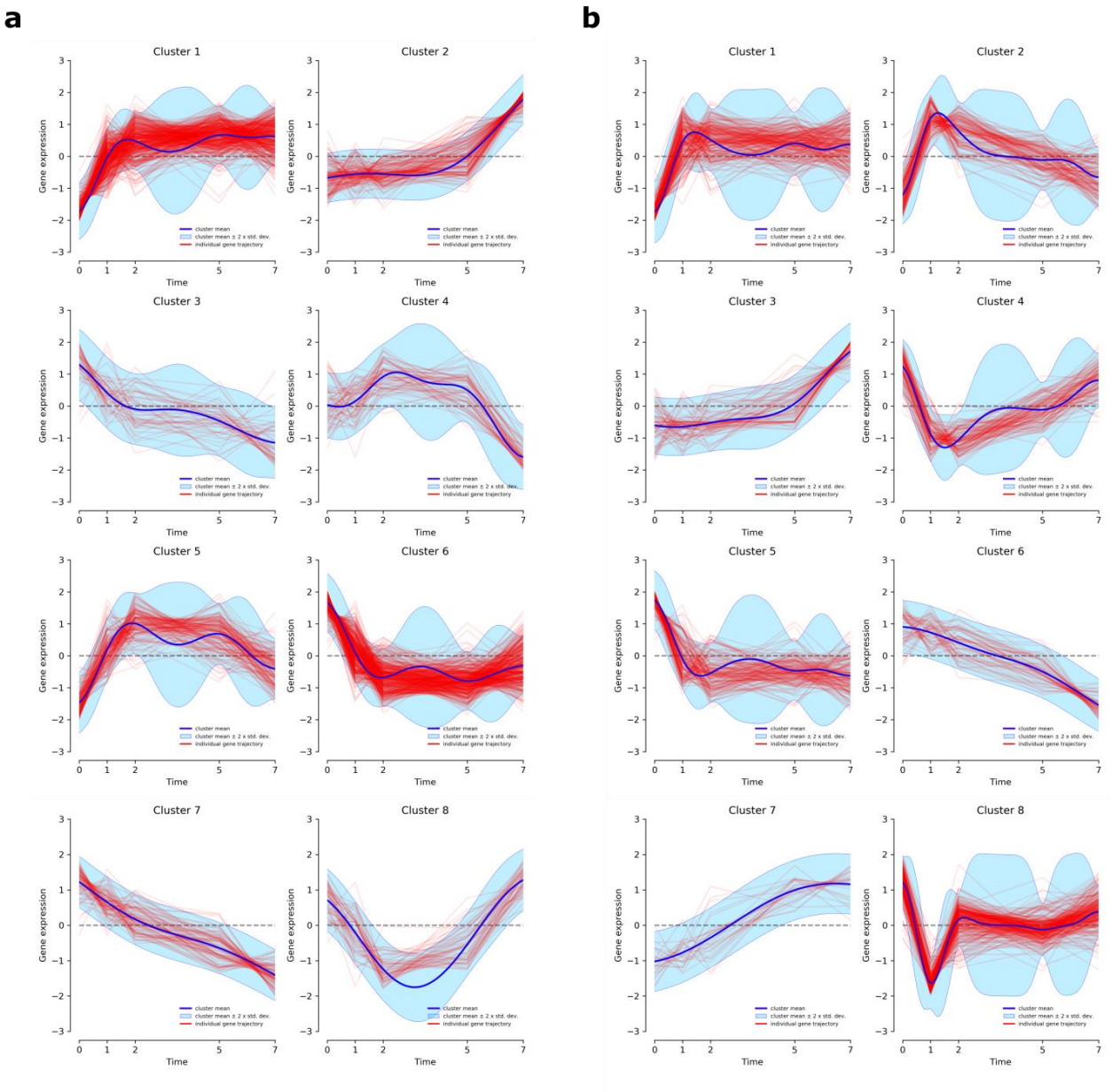

Figure 8: Unsupervised clustering of differentially expressed genes over time

(**a**) Clustering of 1477 differentially expressed genes in T47D under TAM treatment for 1, 2, 5 and 7 months. (**b**) Clustering of 1163 differentially expressed genes in T47D under E2 deprivation for 1, 2, 5 and 7 months. Genes were selected for clustering based on adjusted P-value cut-off for the ANOVA test: TAM: P<0.1, LTED: P<0.25. Plots represent gene expression over time, with each red line being a single gene and the blue line being the mean trend of the cluster.

Table 7: KEGG pathway analysis on selected clusters in E2 deprived T47D

KEGG Pathway	KEGG id	-E2 Cluster 1 p-value	-E2 Cluster 8 p-value
MAPK signaling pathway	hsa04010	0.00182	0.324889
Cell cycle	hsa04110	0.79803	3.19E-28
DNA replication	hsa03030	1	6.83E-13

The unsupervised clustering was not specific enough to serve as the basis for target selection, with most genes showing high fluctuations in comparison to the mean of the respective clusters. To investigate possible mediators of resistance I thus decided to focus on genes differentially expressed at early time points (1 and 2) and further narrowed down on genes that showed an upregulation compared to the non-treated cells (Figure 9 a). The selected gene lists included 786 and 761 genes for TAM treated and E2 deprived cells, respectively. To focus on the commonalities between the two treatments, only the 282 shared upregulated genes were selected for further analysis (Figure 9 b). Pathway analysis using KEGG pathway mapping on this gene list confirmed the results obtained from the cluster analysis, with a significant enrichment for the MAPK signaling pathway (Figure 9 c, red bars).

A gene responsible for resistance development likely will not act independently, but be involved in the regulation of other genes. To identify transcriptional drivers responsible for the regulation of multiple genes in the list, I used the C3 MSigDB transcription factors (TFs) motif collection. Among several predicted TFs binding in the regulatory regions of those genes, only ATF3 was a member of the upregulated gene list itself, therefore being a suitable candidate for further investigations (Figure 9 a, c-blue bars).

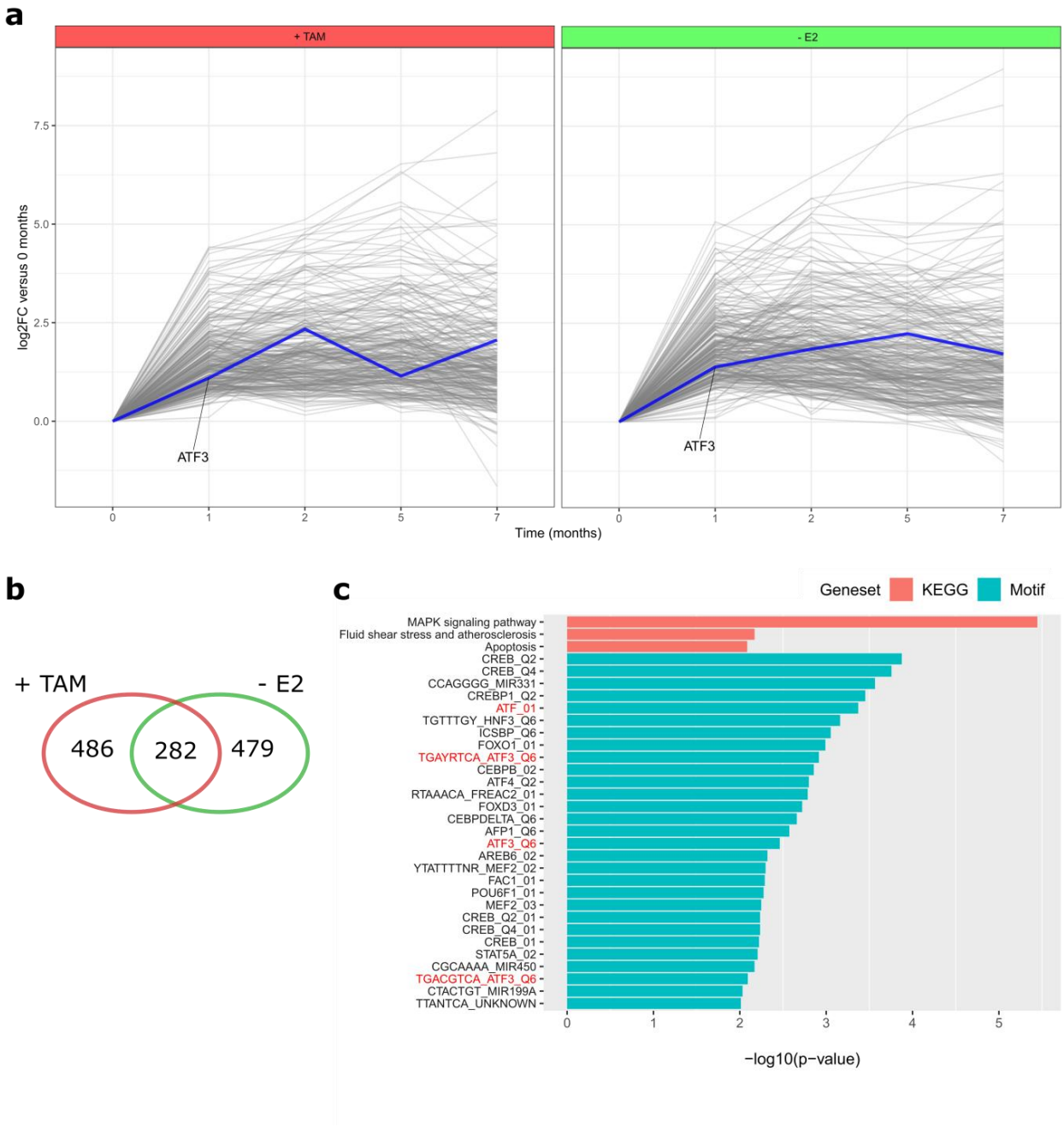

Figure 9: Early upregulated genes in RNA-seq

(**a**) Trend of the differentially expressed genes early upregulated at month 1 and 2 after treatment in T47D treated with TAM or E2 deprivation. ATF3 is highlighted in blue. (**b**) Venn diagram of the absolute number of genes differentially upregulated at month 1 and 2 after treatment. (**c**) Red: pathway enrichment analysis on the 282 common early upregulated genes using KEGG pathways mapping. Blue: predicted transcription factors binding analysis on the 282 common early upregulated genes using Molecular Signature Database C3 collection. The binding sites for ATF/ATF3 are highlighted in red.

Post-translational modifications of histone proteins are tightly associated with changes in gene expression. One of the most known and best studied modification is the acetylation of lysine 27 of histone 3 (H3K27Ac) that has been associated with active promoters and enhancers (Creyghton et al. 2010). To investigate if the changes in gene expression were supported by a higher deposition of this permissive mark, I performed ChIP-seq using cells harvested at the same time points of the RNA-seq profiling. Data preprocessing and peak calling was performed by Giacomo Corleone (ICL). To focus the attention on the genes that were found differentially expressed at different time points, early upregulated genes from Figure 9 and downregulated genes in Cluster 8 of Figure 8 were used. The analysis was done for both treatments, and examples from the E2 deprived cells are shown here. Indeed a substantial increase in the H3k27Ac mark was detected around the transcription start site (TSS) of early upregulated genes 1 month after the start of treatment. This increase was also present at later time points, however, mostly at lower levels (Figure 10 a). This indicates that the increase in gene expression detected at the RNA level is supported by a permissive chromatin structure that promotes TF binding and active transcription. On the other hand, downregulated genes showed a smaller H3K27Ac enrichment after 1 month, and a decrease in all consecutive time points. This supports the fact that these genes have reduced expression levels during resistance development. The difference between H3K27Ac profiles on early up and down genes is evident at all time points except before the treatment, where downregulated genes are having higher levels of the permissive mark (Figure 11 a). This is in agreement with the fact that gene Cluster 8 contains mostly cell cycle related genes, which were probably highly expressed before treatment as cells were cycling. Indeed, after treatment administration, E2 deprived cells undergo a long non-proliferative phase (Figure 6 c) and recover only at late time points. To confirm this at single gene level, a representative gene for each cluster is shown. ATF3 was included in the list of early upregulated genes and predicted to regulate several genes in the list. Indeed the peaks at the two TSS of this gene are showing an enrichment at all time points, with the highest being month 1 (Figure 11 b). On the contrary E2F1, a master regulator of cell cycle included in Cluster 8 shows no changes in the H3K27Ac marks on the promoter region (Figure 11 c).

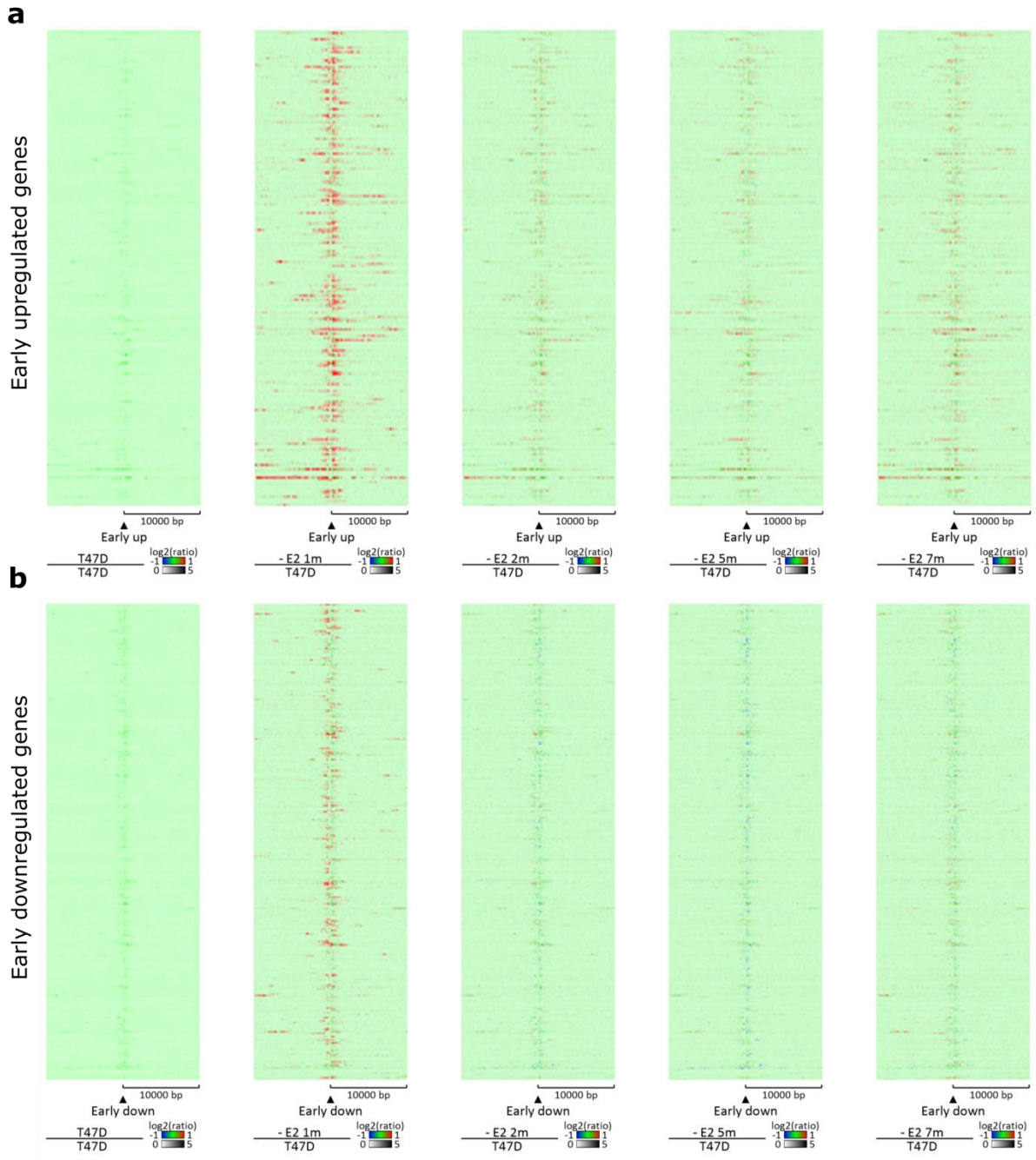

Figure 10: Heatmaps of the H3K27Ac profiles around TSS

(**a**) ChIP-seq H3K27Ac profiles around the TSS of early upregulated genes (Figure 9) under E2 deprivation. (**b**) ChIP-seq H3K27Ac profiles around the TSS of early downregulated genes (Cluster 8) under E2 deprivation. Heatmaps represent ratio between each sample (T47D, -E2 1m, -E2 2m, -E2 5m, -E2 7m) and the untreated sample (T47D). Green, blue and red indicate no change, decrease and increase in the acetylation levels respectively

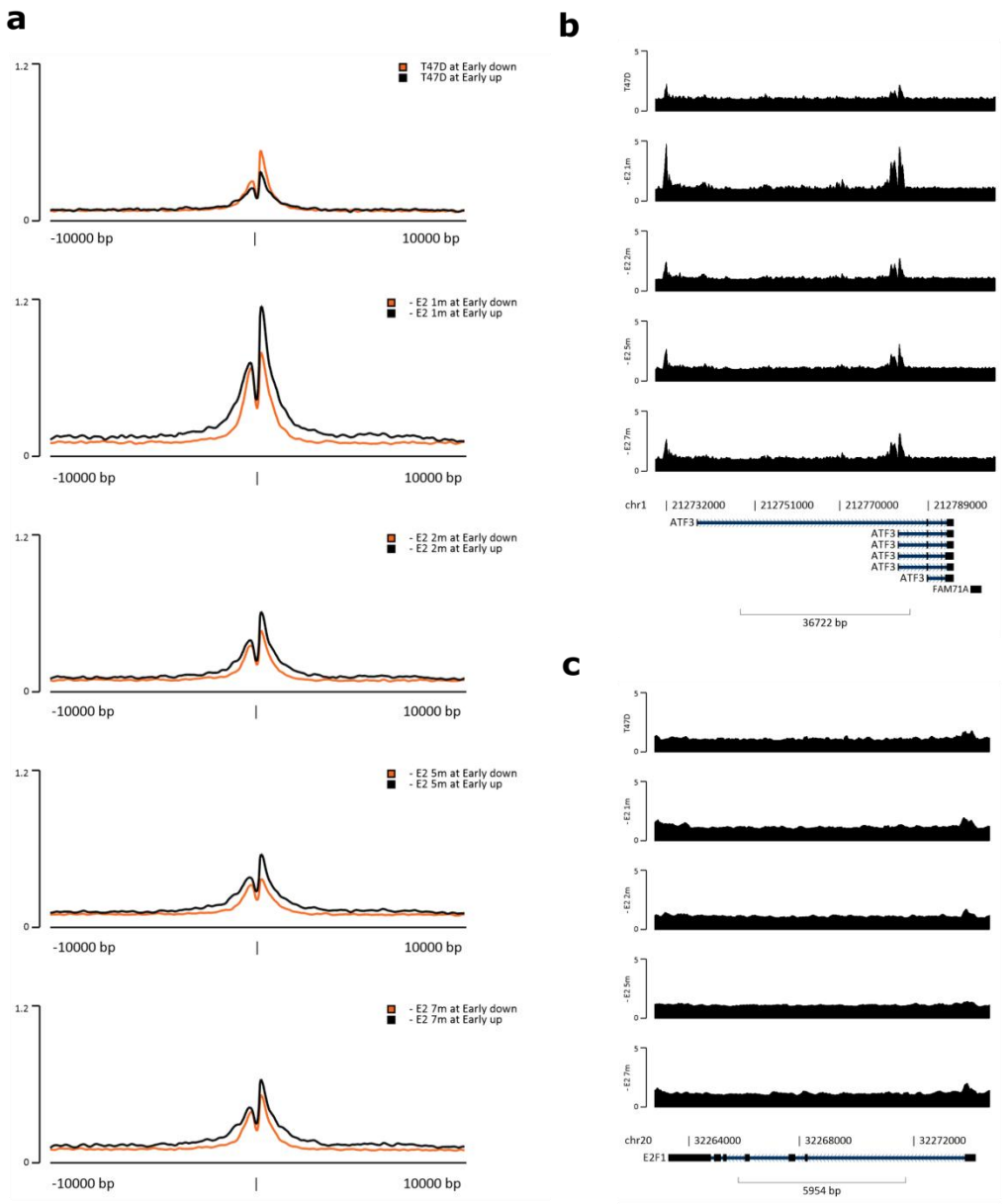

Figure 11: H3K27Ac profiles around TSS of selected genes
(**a**) Average H3K27Ac profiles around TSS of early up and downregulated genes under E2 deprivation for 0, 1, 2, 5 and 7 months (**b**) H3K27Ac peaks at *ATF3* gene locus under E2 deprivation for 0, 1, 2, 5 and 7 months. (**b**) H3K27Ac peaks at *E2F1* gene locus under E2 deprivation for 0, 1, 2, 5 and 7 months.

Overall the Chip-seq data are in agreement with the RNA-seq data and confirm the target selection based on clustering and time-resolved trend of the genes.

To better understand the expression dynamics in the early response to the treatments, MCF7 and T47D cells were treated for 2 weeks and selected genes were assessed with qRT-PCR. In both cell lines, ATF3 was increased after 1 week of treatment, with MCF7 showing also an early increase at 2 hours, probably corresponding to ATF3's role as stress-response gene (Figure 12 a-b). Genes involved in MAPK as RPS6KA5, ERBB2, TGFB2 and JUN, found upregulated in RNA-seq, showed a consistent increasing trend in early times as well in both the cell line models.

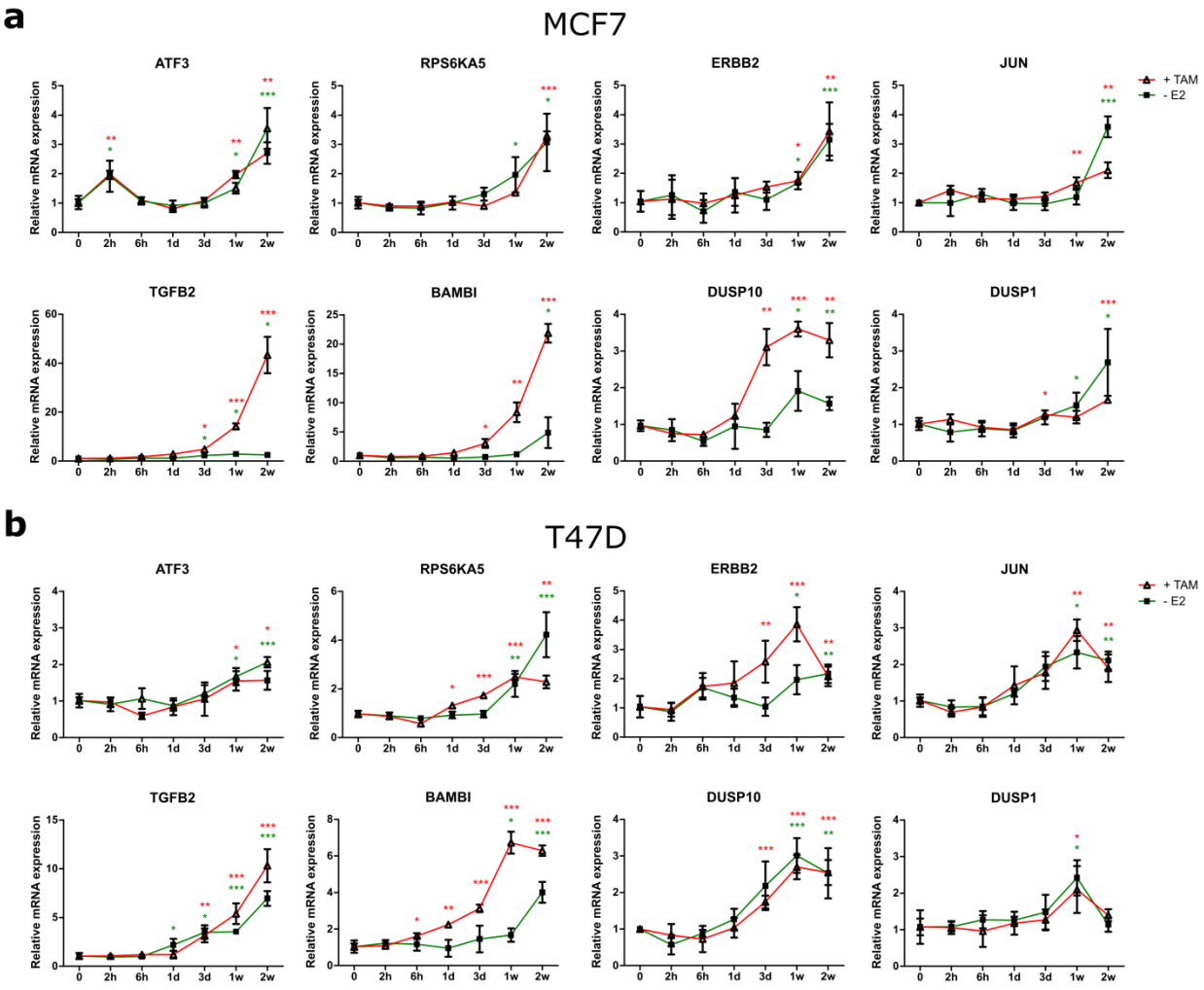

Figure 12: Early upregulated genes under treatment
(**a**) mRNA levels of early upregulated genes determined by qRT-PCR at different time points (2h, 6h, 1d, 3d, 1w, 2w) during TAM treatment and E2 deprivation in MCF7. (**b**) mRNA levels of early upregulated genes determined by qRT-PCR at different time points (2h, 6h, 1d, 3d, 1w, 2w) during TAM treatment and E2 deprivation in T47D. All values are represented as relative values normalized to the untreated control (time 0). Data are shown as mean ± SEM, n=3 (each with 2 technical replicates). *** p-value <0.001, ** p-value <0.01, * p-value <0.05

At the same time, negative regulators of this pathway (BAMBI for TGFB2, DUSP1 and DUSP10 for central kinases of MAPK pathway) showed an parallel increase, suggesting a feedback loop in the cells to try to shut down this processes (Figure 12 a-b). Notably, the increase of BAMBI in MCF7 LTED is limited, as expected from the minimal increase of TGFB2 in this cell line.

These data indicate that the early upregulated genes detected in the RNA-seq screening are already increasing after 3-7 days of treatment in both cell lines.

MAPK pathway is a known de-regulated pathway in endocrine resistance and was previously found to be affected early during therapy administration in the RNA-seq profiling (Peng et al. 2017; Ghayad et al. 2010). To confirm that indeed the MAPK pathway was upregulated in the resistant cells at the proteomic level a targeted proteomic approach was used. Profiling of pathway activation was performed with Reverse Phase Protein Array (RPPA) using antibodies recognizing proteins involved in the MAPK pathway as well as the deepy interconnected PI3K/AKT pathway. To investigate not only the total protein levels, but also the activity of the selected pathways, antibodies recognizing specifically phosphorylated forms of the proteins were used. RPPA profiling revealed indeed an increase in the levels of many proteins involved in these pathways in both MCF7 and T47D resistant cells. In the two cell lines both proteins upstream of these pathway, as ERBB family members and RTK associated proteins like SOS and GAB1, and downstream effectors like MSKs, phospho-c-JUN and p-eIF4B showed a consistent increase across resistant cell lines. Of note also several central phosphorylated kinases, like AKT, MEK, RAF and p38 showed an augmented activity.

These data therefore confirms the deregulation of the MAPK and PI3K-AKT pathways also at the protein level in the resistant model cell lines.

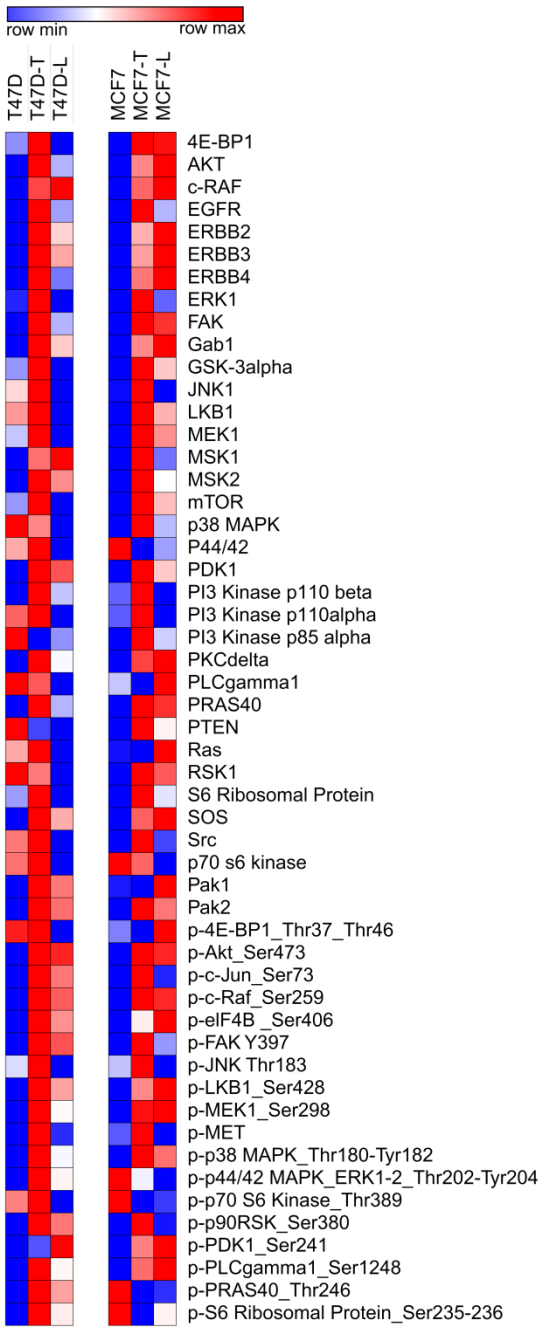

Figure 13: Heatmaps of RPPA-screened proteins in resistant cells
Heatmaps of 35 total proteins and 18 phospho-proteins involved in MAPK and PI3K/AKT signaling pathways in MCF7 and T47D parental and resistant cells. Log2 normalized signal intensities for each protein are plotted and color-coding refers to relative intensities in each row and each cell line independently.

4.1.4 Validation of the role of ATF3 in resistance

RNA-seq results identified ATF3 as an early-upregulated gene. Its annotated function as transcription factor and its role under stress conditions let me hypothesize that the encoded protein could also be important in the regulation of gene expression changes during resistance development (Hai and Hartman 2001; Hai et al. 1999). Indeed, during early phases of resistance development in T47D, ATF3 was found upregulated in both TAM treated and E2 deprived cells (Figure 14 a, Figure 12 a-b). qRT-PCR analysis of resistant T47D cells demonstrated that ATF3 remained high also in resistant cells (Figure 14 c). Additionally, RNA-seq and qRT-PCR data confirmed that ATF3 was upregulated also in resistant MCF7, even if the levels were not as high in MCF7-L cells. (Figure 14 b, d). Finally, to check if the RNA levels were reflected also at the protein levels, all cell lines were investigated with WB. As ATF3 protein levels are low at baseline levels, anisomycin stimulation was used to induce its expression. Anisomycin is an antibiotic that inhibits DNA and protein synthesis, therefore inducing several stress pathways in the cells, including ATF3 expression (Lu, Chen, and Hai 2007; Hazzalin et al. 1998). Indeed, when stimulated with anisomycin, ATF3 became detectable in all the conditions and the resistant cells showed higher ATF3 protein expression compared to the parental cells in both cell lines (Figure 14 e).

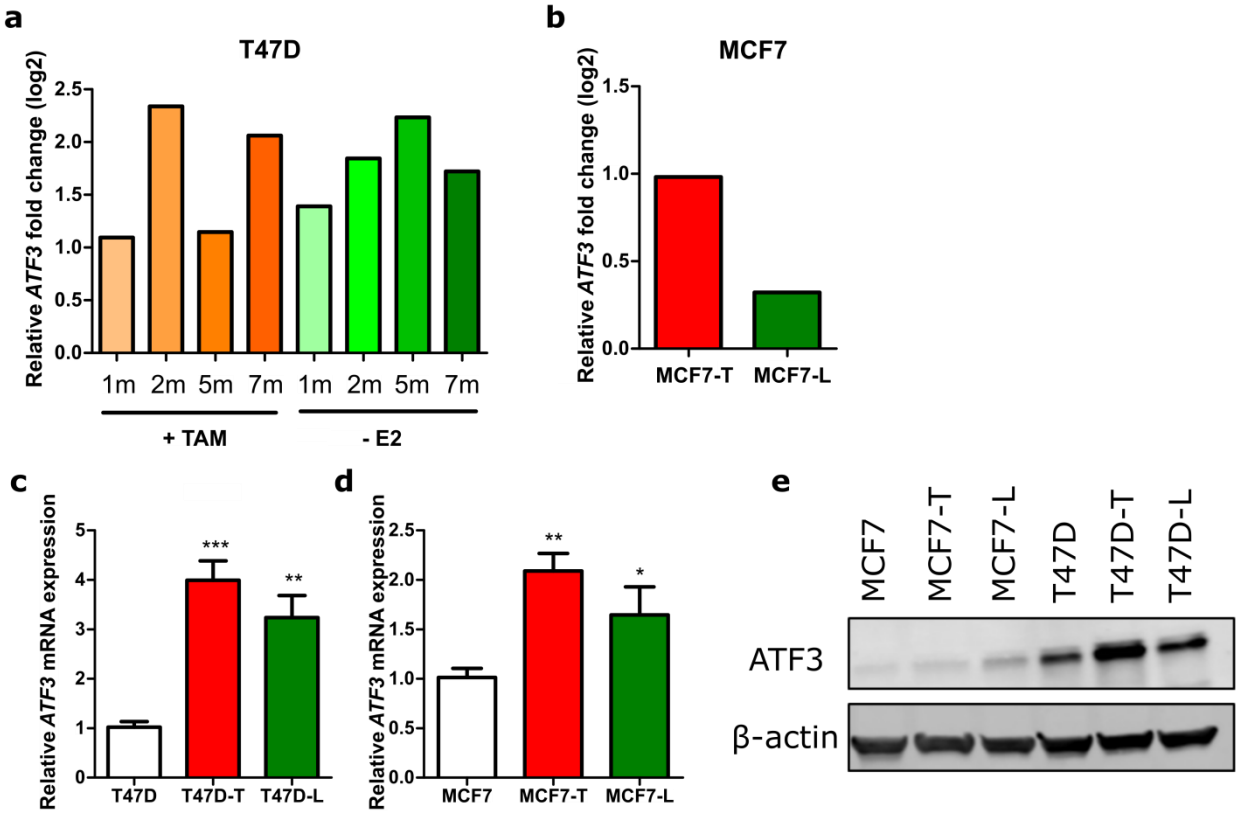

Figure 14: ATF3 expression levels are increased in resistant cell lines
(**a**) Relative ATF3 mRNA levels determined by RNA-Seq in T47D at defined time points (1m, 2m, 5m, 7m) during resistance development against TAM and E2. (b) Relative ATF3 mRNA levels determined by RNA-Seq in resistant MCF7 cell lines (**c-d**) Relative ATF3 mRNA levels determined by qRT-PCR in parental and resistant T47D and MCF7 SE. (**e**) ATF3 protein levels in parental and resistant MCF7 and T47D determined by WB after 2h anisomycin stimulation. β-actin levels are used as loading control. For RNA-Seq values are represented as relative Log2 Fold Change compared to parental cells. For qRT-PCR data are normalized to *ACTB* and then to parental cells and represented as mean + SEM, n=3 (each with 3 technical replicates). *** p-value <0.001, ** p-value <0.01, * p-value <0.05

4.1.5 Knockdown of ATF3 affects cell number and apoptosis

To establish a potential role of ATF3 in the resistance process I next performed an RNAi knockdown both in the parental and resistant cell lines. First, to decide if to use a specific siRNA or a pool, knockdown efficiency was evaluated both in MCF7 and T47D. The four siRNA tested showed a knockdown efficiency higher than 80% in MCF7 and slightly lower in T47D (Figure 15

a-b). To exclude possible off target effects of one of the siRNA, viability was assessed 7 days after transfection. All the siRNA showed a decrease in cell number of around 80% for MCF7 and of similar amplitude in T47D, even though with higher variance (Figure 15 c-d). As no siRNA showed low knockdown efficiency or any outlier effect on viability, I choose to use the siRNA pool to test the effect of the knockdown on the cells. Therefore from now on I will refer to the siRNA pool as siATF3. As resistant cells have higher levels of ATF3 compared to their sensitive counterpart the knockdown efficiency was tested for each cell line individually. Indeed ATF3 was strongly downregulated both at the mRNA and protein level in all the tested cell lines (Figure 15 e-f).

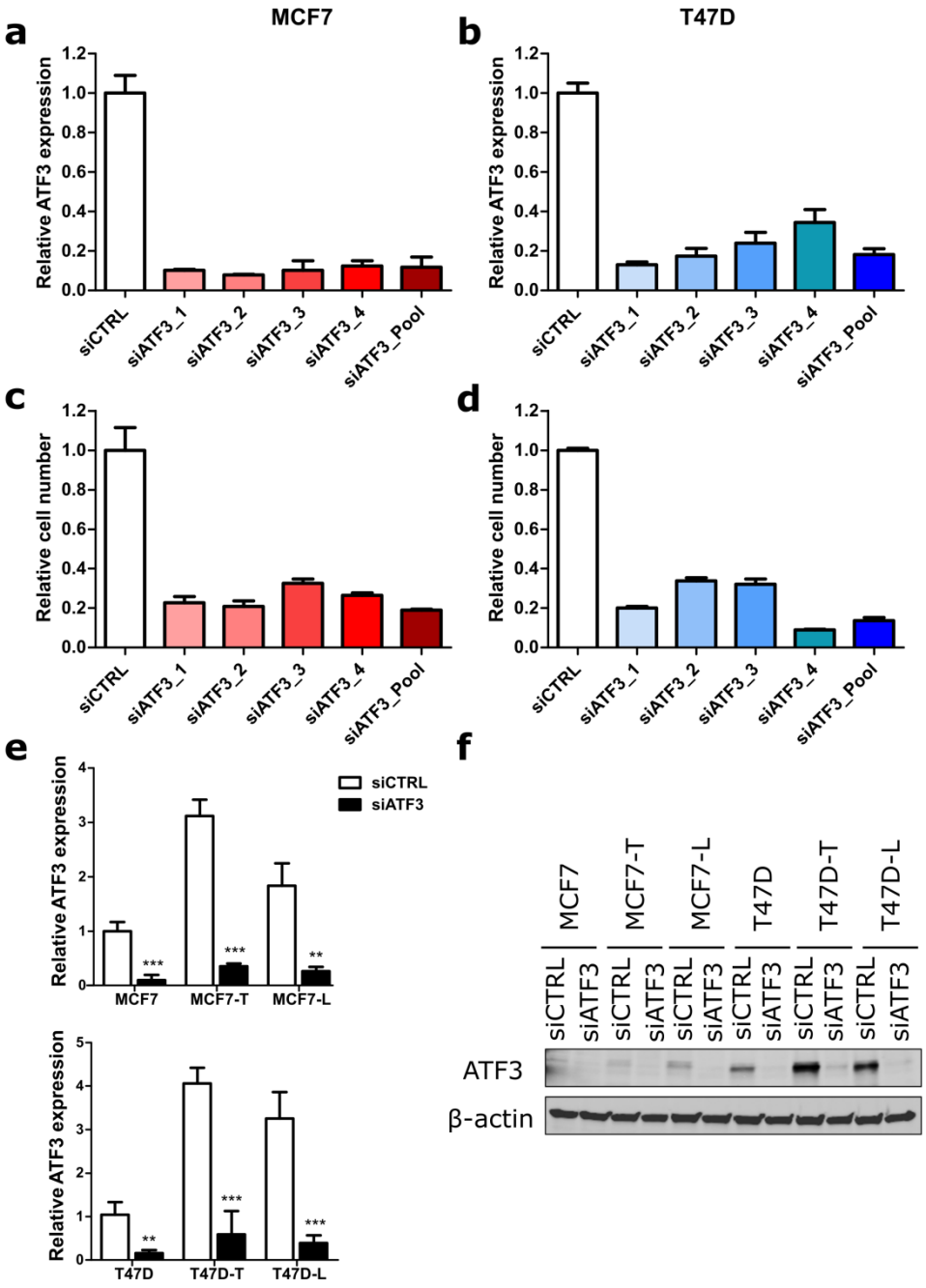

Figure 15: RNAi leads to efficient knockdown of ATF3 at RNA and protein levels
(**a-b**) *ATF3* mRNA levels determined by qRT-PCR 3 days after transfection with 4 single siRNA for ATF3 and the siATF3 pool. (**c-d**) Nuclei count measured with fluorescent microscopy 6 days after transfection with 4 single siRNA for ATF3 the siATF3 pool. (**e**) *ATF3* mRNA levels determined by qRT-PCR 3 days after transfection with siCTRL and siATF3 pool. (**f**) ATF3 protein levels determined by WB 3 days after transfection with siCTRL and siATF3 pool and 2h stimulation with anisomycin. β-actin levels are used as loading control. For the qRT-PCR the values are normalized to *ACTB* levels and to the siCTRL. Data are represented as mean + SD of 3 technical replicates for the

deconvolution and as mean + SEM, n=3 (each with 3 technical replicates) for panel **e**. For the nuclei count the values are normalized to the seeding control and then to the siCTRL control. Data are represented as mean + SD of 5 technical replicates. *** p-value <0.001, ** p-value <0.01, * p-value <0.05

Next, I tested if ATF3 knockdown was able to affect the levels of MAPK pathway-related genes. Indeed upon knockdown of ATF3, the expression of RPS6KA5 and ERBB2 was significantly decreased (Figure 16). Of note this decrease was only detected in resistant cells with elevated ATF3 expression, while the expression of the two genes did not change in wildtype cells. A known direct target of ATF3, DDIT3, was used as a positive control (Liu et al. 2012). Interestingly two downregulators of the MAPK pathway, DUSP10 and DUSP1, showed an opposite trend, as both were upregulated in the resistant cells upon ATF3 knockdown (Figure 16). This indicates that ATF3 might directly or indirectly affect downstream targets in different ways to induce and maintain the upregulation of MAPK signaling.

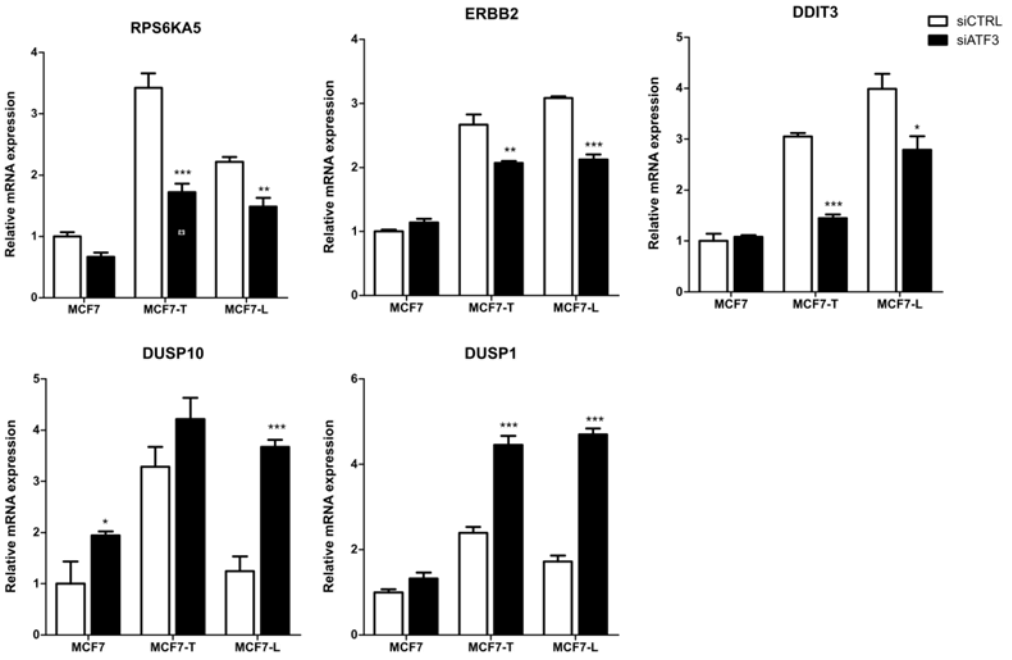

Figure 16: Effect of *ATF3* knockdown on upregulated genes
mRNA levels of early upregulated genes determined by qRT-PCR in parental and resistant MCF7. Data are normalized to *ACTB* and then to parental cells and represented as mean + SEM, n=3 (each with 2 technical replicates). *** p-value <0.001, ** p-value <0.01, * p-value <0.05

To test effect of ATF3 knockdown on cellular processes, cell viability was assessed 6 days after transfection, to allow the. ATF3 knockdown drastically affected the cell number both in the sensitive and resistant cells with a decrease of more than 50% in both MCF7 and T47D compared to the siCTRL transfected cells (Figure 17 a-d). The effect of siRNA was enhanced in both the parental cells treated with TAM or deprived from estrogen compared to the ones kept in E2 containing media, therefore increasing the sensitivity to the drug (Figure 17 a, c). These data show that ATF3 is essential for the cells both in normal condition and in the response to the drug and that its knockdown is highly toxic for the cells.

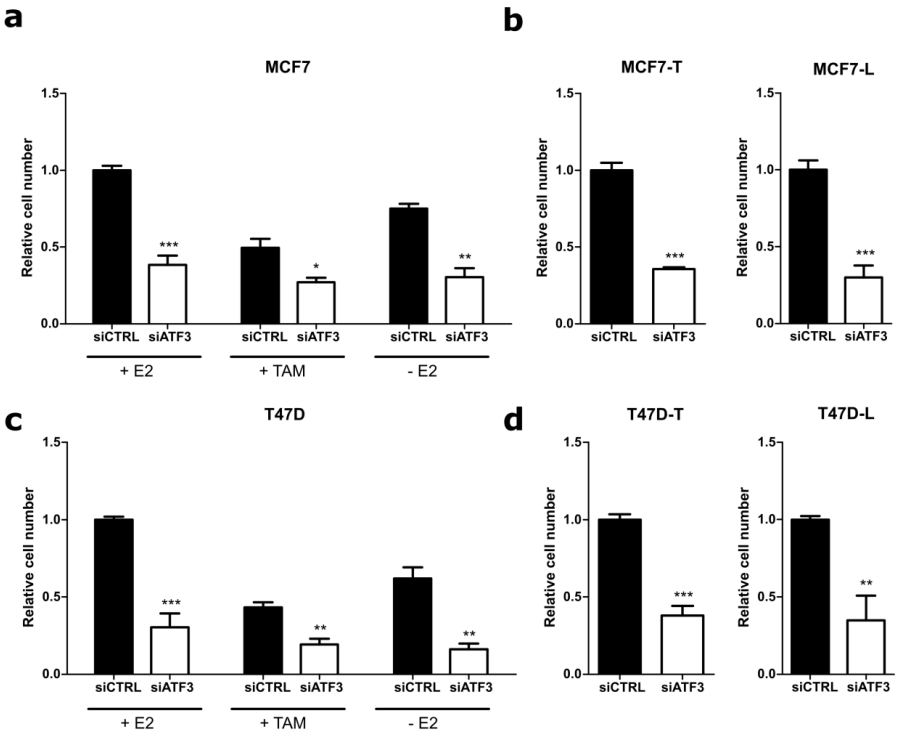

Figure 17: Knockdown of ATF3 drastically affects cell viability
(**a-d**) Nuclei count measured with fluorescent microscopy 6 days after transfection. Parental cells were treated with the indicated media (+E2, +TAM, -E2) for the time of the assay. Resistant cells were kept in their respective media. All values are normalized to seeding control and then to the siCTRL control. Data are represented as mean + SEM, n=3 (each with 5 technical replicates). *** p-value <0.001, ** p-value <0.01, * p-value <0.05

To test if the observed decrease in cell number was accompanied by an increase in apoptosis, cells were analyzed after Annexin V/PI staining. Knockdown of ATF3 indeed induced a

significant increase in the percentage of both early and late apoptotic cells in MCF7-T, and only in late apoptotic cells apoptosis in MCF7-L (Figure 18 b, d). No significant difference was detected in the parental cells, even though an increase in the percentage of early apoptotic cells was evident in all the conditions(Figure 18 a, c). In parental T47D, ATF3 knockdown induced an increase in the early apoptotic cells fraction in presence of TAM or E2 deprivation, while no effect was detected in the untreated cells (Figure 18 e, g). This supports the importance of ATF3 in stress conditions. In resistant cells a significant increase in the percentage of both early and late apoptotic cells was evident in T47D-T. While there was no significant effect in the T47D-L, an increase in the percentages is evident in both the populations (Figure 18 f, h).

Collectively, these results indicate a role of ATF3 in avoiding programmed cell death both in sensitive cells under endocrine stress (at least for T47D) and in the resistant cells.

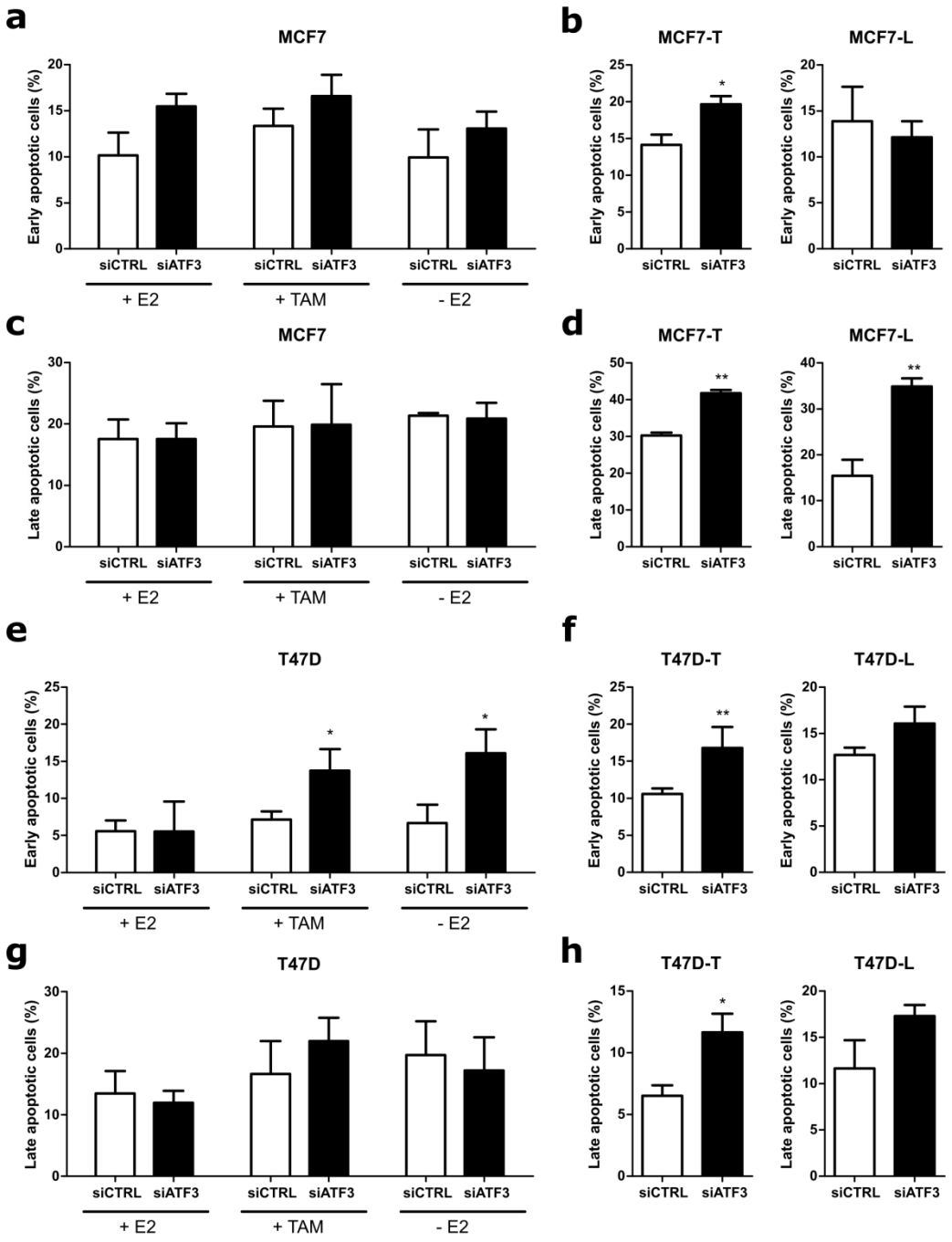

Figure 18: Effect of ATF3 knockdown on apoptosis

(**a-h**) Measurement of apoptosis rate 4 days after transfection with siCTRL and siATF3. Parental cells were treated with the indicated media (+E2, +TAM, -E2) for the time of the assay. Resistant cells were kept in their respective media. Plots represent the percentage of early and late apoptotic cells determined by Annexin V/PI staining. Data are represented as mean + SEM, n=2 (each with 3 technical replicates). *** p-value <0.001, ** p-value <0.01, * p-value <0.05

4.1.6 CRISPR-Cas9 knockout of ATF3 affects cell proliferation, cell cycle, apoptosis and invasion

Since the transient knockdown of ATF3 with siRNA showed high toxicity, I decided to develop stable knockout cell lines to better investigate the role of ATF3 in resistance-related cellular processes. To exclude phenotypic effects related to off-target effects, 2 individual sgRNA targeting exon 3 of ATF3 gene were designed. Knockout was validated in clones derived from single cells using Sanger sequencing. Two selected clones, representing the two different sgRNAs, presented an insertion of 1 bp and a deletion of 17 bp, respectively (Figure 19 a). The Sanger sequencing results also confirmed purity of the clones, with editing efficacy higher than >98% (Figure 19 b). The sequencing identified these clones as homozygous biallelic knockouts, having the exact same mutation on both the alleles. The efficacy of the knockout was verified with WB and, given the low expression of ATF3 at the basal level, anisomycin was used to stimulate its expression. Indeed, after anisomycin stimulation, the WT cells showed a band for ATF3, while still no bands were detectable for the two knockout clones.

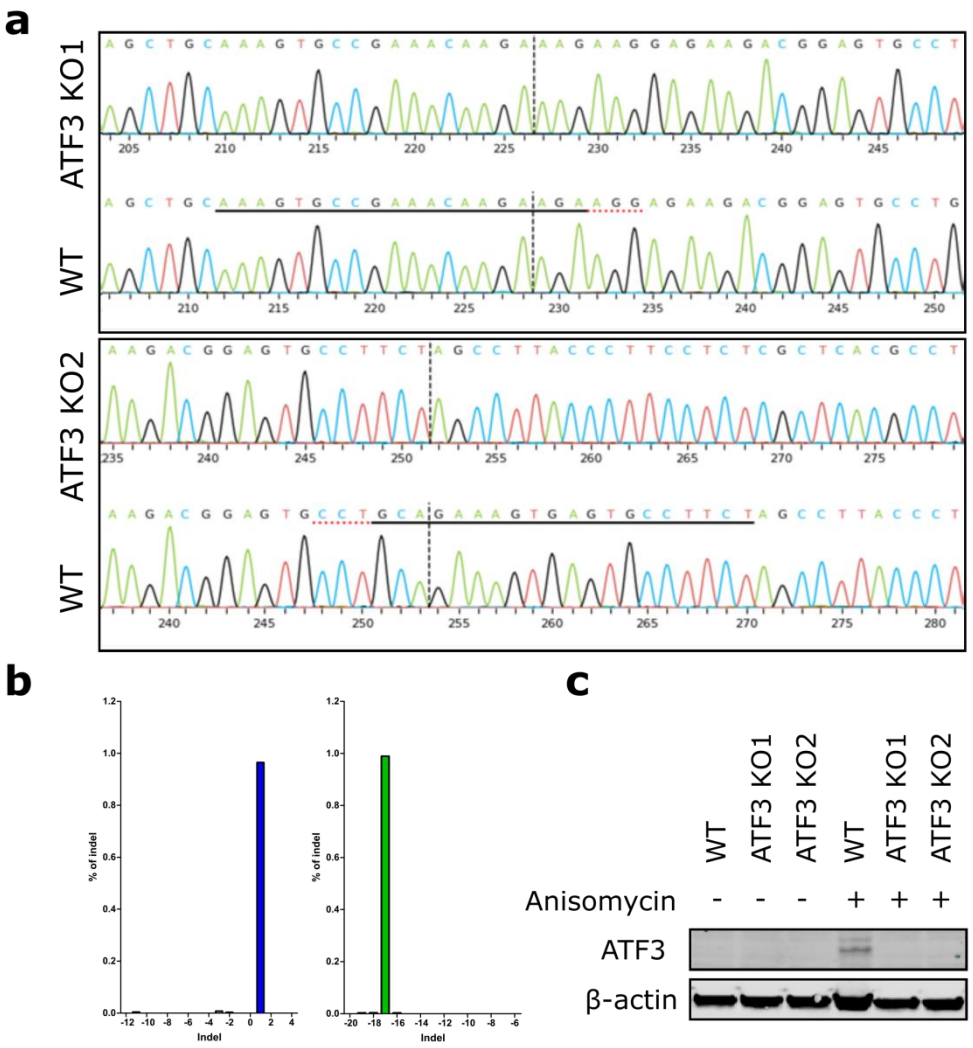

Figure 19: Crispr/Cas9 mediated knockout of ATF3 in MCF7 cells
(**a**) Sanger sequencing visualization of the respective alterations in the *ATF3* gene that have been induced by sgRNA-mediated CRISPR/Cas9 knockout, compared to the wildtype (WT) *ATF3* gene sequence. Sequences of respective sgRNAs are underlined (above the WT sequence track) and PAM-sequences (AGG) are indicated there with a red dotted line. (**b**) Percentage of indels contribution in the total population measured by Sanger sequencing. (**c**) Western blot validation of ATF3 knockout efficiency with or without 2h anisomycin stimulation. β-actin is used as loading control.

To test the effect of ATF3 knockout on proliferation and viability, the cells were measured both in baseline and under treatment conditions. In presence of E2 the cells presented a similar proliferation rate, with KO1 showing a minimal but significant decrease in proliferation

compared to the WT, while KO2 showed the opposite trend (Figure 20 a). In presence of TAM and estrogen deprivation, however, the two ATF3 knockout clones displayed a significantly slower proliferation rate, with KO1 being the slowest (Figure 20 b, c). At the same time, the two knockout clones showed a significant reduction in the viability 8 days after estrogen deprivation. A similar reduction, even if smaller in size and significant only for KO1, was detected for the viability under TAM treatment (Figure 20 d). Altogether this data demonstrate that ATF3 plays a role in cellular response to treatment and that the lack of ATF3 increases the sensitivity of the cells to endocrine treatments.

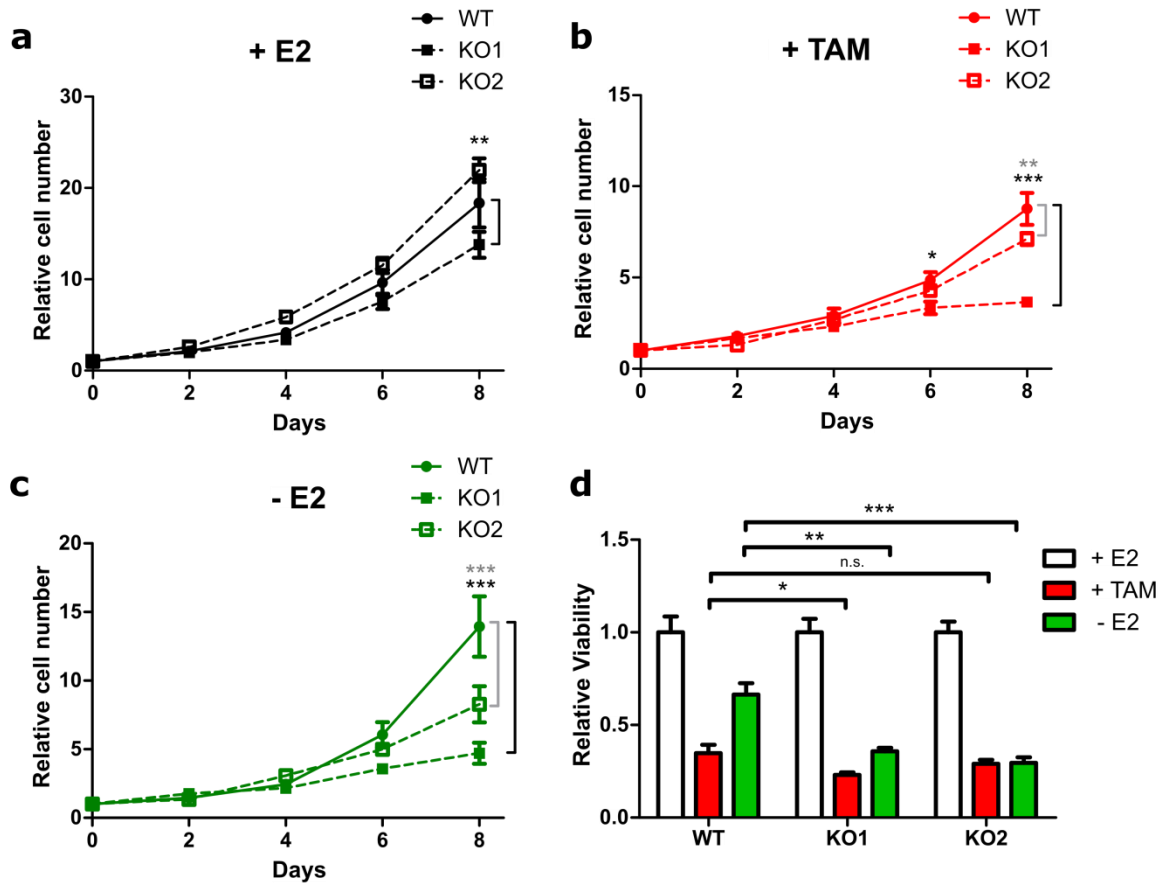

Figure 20: Effect of ATF3 knockout on proliferation and viability
(**a**) Cell proliferation of MCF7 treated for 8 days with E2 and measured at indicated time points with nuclei count in fluorescent microscopy. (**b**) Cell proliferation of MCF7 treated for 8 days with TAM and measured at indicated time points with nuclei count in fluorescent microscopy. (**c**) Cell proliferation of MCF7 deprived for 8 days from E2 and measured at indicated time points with nuclei count in fluorescent microscopy. (**d**) Cell viability of MCF7 after 8 days of treatment with E2, TAM or without E2 measured with CellTiterGlo. All values for the proliferation assays are normalized to a seeding control. Values for the viability assay are normalized to the respective cell

treated with E2. Data are represented as mean ± SEM, n=3 (each with 5 technical replicates). *** p-value <0.001, ** p-value <0.01, * p-value <0.05

To understand if the effect of ATF3 knockout on proliferation and viability under treatment was mediated by changes in other relevant cellular process, the cells were next tested for their cell cycle distribution and apoptosis rate. While no differences in the cell cycle distribution were detected in baseline condition (+E2 in Figure 21 a), knockout clones showed a striking reduction in the percentage of cells entering S phase compared to their WT counterpart with both TAM and -E2 treatments (Figure 21 a). Interestingly, ATF3 knockout also affected the percentage of apoptotic cells under treatment. As before, no difference was observed in untreated condition with a similar number of early and late apoptotic cells. However, after TAM treatment and E2 deprivation, both ATF3 KO clones showed a significant increase in the percentage of early apoptotic cells (Figure 21 b). Overall these results show that ATF3 knockout augments the sensitivity to endocrine therapy both by affecting cell cycle and increasing the apoptosis rate.

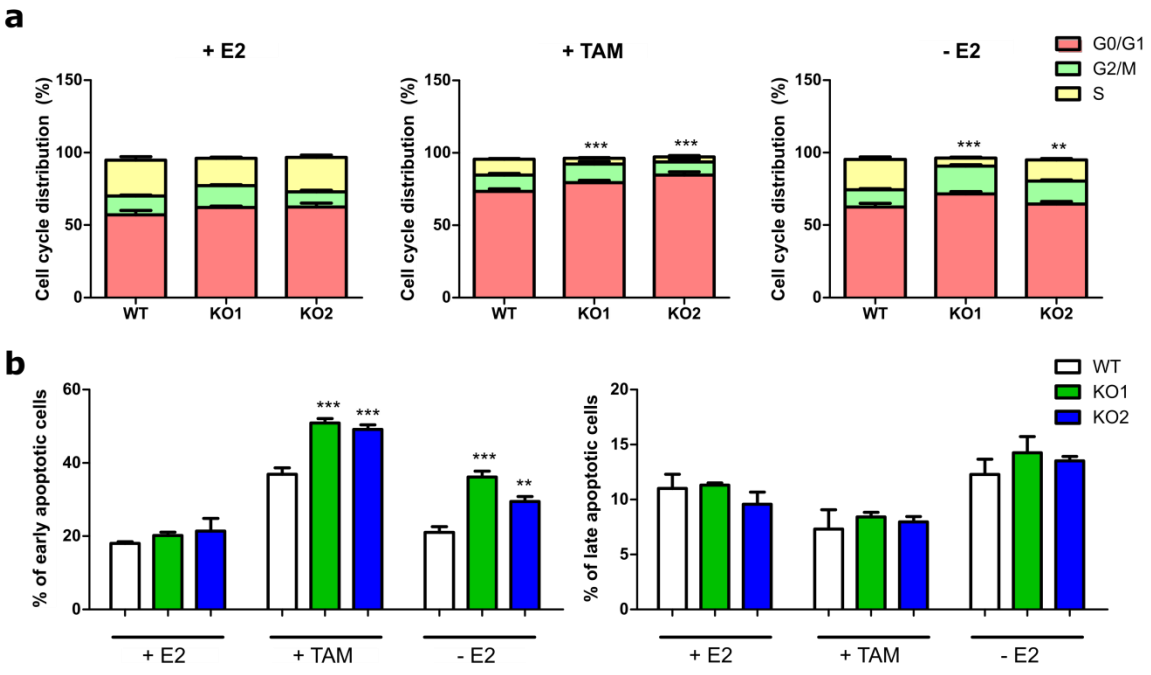

Figure 21: Effect of ATF3 knockout on cell cycle and apoptosis
(**a**) Cell cycle distribution of MCF7 treated for 4 days with E2, TAM or without E2. Plots represent the percentage of cells in the different cell cycle phases determined by BrdU/7AAD staining. Statistics performed on the S phases (yellow bars) (**b**) Measurement of apoptosis rate in MCF7

treated for 4 days with E2, TAM and without E2. Plots represent the percentage of early and late apoptotic cells determined by Annexin V/PI staining. Data are represented as mean + SEM, n=3 (each with 3 technical replicates). *** p-value <0.001, ** p-value <0.01, * p-value <0.05

ATF3 has been implicated in the regulation of cellular invasion in several cancer entities (Jiang et al. 2016; Xuebing Li et al. 2017). To assess if the knockout induced altered invading capabilities cells were tested in a transwell matrigel assay. MCF7 are not highly invading cells, and in baseline conditions they have limited motility. Indeed without stimulation the cells showed low invading abilities even though KO2 displayed even less invading cells (Figure 22 a-b). However, upon TFGβ1 stimulation, the WT cells showed the expected increase in invasion, while the two knockouts did not invade more than in the unstimulated condition (Figure 22 a-b). These data suggest a potential role of ATF3 in TGFβ1-induced regulated invasion in breast cancer.

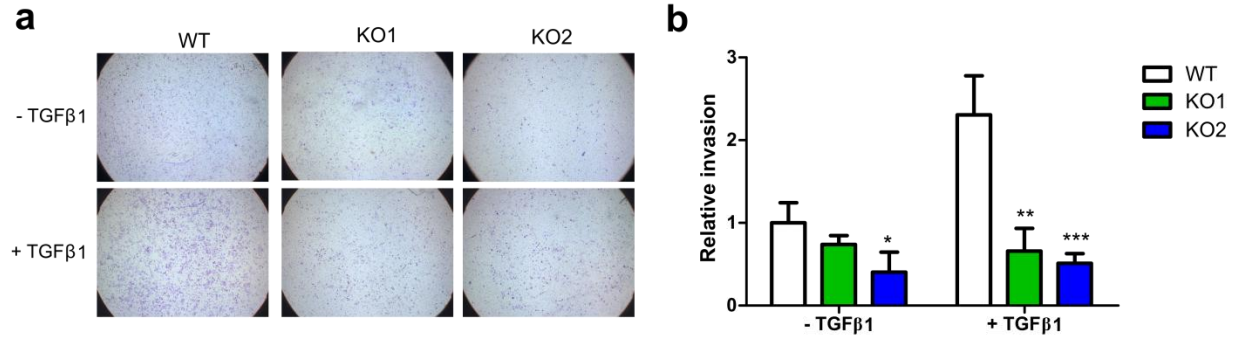

Figure 22: Effect of ATF3 knockout on invasion
(**a**) Representative microscopy images of transwell invasion assay through Matrigel. (**b**) Quantification of the number of invading cells. Values are expressed as relative to the unstimulated WT control. Data are represented as mean + SEM, n=3 (each with 2 technical replicates). *** p-value <0.001, ** p-value <0.01, * p-value <0.05

4.1.7 ATF3 overexpression induces resistance to endocrine therapy

Since ATF3 knockout increased the sensitivity of WT MCF7 to TAM treatment and E2 deprivation, I wanted to test if its overexpression could instead render these cells more resistant. For this reason stably overexpressing MCF7 and T47D were created by the DKFZ stable isogenic cell lines core facility. *ATF3* overexpression was indeed evident at the mRNA level, with both overexpressing cell lines expressing high levels of *ATF3* compared to cells infected with an empty vector (Figure 23 a-b). Accordingly, overexpression was detected also at the protein level in both cell lines (Figure 23 c).

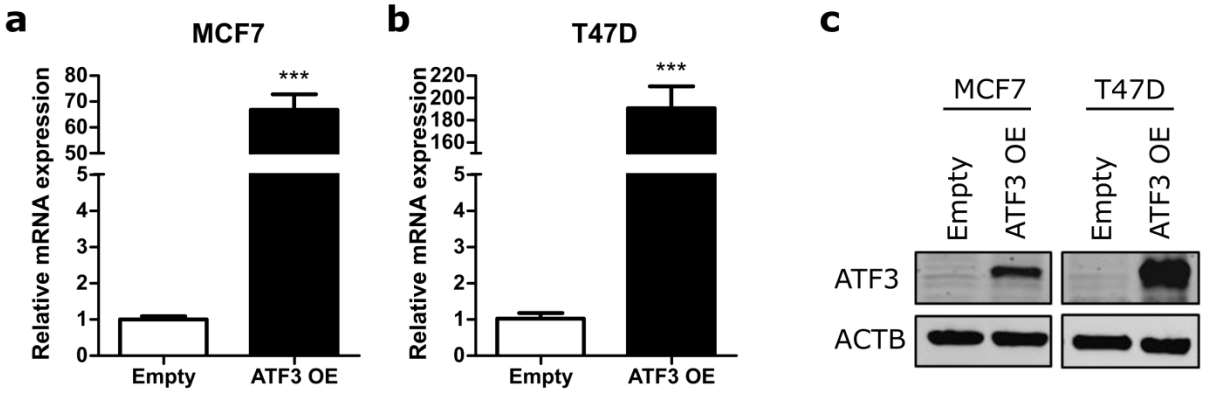

Figure 23: ATF3 overexpression in parental MCF7 and T47D
(**a-b**) *ATF3* mRNA levels determined by qRT-PCR in empty vector and ATF3 overexpressing MCF7 and T47D cells. (**c**) Western blot validation of overexpression efficiency. Data are represented as mean + SEM, n=2 (each with 3 technical replicates). *** p-value <0.001, ** p-value <0.01, * p-value <0.05

To test the effect of ATF3 overexpression on proliferation and viability, the cells were measured both in baseline and under treatment conditions. In MCF7, while in presence of E2 the cells showed a similar proliferation rate, TAM treatment strongly affected growth in empty control cells while the ATF3 overexpressing cells proliferated significantly faster (Figure 24 a-b). The response to E2 deprivation, however, was not different between the two cell lines (Figure 24 c) suggesting that overexpression of ATF3 alone was not sufficient to explain the resistant phenotype. Indeed, viability measurements confirmed this difference, with ATF3

overexpressing cells showing a significantly increased viability under TAM treatment, while no difference was observed in E2 deprivation conditions (Figure 24 d). T47D cells overexpressing ATF3 instead displayed already higher proliferation than the empty control in presence of E2 (Figure 24 e). However, the difference was increased when the cells were kept in presence of TAM or without E2, suggesting a more resistant phenotype of the ATF3 overexpressing cells (Figure 24 f-g). Viability measurements confirmed this trend, with the overexpressing cells showing significantly higher viability in presence of TAM as well as a not significant increase in E2 deprivation (Figure 24 h).

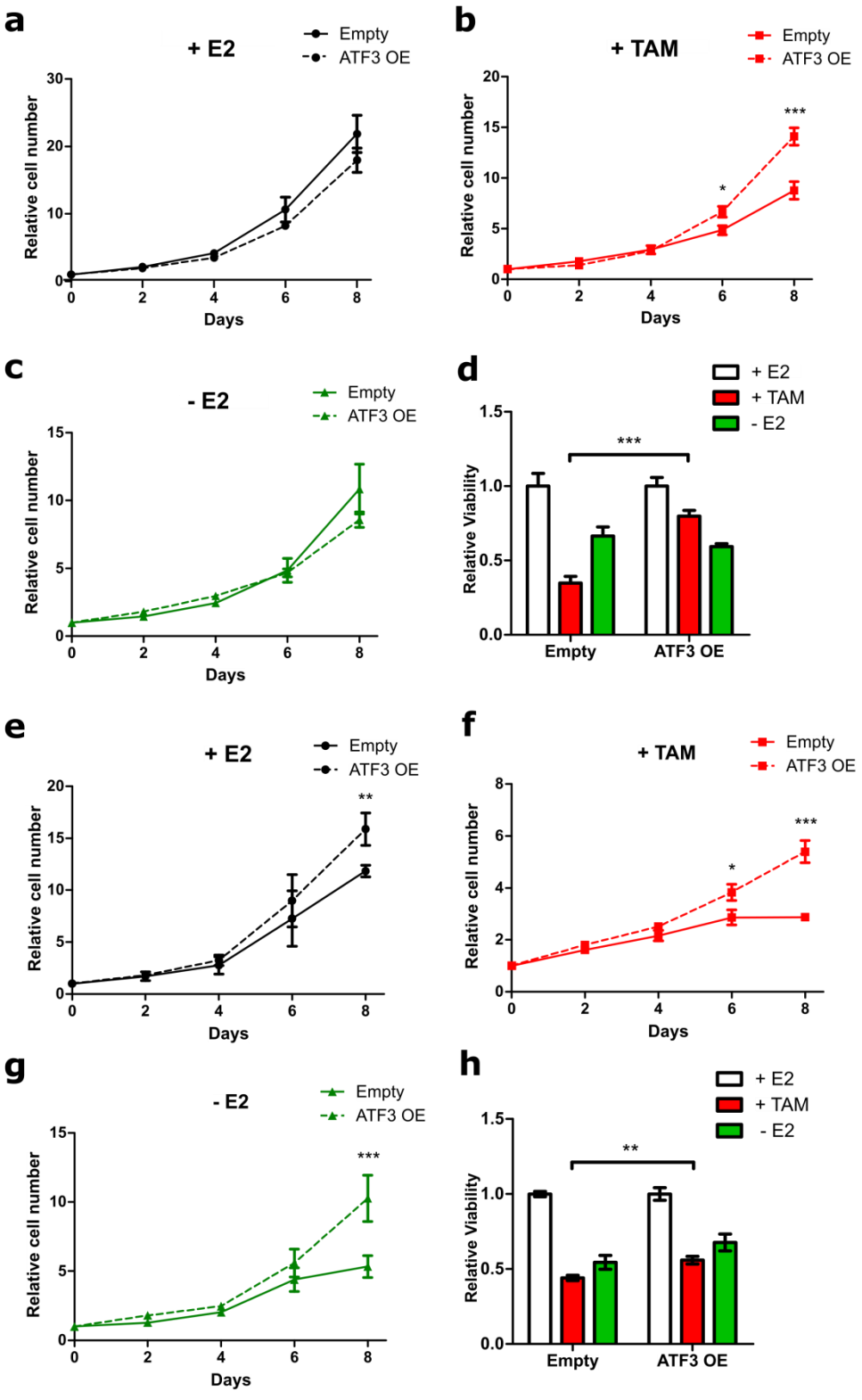
a
+ E2
Empty
ATF3 OE
Relative cell number
Days
b
+ TAM
Empty
ATF3 OE
*
***
Relative cell number
Days
c
- E2
Empty
ATF3 OE
Relative cell number
Days
d
+ E2
+ TAM
- E2
***
Relative Viability
Empty
ATF3 OE
e
+ E2
Empty
ATF3 OE
**
Relative cell number
Days
f
+ TAM
Empty
ATF3 OE
*
***
Relative cell number
Days
g
- E2
Empty
ATF3 OE
***
Relative cell number
Days
h
+ E2
+ TAM
- E2
**
Relative Viability
Empty
ATF3 OE

Figure 24: Effect of ATF3 overexpression on proliferation and viability
(**a**) Cell proliferation of MCF7 treated for 8 days with E2 and measured at indicated time points with nuclei count in fluorescent microscopy. (**b**) Cell proliferation of MCF7 treated for 8 days with TAM and measured at indicated time points with nuclei count in fluorescent microscopy. (**c**) Cell proliferation of MCF7 deprived for 8 days from E2 and measured at indicated time points with nuclei count in fluorescent microscopy. (**d**) Cell viability of MCF7 after 8 days of treatment with E2, TAM or without E2 measured with CellTiterGlo. (**e**) Cell proliferation of T47D treated for 8 days with E2 and measured at indicated time points with nuclei count in fluorescent microscopy. (**f**) Cell proliferation of T47D treated for 8 days with TAM and measured at indicated time points with nuclei count in fluorescent microscopy. (**g**) Cell proliferation of T47D deprived for 8 days from E2 and measured at indicated time points with nuclei count in fluorescent microscopy. (**h**) Cell viability of T47D after 8 days of treatment with E2, TAM or without E2 measured with CellTiterGlo. All values for the proliferation assays are normalized to a seeding control. Values for the viability assay are normalized to the respective cell treated with E2. Data are represented as mean ± SEM, n=3 (each with 5 technical replicates). *** p-value <0.001, ** p-value <0.01, * p-value <0.05

Next, I wanted to test the effect of ATF3 overexpression on cell cycle and apoptosis. In MCF7, when assessed in E2 containing media no difference was observed in the number of cells entering in S phase between the empty control and the overexpressing cells. Under TAM treatment and E2 deprivation, however, ATF3 overexpressing cells showed an increase in S phase, demonstrating less sensitivity to the treatments (Figure 25 a). Additionally, while no difference in the apoptosis rate was observed between the empty and the OE cells with or without E2, the percentage of early apoptotic cells that was induced upon TAM treatment was significantly lower in the ATF3 overexpressing cells (Figure 25 b). Similarly, in T47D no difference was observed in in the percentage of cycling cells between empty and overexpressing cells kept in E2 media. As in MCF7, ATF3 overexpression was able to prevent the cell cycle arrest induced my TAM, while no difference was observed under E2 deprivation (Figure 25 c). At the same time, the overexpression was able to significantly reduce also TAM-induced early apoptosis compared to the empty control. A descrease in the early apoptotic cells, even if not statistically significant, was detected in E2 deprived overexpressing cells (Figure 25 d). Overall these data demonstrate that ATF3 overexpression in able to induce resistance to TAM, in terms of higher proliferation and cell cycle and lower apoptosis rate under treatment, and in a lower extent to E2 deprivation, as reflected on the higher percentage of actively cycling cells in MCF7 and the higher proliferation rate in T47D.

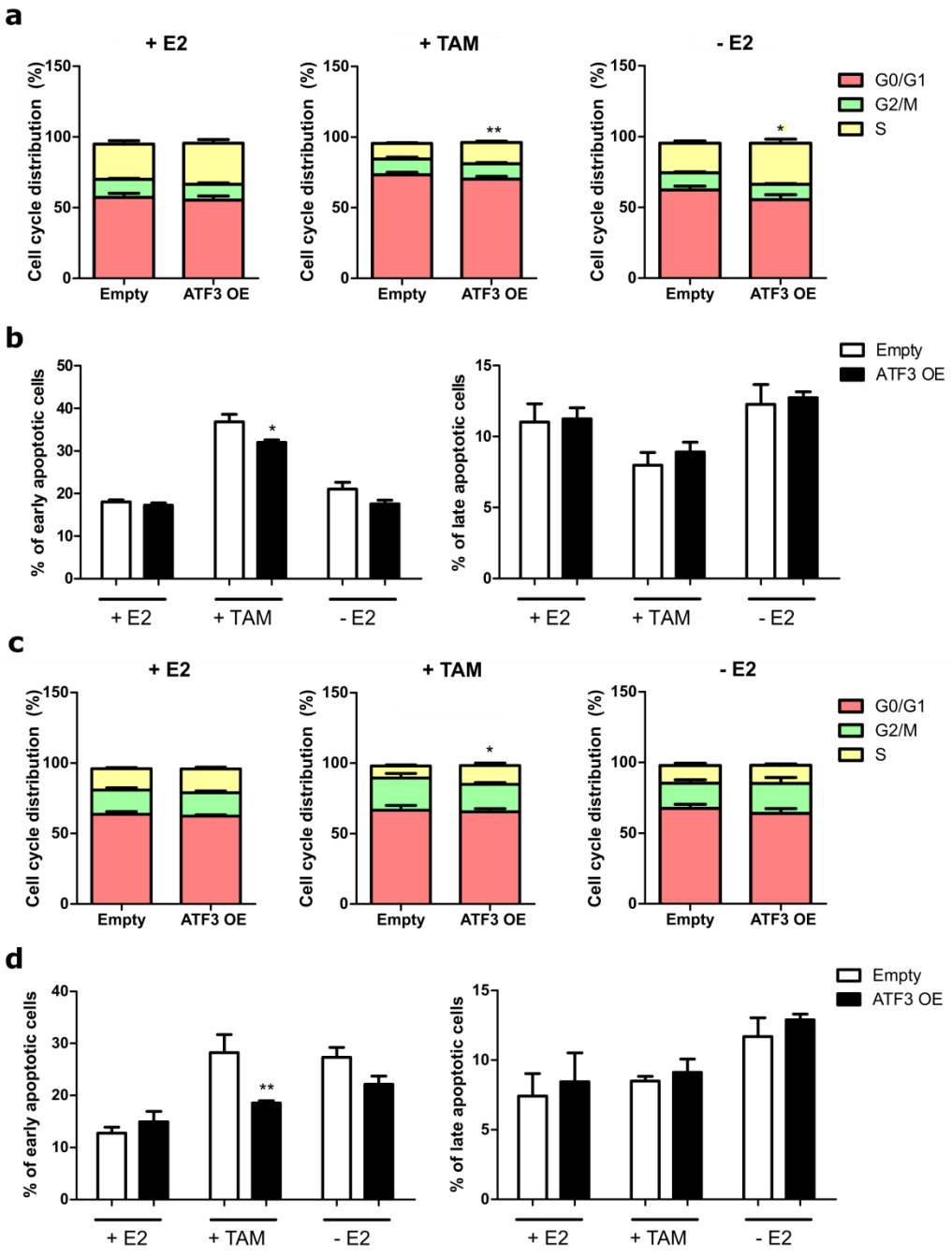

Figure 25: Effect of ATF3 overexpression on cell cycle and apoptosis
(**a**) Cell cycle distribution of MCF7 treated for 4 days with E2, TAM or without E2. (**b**) Measurement of apoptosis rate in MCF7 treated for 4 days with E2, TAM and without E2. (**c**) Cell cycle distribution of T47D treated for 4 days with E2, TAM or without E2. (**d**) Measurement of apoptosis rate in T47D treated for 4 days with E2, TAM and without E2. Cell cycle distribution plots represent the percentage of cells in the different cell cycle phases determined by BrdU/7AAD staining. Statistics performed on the S phases (yellow bars). Apoptosis plots represent the percentage of early and late

apoptotic cells determined by Annexin V/PI staining. Data are represented as mean + SEM, n=3 (each with 3 technical replicates). *** p-value <0.001, ** p-value <0.01, * p-value <0.05

Since ATF3 knockout affected the invasion capabilities of MCF7, I decided to test if the overexpression was able to induce the opposite phenotype. While in unstimulated conditions ATF3 OE MCF7 cells displayed a similar number of invading cells as the empty control, upon stimulation the increase in invasion was enhanced in the overexpressing cells (Figure 26 a-b). Both T47D cell lines (empty control and ATF3 OE) were not able to invade through matrigel (data not shown). These data strengthen the indications obtained from the knockouts on the role of ATF3 in invasion and show similarities in the invasion capabilities of ATF3 overexpressing and resistant cells.

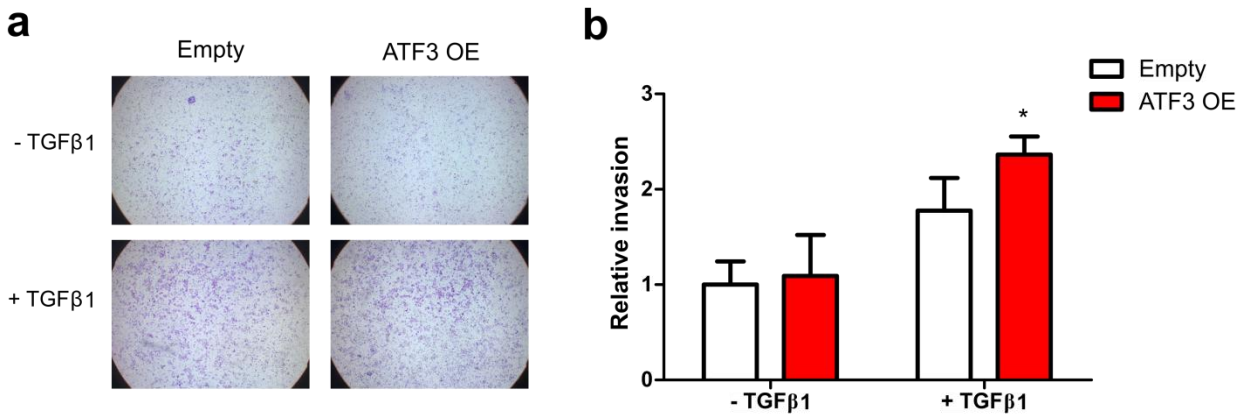

Figure 26: Effect of ATF3 overexpression on invasion in MCF7
(**a**) Representative microscopy images of transwell invasion assay through Matrigel. (**b**) Quantification of the number of invading cells. Values are expressed as relative to unstimulated empty control. Data are represented as mean + SEM, n=3 (each with 2 technical replicates). *** p-value <0.001, ** p-value <0.01, * p-value <0.05

4.1.8 ATF3 modulation affects downstream pathway activities

RNA-seq revealed that during resistance development, the cells rewire their cellular processes, particularly affecting genes involved in MAPK pathway (Figure 9). Resistant cells were additionally proven to have higher activation of many phospho-proteins involved in this

pathway (Figure 13). To investigate if the knockout of ATF3 would directly affect the pathway activation profile of the cells under treatment I followed a targeted proteomic approach with the WT and the knockout clones after treatment either with TAM or E2 deprivation, using RPPA. The pathways chosen for investigation were MAPK for its role in upstream and downstream of ATF3, as well as PI3K/AKT due to its deep interconnection with MAPK and its previously demonstrated role in resistance (Figure 13) (Ma, Crowder, and Ellis 2011; Tokunaga et al. 2006)

Acute treatment of WT MCF7 induced the upregulation of many proteins upstream of both the pathways, from tyrosin kinase receptors like ERBB family members to adjuvant proteins as SOS and GAB1, as well as downstream branches of effector kinases, like FAK, PAK1, and PAK2. Of note, also most of the investigated phospho-proteins revealed higher signals (Figure 27). In the PI3K/AKT pathway, several kinases as PDK1, AKT and PRAS40 showed a higher signal upon treatment, while consistently the phosphorylation of the downstram negative regulator of translation 4E-BP1 displayed a decrease. In parallel, MAPK pathwas showed increased activity by means of higher phosphorylation of p38, MEK1 and JNK, with only ERK1/2 showing decreased activity upon treatment (Figure 27).

In the two knockouts, upon treatment administration, the pathway activation profile was drastically different. While some of the upregulated proteins in WT MCF7 upon TAM and E2 deprivation treatment were not affected by the knockout (ERBB2/3, 4E-BP1, p42/44, Src), several other total and phospho-proteins did not show the same upregulation seen in the WT cells under treatment (Figure 27). Notably, this was the case for most of the phospho proteins, including the phosphorylated forms of AKT, cRAF, MEK and eIF4B. On the other hand, phospho-proteins that displayed downregulation upon treatmnent in the WT were upregulated in the knockouts, as pERK1/2 and p4E-BP1. These results indicate that ATF3 knockout indeed affects the regulation of several branches of the MAPK and PI3K/AKT pathways in response to the drug and the lack of ATF3 prevents the cells from augmenting the expression and activities of central proteins involved in these pathways.

As ATF3 overexpression induced the opposite phenotypic effects compared to the knockouts, i.e. increasing the resistance of sensitive cells to treatment, RPPA analysis was used to compare the ATF3 overexpression to the empty vector control. In MCF7, even though the effect on pathway alteration was not as strong as for the knockout, consistent changes in central proteins were detected. While upon TAM treatment a clear activation of these pathways was visible in the empty control, a stronger upregulation in the MAPK and PI3K/AKT pathways activation was detected in the overexpressing cells under E2 deprivation. Here, many phosphorylated protein such as LKB1, FAK and p38 showed an increase only in the E2 deprived ATF3 overexpressing cells (Figure 28 a). This finding was surprising as the phenotypic effect of the overexpression was stronger upon TAM treatment rather than in E2 deprivation (Figure 24, Figure 25). This could be mediated by specific proteins as pERK1 or peIF4B, which showed an upregulation upon both treatments in the overexpressing cells. However the fact that the MAPK and PI3K/AKT pathways are already highly induced in the empty vector control upon TAM treatment might mask further changes. In T47D the effect was less prominent, with some phospho-proteins being already upregulated in the treated empty control, particularly upon E2 deprivation (Figure 28 b). However, specific upregulation in the treated ATF3 overexpressing cells are visible, as phosphorylated p70 S6 kinase, FAK and PLCγ. This indicates that ATF3 overexpression might influence differently MCF7 and T47D in terms of downstream pathway activation. This could be mediated also by the background of somatic mutations present in these two cell lines as well as their different baseline levels of ATF3.

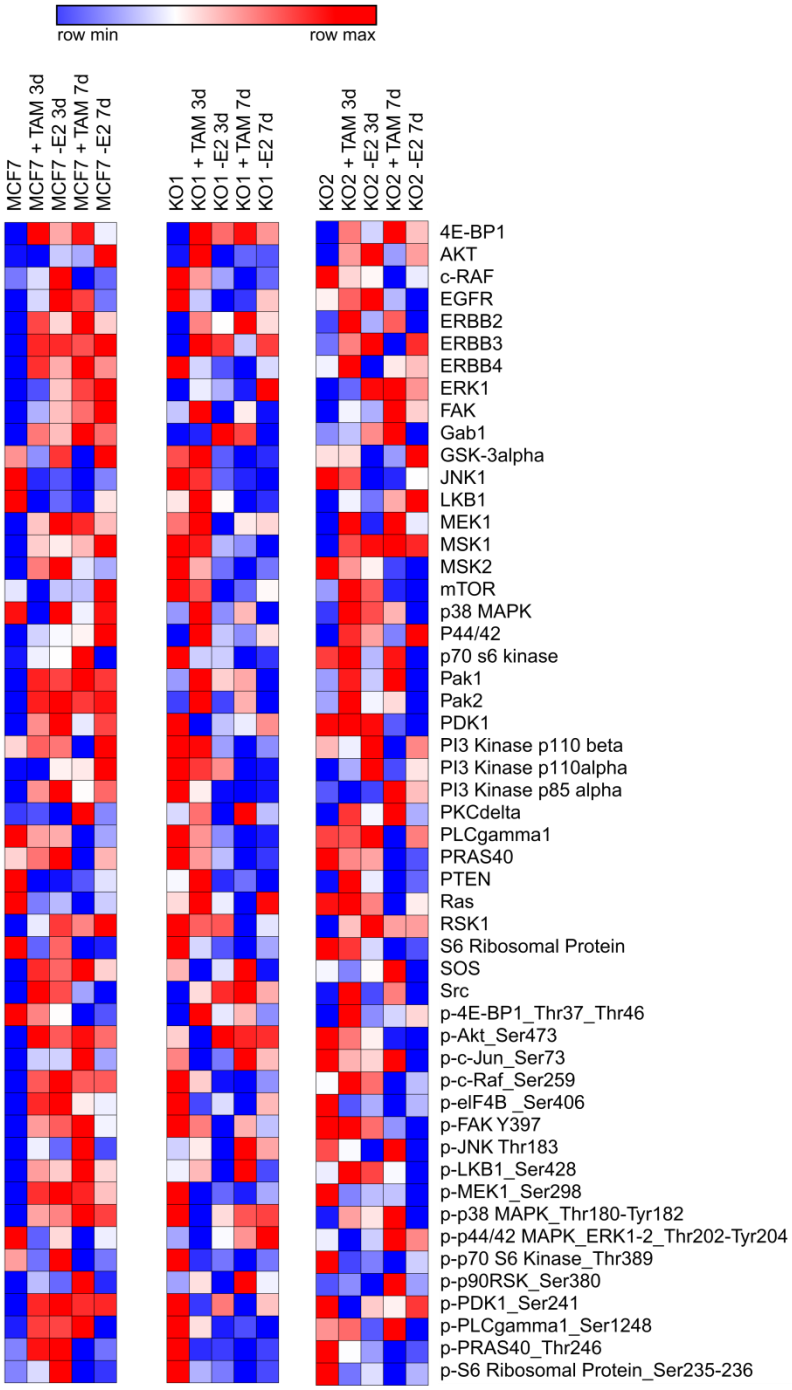

Figure 27: Heatmaps of RPPA-screened proteins in ATF3 knockout cells
Heatmaps of 35 total proteins and 18 phospho-proteins involved in PI3K-AKT-MAPK signaling pathway in MCF7 WT and ATF3 KO clones. Log2 normalized signal intensities for each protein are plotted and color-coding refers to relative intensities in each row and each cell line independently.

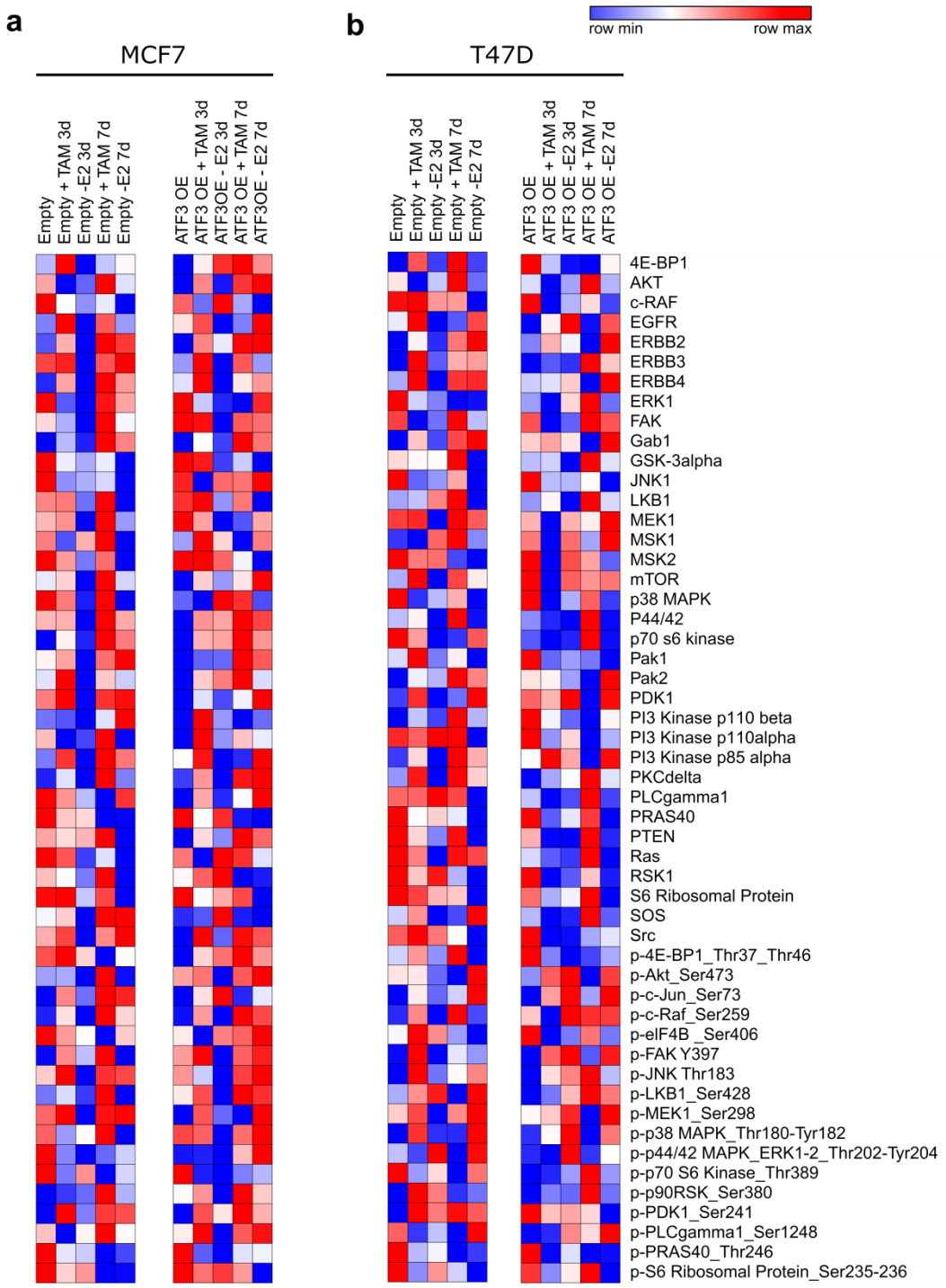

Figure 28: Heatmaps of RPPA-screened proteins in ATF3 overexpressing cells
(**a-b**) Heatmaps of 35 total proteins and 18 phospho-proteins involved in PI3K-AKT-MAPK signaling pathway in MCF7 and T47D Empty and ATF3 overexpressing (OE) cell lines. Log2 normalized signal intensities for each protein are plotted and color-coding refers to relative intensities in each row and each cell line independently.

4.1.9 ATF3 stable knockdown does not re-sensitize resistant cells

Modulation of ATF3 in sensitive cells affected their acute response to drugs, with the knockout increasing their sensitivity while overexpression conferred resistance. This demonstrates a role of ATF3 in drug response and resistance development. Then, I wanted to assess if the knockout of ATF3 was able to re-sensitize resistant cells. As the CRISPR approach requires single clone selection and a long drug holiday that might affect cellular behavior, I decided to use shRNAs knockdown, where antibiotic selection can be used to select transfected cells. Two different ATF3 shRNAs were used and a SCRAMBLE shRNA was transduced as a control. Knockdown of ATF3 was effective at the protein level in all the resistant cell lines, even though residual levels were still detected (Figure 29 a). However, as ATF3 levels are only 2 to 3 fold increased in resistant compared to the parental cells, this knockdown reduced ATF3 levels to the original baseline level (Figure 14).

To assess the effect of ATF3 knockdown on treatment response, the cells were tested for their proliferative capabilities. Under TAM treatment, no difference was observed in the cell lines, with the two shATF3 and the shSCR showing the same proliferation rate (Figure 29 b, d). In the LTED cells, one of the T47D-L knockdowns showed a significantly slower proliferation, while the other shATF3 displayed the same proliferation as the shSCR (Figure 29 c). On the other hand, in MCF7-L shATF3_2 showed a higher proliferation rate, however in this cell the knockout had low efficiency (Figure 29 a, e). This data suggest that ATF3 knockdown is not able to re-sensitize already resistant cells to either TAM treatment and or E2 deprivation.

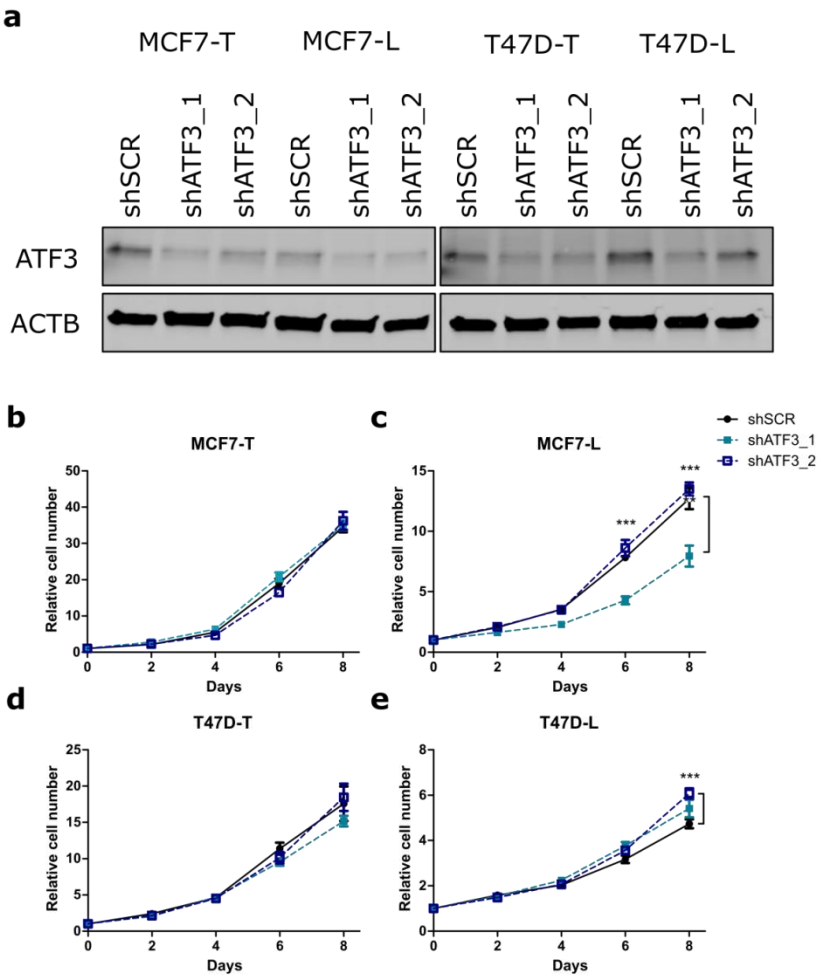

Figure 29: Effect of ATF3 stable knockdown on resistant cells' proliferation
(**a**) Western blot validation of knockdown efficiency with two shRNA compared to a shSCR control (**b-e**) Cell proliferation of resistant MCF7 and T47D with nuclei count in fluorescent microscopy. All values for the proliferation assays are normalized to a seeding control. Data are represented as mean ± SEM, n=2 (each with 5 technical replicates). *** p-value <0.001, ** p-value <0.01, * p-value <0.05

To confirm these results I also tested the effect of the stable knockdown on cell cycle and apoptosis. Indeed no significant difference was detected in all the resistance cell lines regarding the number of cycling cells, apart from MCF7-T shATF3_2 which showed a reduction compared to the shSCR (Figure 30 a, b). At the same time, no difference was observed in the percentage of apoptotic cells, with only a decrease in the number of early apoptotic cells in T47D-T shATF3_1 cells (Figure 30 c, d). Overall these data are in agreement with the proliferation assay, showing no effect of the knockdown of ATF3 in resistant cells.

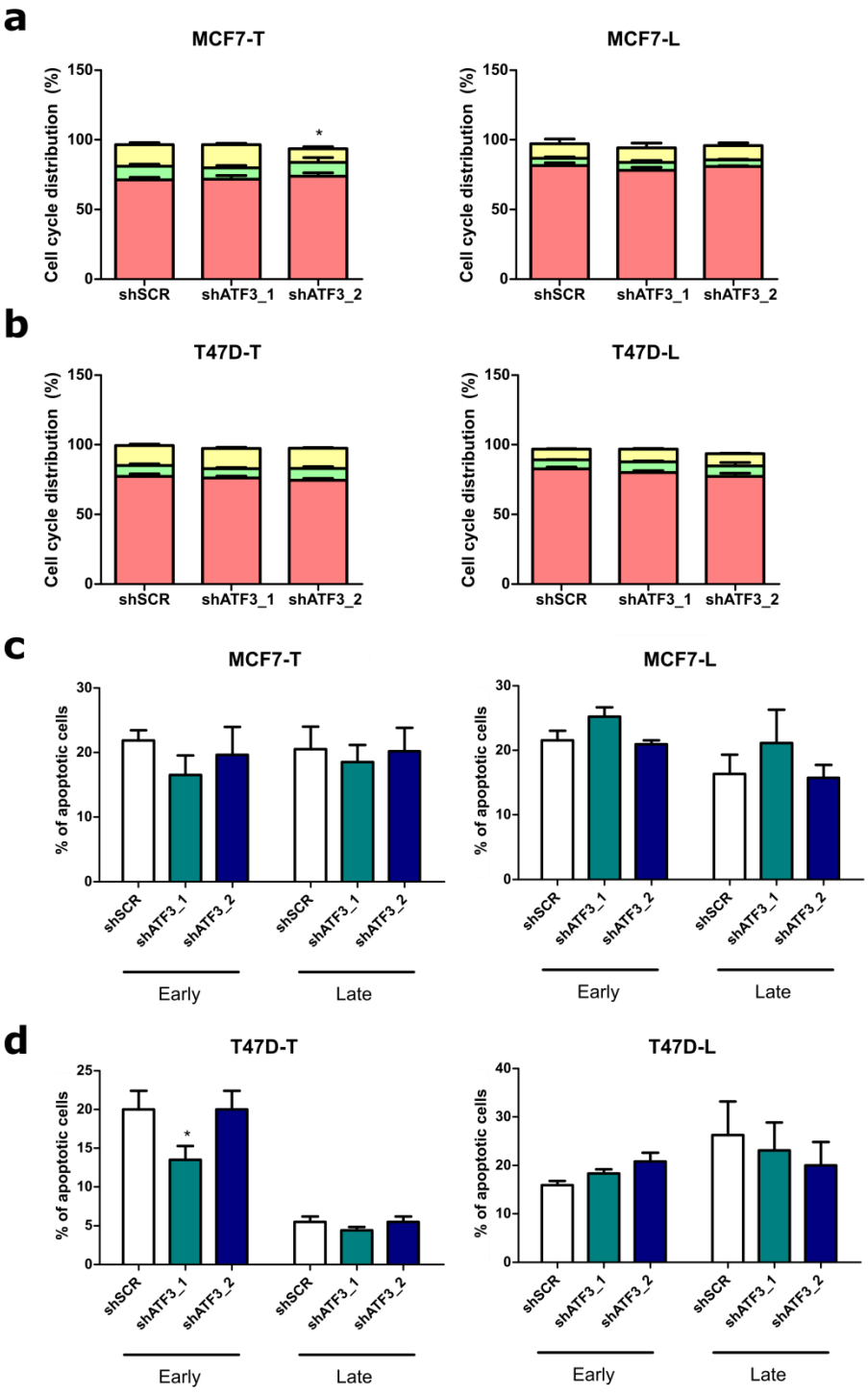

Figure 30: Effect of ATF3 stable knockdown on resistant cells' cell cycle and apoptosis
(**a-b**) Cell cycle distribution of resistant MCF7 and T47D. Plots represents the percentage of cells in the different cell cycle phases determined by BrdU/7AAD staining (**c-d**) Measurement of apoptosis rate in resistant MCF7 and T47D. Plots represent the percentage of early and late apoptotic cells

determined by Annexin V/PI staining. Data are represented as mean + SEM, n=2 (each with 3 technical replicates). *** p-value <0.001, ** p-value <0.01, * p-value <0.05

4.1.10 ATF3 regulates TGFB2 expression

ATF3 was selected as a target based on its predicted role in regulating several genes upregulated in resistance. Indeed ATF3 knockout reduced the MAPK pathway activation upon treatment, confirming ATF3 as a putative regulator of this pathway. To understand if the ATF3 effect on MAPK upregulation could be mediated by other proteins, I investigated the list of early upregulated genes for MAPK inducers. TGFβ2 was in the list of early upregulated genes and is a predicted ATF3 target. TGFB ligands are known inducers of the MAPK and PI3K/AKT signaling pathways in a SMAD-independent way, especially in cancer (Chapnick et al. 2011; Zhang 2009). While TGFβ1 has been deeply characterized as a mediator of resistance to endocrine therapies, TGFβ2 was reported to be upregulated under tamoxifen treatment, but its role in this context has not been investigated (Perry, Kang, and Greaves 1995; Yoo et al. 2008; Brandt et al. 2003). Still, the known role of TGFβ1 and the fact that both TGFβ1 and 2 act on the same receptor, make TGFβ2 a promising downstream target of ATF3. Therefore, together with Zuzana Koskova, a bachelor student I directly supervised, I decided to investigate the crosstalk between ATF3 and TGFβ2.

TGFβ2 upregulation was detected in both resistant cell lines, with only MCF7-L not showing a difference in the RNA-seq data (Figure 31 a). TGFβ1, however, showed a decrease in early phases of resistance development in T47D, while no difference was visible in MCF7 (Figure 31 c). This indicates a specific upregulation of TGFβ2 in these resistant models. qRT-PCR confirmed these results, showing strongly elevated levels of TGFβ2 IN MCF7-T and also a small increase in the MCF7-L (Figure 31 b). Finally, ELISA was used to test if the high levels seen in mRNA were actually translated in secreted protein by the cells. Indeed increased levels of TGFβ2 were detected in the supernatant of all resistant cells, apart from MCF7-L (Figure 31 d).

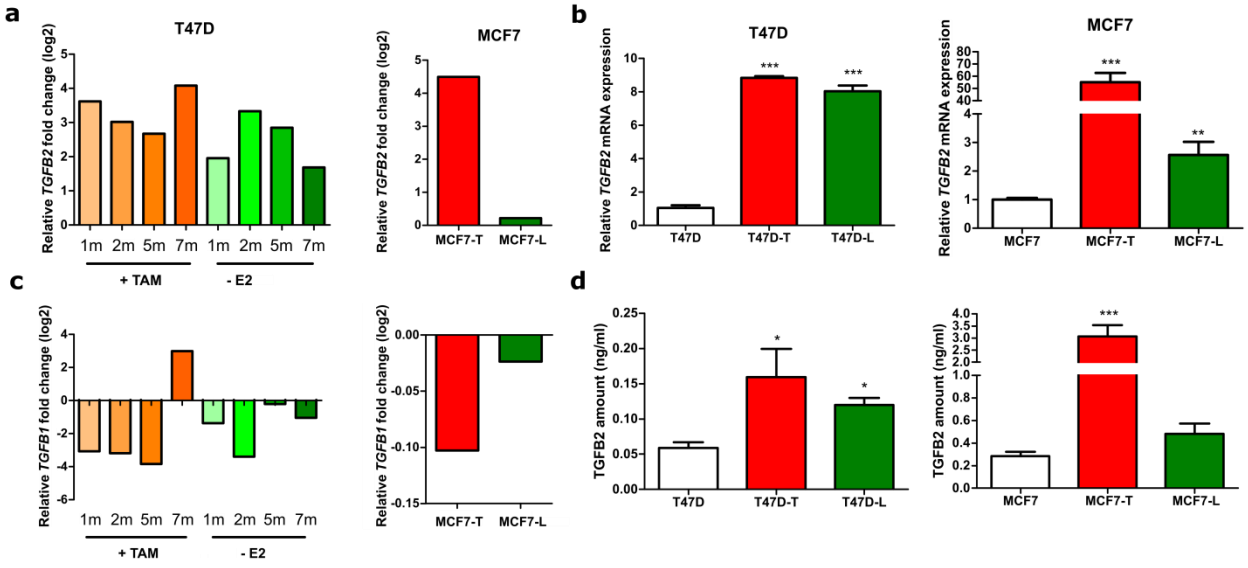

Figure 31: TGFβ2 levels in resistant cell lines
(**a-c**) Relative TGFB1 and TGFB2 mRNA levels determined RNA-Seq in T47D at defined times (1m, 2m, 5m, 7m) during resistance development against TAM and E2 and in MCF7 resistant to 100nM TAM (MCF7-T) and E2 deprivation (MCF7-L). (**b**) Relative ATF3 mRNA levels determined by qRT-PCR in resistant T47D and MCF7. (**d**) ATF3 protein levels determined by ELISA in resistant T47D and MCF7. For RNA-Seq values are represented as relative Log2 Fold Change compared to parental cells. For qRT-PCR data are normalized to parental cells and represented as mean + SEM, n=3 (each with 3 technical replicates). For ELISA results are shown as total protein amount quantified via GloMax and represented as mean + SEM, n=3 (each with 2 technical replicates) *** p-value <0.001, ** p-value <0.01, * p-value <0.05

To test if ATF3 indeed regulates TGFβ2 expression, ATF3 was silenced in both MCF7 and T47D parental and resistant cells. Upon ATF3 knockdown TGFβ2 was reduced both at the mRNA and, to a lesser extent, at protein levels in all MCF7 cell lines (Figure 32 a-b). Surprisingly, however, ATF3 knockdown in T47D had the opposite effect, inducing an upregulation of TGFβ2 (Figure 32 a-b). Since TGFβ1 has been proven to induce ATF3 expression, we also tested if TGFβ2 expression might affect ATF3. While the silencing was effective both at the mRNA and protein levels, no difference in ATF3 expression was detected in any cell line (Figure 32 c-e).

These results suggest a role of ATF3 in the regulation of TGFβ2, even though with completely distinct effects in MCF7 and T47D.

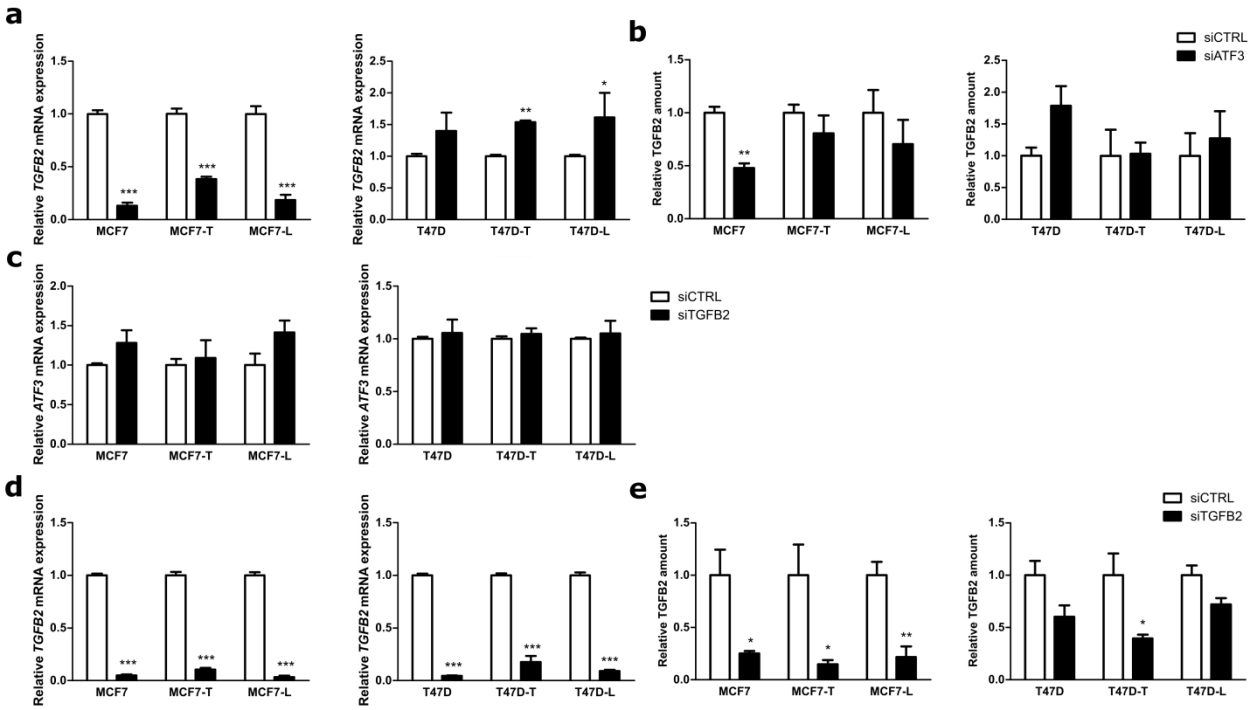

Figure 32: Effect of ATF3 knockdown on TGFB2 expression
(**a**) Relative TGFB2 mRNA levels determined by qRT-PCR in siCTRL and siATF3 transfected cells. (**b**) Relative TGFB2 protein levels determined by ELISA in siCTRL and siATF3 transfected cells. (**c-d**) Relative ATF3 and TGFB2 mRNA levels determined by qRT-PCR in siCTRL and siTGFB2 transfected cells. (**f**) Relative TGFB2 protein levels determined by ELISA in siCTRL and siTGFB2 transfected cells. mRNA values are normalized to siCTRL for each cell line. ELISA's values is normalized to RNA concentrations and then to siCTRL for each cell line. Data are represented as mean + SEM, n=3 (each with 3 technical replicates). *** p-value <0.001, ** p-value <0.01, * p-value <0.05

Even though the knockdown of TGFβ2 did not affect the levels of ATF3, I tested if the stimulation with recombinant TGFβ2 could induce an upregulation in ATF3. In MCF7 TGFβ2 stimulation increased ATF3 expression as a delayed response after 7 days, while no effect was seen in T47D (Figure 33 a). As a control for the stimulation BAMBI, a pseudo-receptor for TGFβ, was tested and was indeed upregulated in both cell lines (Figure 33 b). To test if TGFβ2 stimulation was able to induce activation of the MAPK and PI3K/AKT pathways, the cells were tested with RPPA. As expected, upon stimulation, several total and phospho-proteins involved in the MAPK and PI3k/AKT cascades were found upregulated in both the cell lines, indicating the efficient activation of both pathways (Figure 33 c).

Overall these data connect ATF3 and TGFβ2 and indicate that they are able to induce each other as well as downstream MAPK signaling pathway activation.

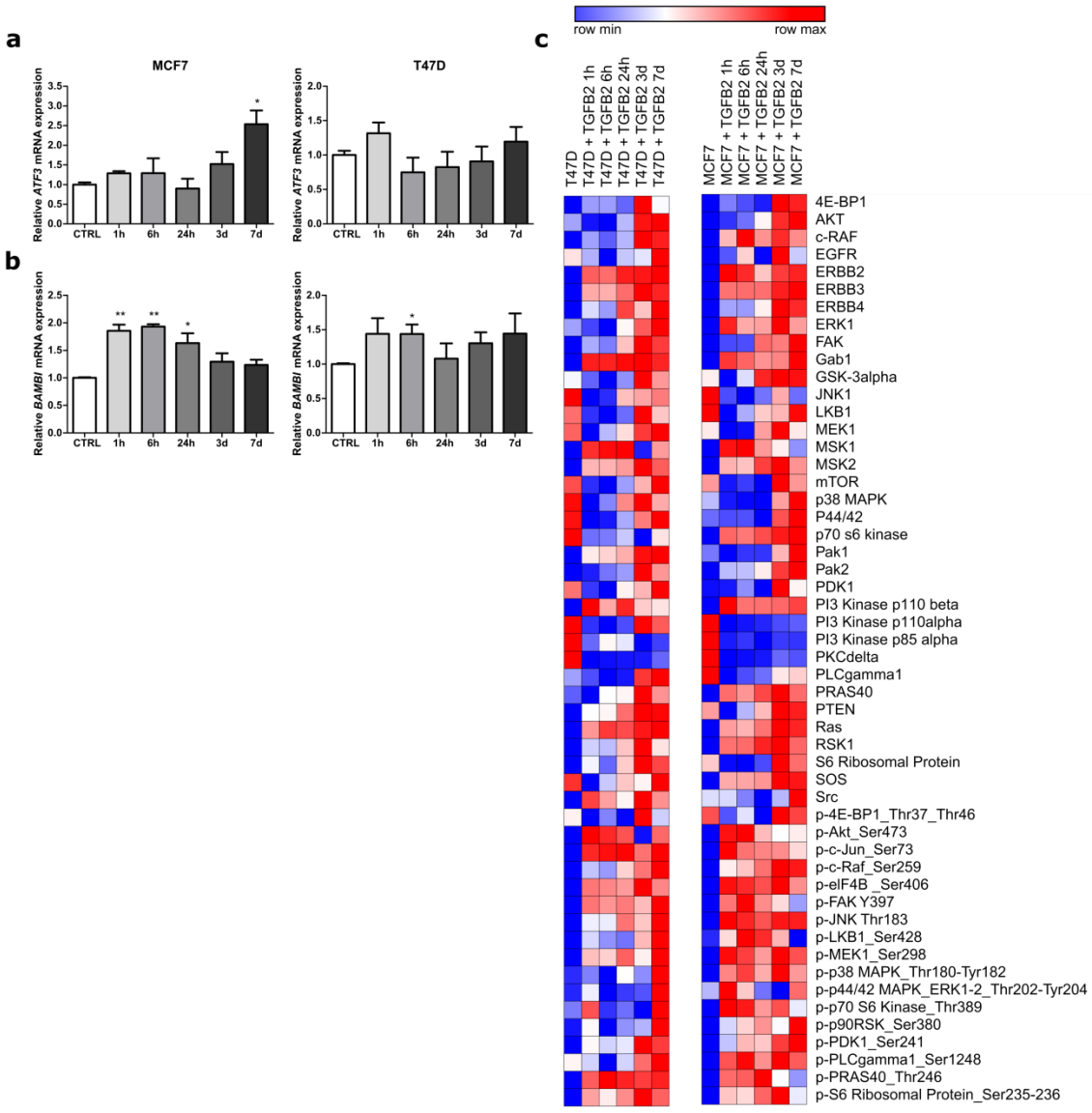

Figure 33: TGFβ2 stimulation affects ATF3 expression and PI3K-AKT-MAPK pathways activation

(**a**) Relative ATF3 mRNA levels determined by qRT-PCR in MCF7 under TGFβ2 stimulation for the indicated times. (**b**) Relative BAMBI mRNA levels determined by qRT-PCR in MCF7 under TGFβ2 stimulation for the indicated times. (**c**) Heatmaps of 35 total proteins and 18 phospho-proteins involved in PI3K-AKT-MAPK signaling pathway in MCF7 and stimulated with TGFβ2 for the indicated times. Log2 normalized signal intensities for each protein are plotted and color-coding refers to relative intensities in each row and each cell line independently.

4.1.11 ATF3 knockout effect on tumor growth *in vivo*

ATF3 knockout had a striking effect on proliferation, cell cycle progression and apoptosis *in vitro*. To assess if this effect was reproducible in an *in vivo* xenograft model, mice were injected with the two ATF3KO clones and their WT counterpart and treated with E2, TAM or Letrozole (LET) pellets. In presence of E2 all the mice in the 3 groups had to be sacrificed due to tumor progression, with the 2 ATF3 knockouts reaching the ethical limit relatively slower than the WT (Figure 34 a, Table 8).

Table 8: Percentage of and average time to sacrifice

	+ E2		**+ TAM**		**+ LET**	
	Percentage of mice sacrificed	Average time to sacrifice	Percentage of mice sacrificed	Average time to sacrifice	Percentage of mice sacrificed	Average time to sacrifice
WT	100%	64,4	33%	98,5	100%	65,8
KO1	100%	97	0%	NA	33%	106,5
KO2	100%	81,6	33%	122,5	50%	102,3

Under TAM treatment, similarly to what was seen *in vitro,* both the ATF3 knockouts showed slower proliferation. Astonishingly, all the mice injected with ATF3 KO1 displayed almost no growth when treated with TAM, with one mouse even showing complete remission (Figure 34 b). Even if less drastic, a growth delay was detected also in the KO2 (Figure 34 c). Here 2 mice had to be sacrificed because of the tumor size, like in the WT, but much later (Table 8). Additionally, of the mice still alive at the end of the experiments, the WT ones presented the biggest tumors, with the two KO having significantly smaller masses (Figure 34 d).

In the WT group no decrease in proliferation was detected in the LET-treated mice compared to the E2-treated ones (Figure 35 a). This can be explained by the fact that we did not used ovariectomized mice and the levels of estrogen available might be enough for the WT cells to sustain a normal proliferation. Notably however, the two ATF3 KO clones presented a slower proliferation (Figure 35 b-c). Specifically, four and three mice from the KO1 and KO2 groups respectively, did not reached the size limit by the end of the experiment, having comparable sizes to the TAM treated groups.

Altogether these data confirm the *in vitro* data and support the role of ATF3 in the regulation of resistance to endocrine therapy.

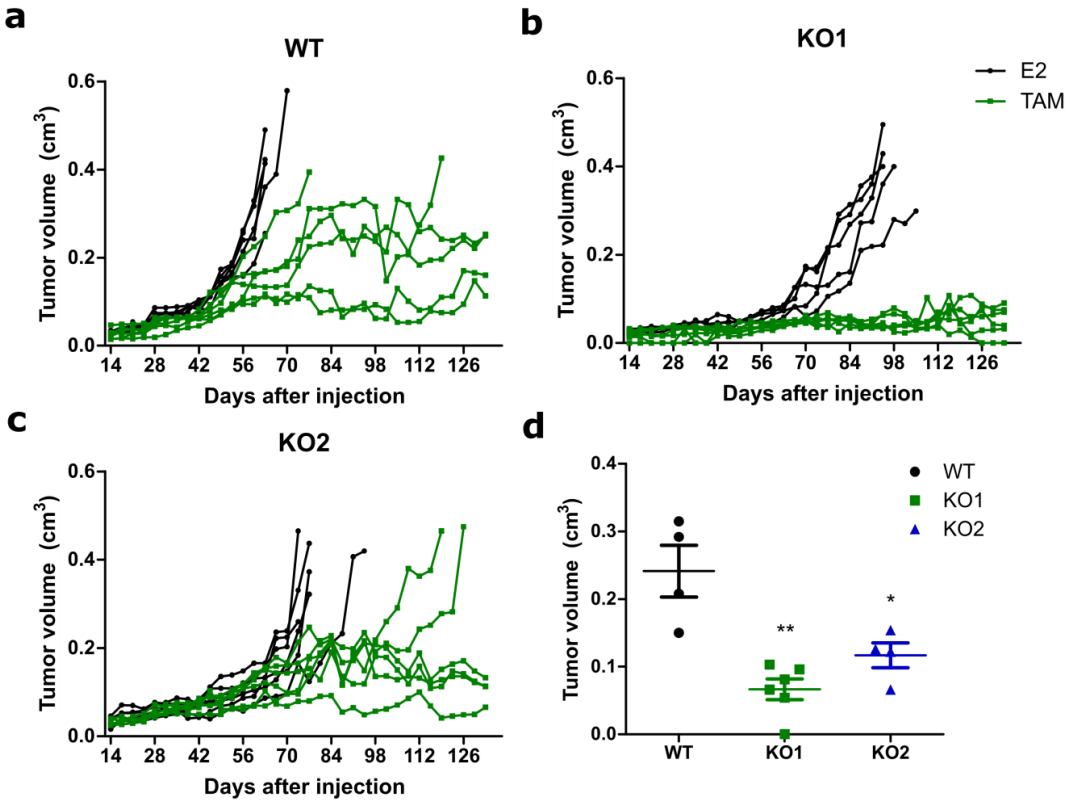

Figure 34: Tumor growth of ATF3 knockdown *in vivo* under TAM treatment
(**a**) Tumor volume in mice injected with MCF7 WT and treated with E2 or TAM for 120 days. (**b**) Tumor volume in mice injected with MCF7 ATF3KO1 and treated with E2 or TAM for 120 days. (**c**) Tumor volume in mice injected with MCF7 ATF3KO2 and treated with E2 or TAM for 120 days. (**d**) Tumor volume of mice still alive after 120 days of treatment. For tumor curves, each line represents a mice and each dot represents a measurement. For tumor volumes at the end, values are represented as mean ± SEM. *** p-value <0.001, ** p-value <0.01, * p-value <0.05

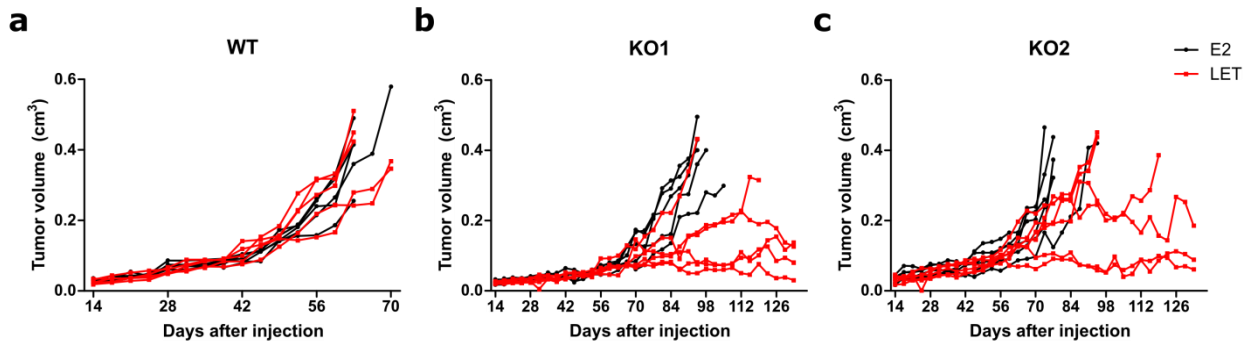

Figure 35: Tumor growth of ATF3 knockdown *in vivo* under LET treatment
(**a**) Tumor volume in mice injected with MCF7 WT and treated with E2 or LET for 120 days. (**b**) Tumor volume in mice injected with MCF7 ATF3KO1 and treated with E2 or LET for 120 days. (**c**) Tumor volume in mice injected with MCF7 ATF3KO2 and treated with E2 or LET for 120 days. (**d**) Each line represents a mice and each dot represents a measurement.

4.1.12 ATF3 expression in patients datasets

To evaluate the clinical relevance of the *in vitro* findings I decided to investigate ATF3 levels in publicly available datasets with gene expression data from patients treated with endocrine therapy. The GEO database contained 6 datasets suitable for analysis, having matched samples before and after therapy administration collected in different studies. Indeed, ATF3 was found significantly upregulated after therapy administration in 5 out of the 6 datasets (Figure 36 a-f). In all the datasets with more than one time point, ATF3 was mostly upregulated in the last (>90 days of treatment), while only in the GSE80077 ATF3 was already upregulated after 14 days of treatment.

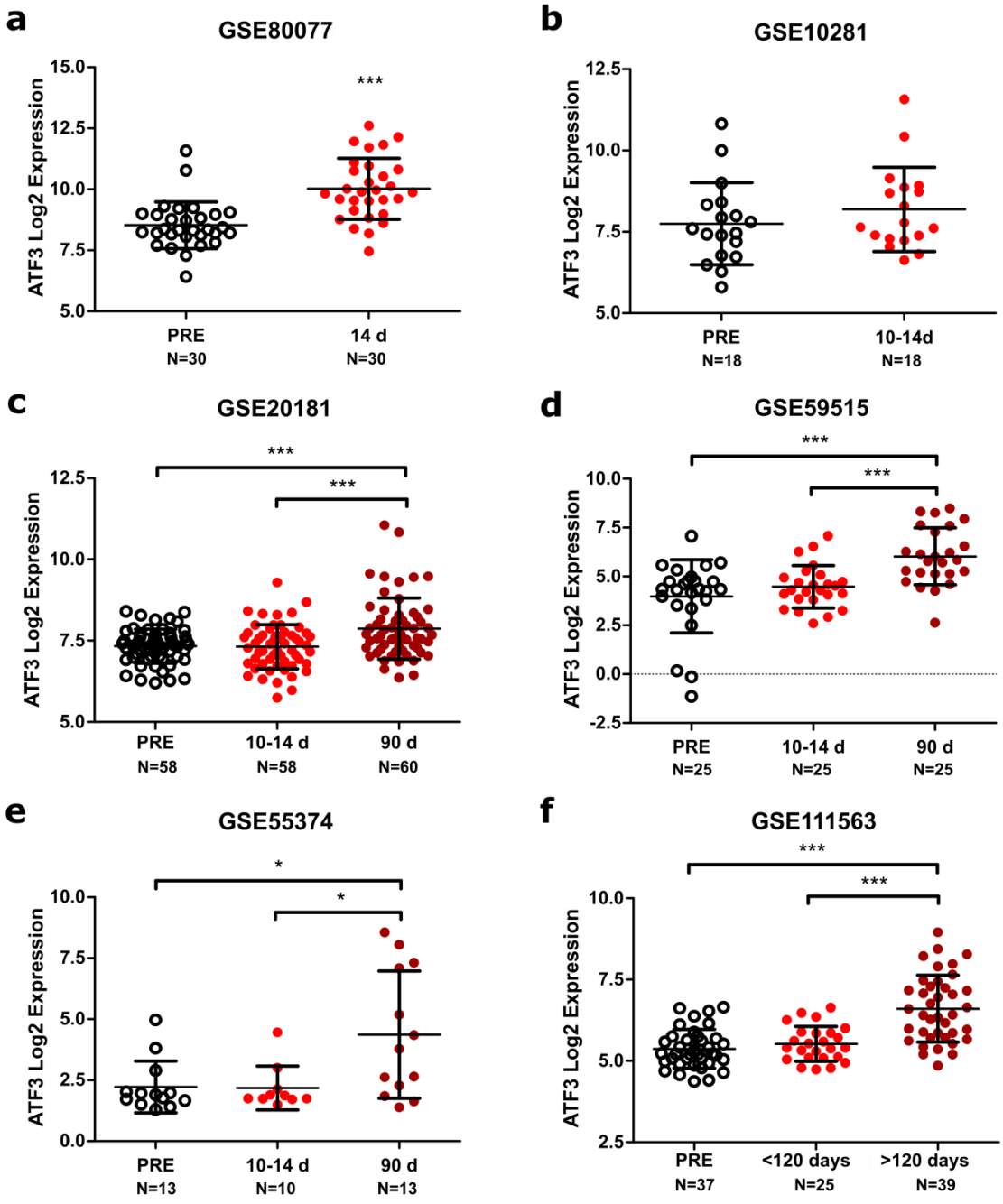

Figure 36: ATF3 expression in GEO datasets of patients treated with endocrine therapy
(**a**) ATF3 expression in GSE80077 dataset, made of matched tumors before and 14 days after tamoxifen or letrozole administration. (**b**) ATF3 expression in in GSE10281 dataset, made of matched tumors before and 10 to 14 days after letrozole administration. (**c**) ATF3 expression in GSE20181 dataset, made of matched tumors before, 10-14 and 90 days after letrozole administration. (**d**) ATF3 expression in in GSE59515 dataset, made of matched tumors before, 10-14 and 90 days after letrozole administration. (**e**) ATF3 expression in GSE55374 dataset, made of

matched tumors before, 10-14 and 90 days after letrozole administration. (**d**) ATF3 expression in in GSE111563 dataset, made of matched tumors before, in the first 120 days and after 120 days of letrozole administration. All values are represented as Log2 expression of the respective probe in individual patients ± SD. *** p-value <0.001, ** p-value <0.01, * p-value <0.05

Strikingly, when analyzing the gene expression data from GSE111563 with the GEO2R function, *ATF3* was found to be the top differentially expressed gene between the three time points (Table 9). Notably, many of the other top differentially expressed genes are predicted targets of ATF3, as well as upregulated genes in the early time points cell line model (*EGR1*, *DUSP1*, *FOSB*, *JUN*), corroborating the relevance of ATF3 in the regulation of the response to endocrine therapy. This finding suggested that a similar gene pattern was induced both in cell lines and patients biopsies. Indeed the early upregulated gene set (Figure 9) showed an enrichment in the treated samples compared to the pre-treatment biopsies in patients from GSE111563 (Figure 37). This overlap is a strong confirmation of the relevance of the cell line model used as recapitulate effectively *in vitro* the *in vivo* gene expression profiles of treated tumors.

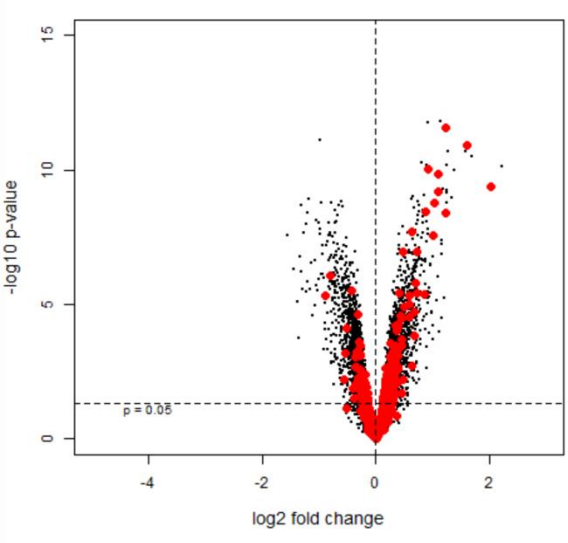

Figure 37: Early upregulated genes in GSE111563
Volcano plot of the early upregulated gene set (Figure 9) in the GSE111563 plotting the Log2 fold change between >120 days and pre-treatment time points. Red dots represent genes in the early upregulated gene set.

Overall these data confirm the increase in expression of ATF3 upon therapy administration and indicate the relevance of ATF3 in the clinical setting.

Table 9: Top 10 differentially expressed probes in GSE111563

ID	adj.P.Val	P.Value	Gene.symbol	Gene.title
ILMN_2374865	0.00000239	1.08e-10	ATF3	activating transcription factor 3
ILMN_2410145	0.00001972	1.78e-09		
ILMN_1735014	0.00003592	5.72e-09	KLF6	Kruppel like factor 6
ILMN_1751607	0.00003592	7.68e-09	FOSB	FosB proto-oncogene, AP-1 tran...
ILMN_1781285	0.00003592	8.12e-09	DUSP1	dual specificity phosphatase 1
ILMN_1762899	0.00005227	1.58e-08	EGR1	early growth response 1
ILMN_1720829	0.00005227	1.65e-08	ZFP36	ZFP36 ring finger protein
ILMN_1715984	0.00005493	1.99e-08	GREB1	growth regulation by estrogen in ...
ILMN_1806023	0.00005968	2.43e-08	JUN	Jun proto-oncogene, AP-1 transc...
ILMN_2197365	0.00007655	3.46e-08	RGS2	regulator of G-protein signaling 2

4.2. Part II: Barcoding of luminal A cell lines reveals treatment and cell-line specific mechanisms of endocrine resistance development

4.2.1 Barcoding of luminal A cell lines

Resistance to endocrine therapy can be mediated by different genetic and epigenetic alterations. Even though different molecular pathways and cellular processes have been correlated to this process, the mechanisms underlying the initiation and selection of resistant cells is still unknown. To address this question, I used a cellular barcoding approach by employing the ClonTracer library (Bhang *et al.*, 2015). This pooled barcode library, composed of more than 1 million unique barcodes, was used to tag MCF7 and T47D cells and track the clonal evolution of individual barcoded clones over the resistance development process (Figure 38). To do so, 100,000 cells were infected with the library with an extremely low MOI (0.05) to ensure the presence of a single barcode per each cell. The barcoded cells were then expanded to obtain sufficient cells to start the resistance development and to extract initial DNA as zero time point control. To be able to investigate the mechanisms of resistance, cells were cultivated for 8 months in presence of E2 as control, with 100nM TAM or without E2, each condition having five independent replicates. DNA from each replicate was then extracted, the barcodes were PCR amplified and sequenced (Figure 38).

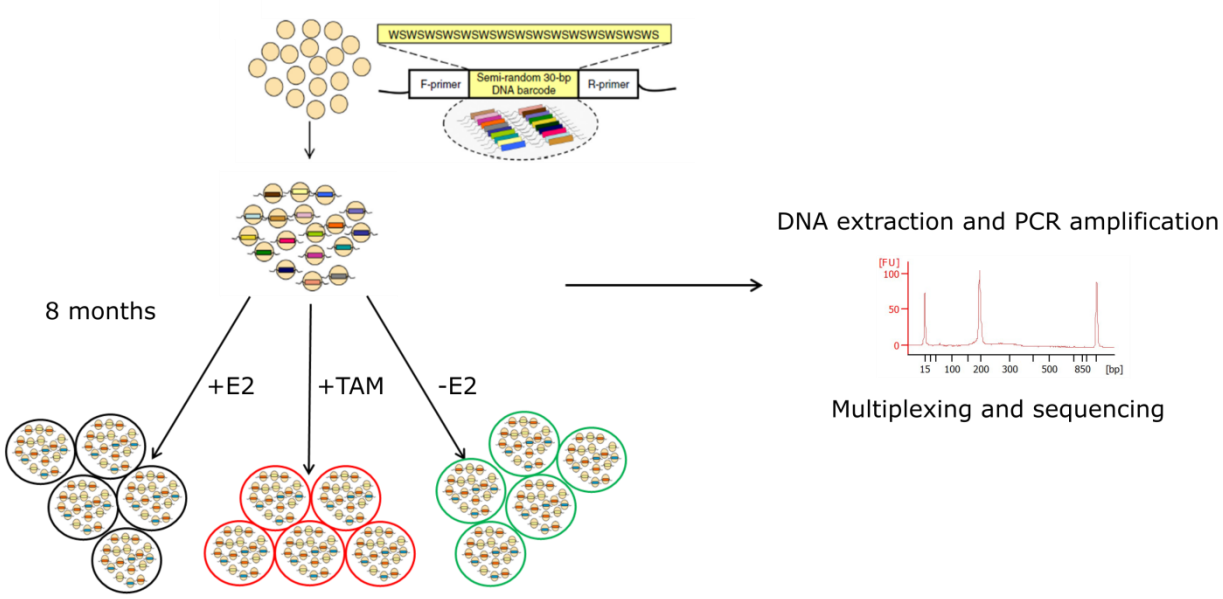

Figure 38: Schematic representation of the barcoding experiment
Scheme representing the steps used for the barcoding experiment: library transduction in MCF7 and T47D cells, chronic treatment for 8 months to induce resistance development in 5 independent replicates for each condition (+E2, +TAM, -E2), PCR amplification of the barcodes and DNA sequencing. (Modified from HE Bhang et al. 2015)

To assess the resistance development after 8 months of treatment, cells were tested in a proliferation assay over 7 days. For TAM treatment, the resistant cells treated with the drug showed significantly faster proliferation compared to the sensitive cells, even though they did not proliferate as fast as the untreated cells (Figure 39 a-b). To assess the estrogen deprivation effect in the sensitive clones, cell were pre-treated for 14 days as the proliferation arrest is delayed compared to TAM treatment. Indeed, sensitive cells showed almost no proliferation when deprived of E2, while resistant cells showed active proliferation, even if slower than the untreated sensitive cells (Figure 39 c-d). This data indicate that the treated clones in both cell lines had acquired resistance to both TAM and E2 deprivation after 8 months of chronic treatment.

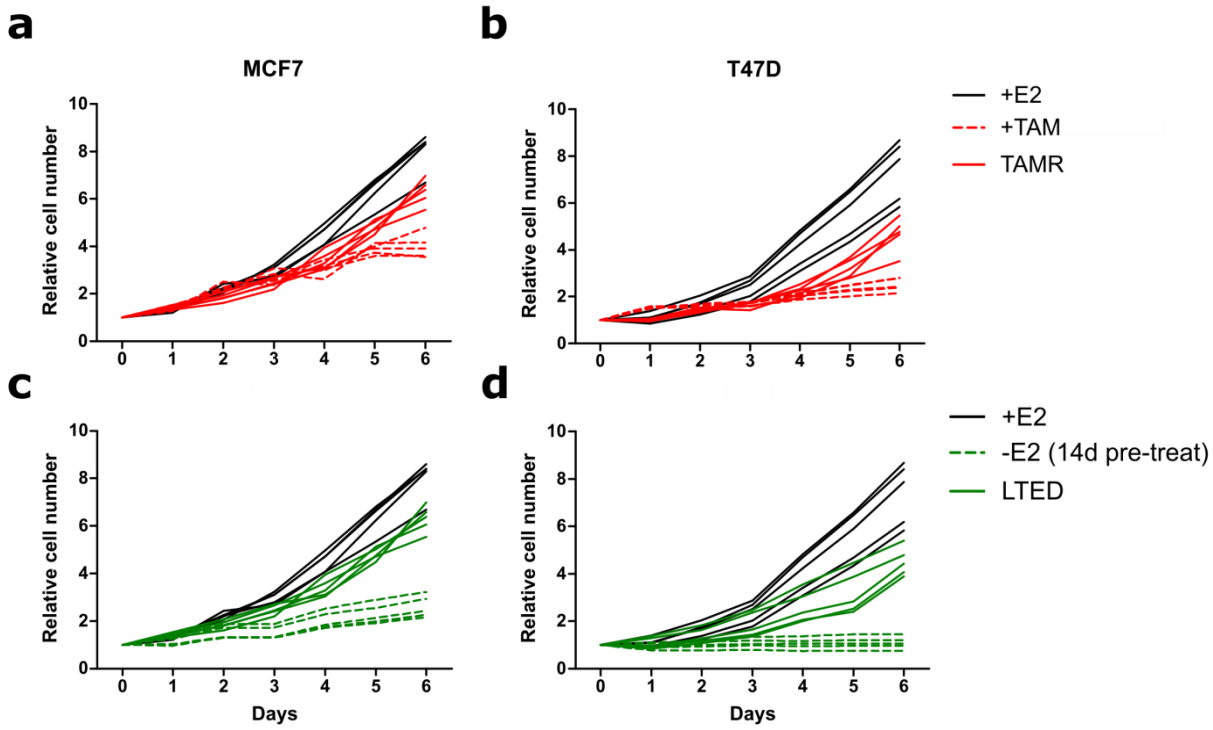

Figure 39: Proliferation of barcoded MCF7 and T47D
(**a**) Cell proliferation of barcoded MCF7 (treated for 6 days with E2 or TAM) and TAMR cells (treated with TAM) measured as RFP positive cells with fluorescent microscopy. (**b**) Cell proliferation of barcoded T47D (treated for 6 days with E2 or TAM) and TAMR cells (treated with TAM) measured as RFP positive cells with fluorescent microscopy. (**c**) Cell proliferation of barcoded MCF7 (treated with E2 for 6 days or deprived from E2 14d before the assay) and LTED cells (deprived form E2) measured as RFP positive cells with fluorescent microscopy. (**d**) Cell proliferation of barcoded T47D (treated with E2 for 6 days or deprived from E2 14d before the assay) and LTED cells (deprived form E2) measured as RFP positive cells with fluorescent microscopy. Each line represents the mean of 5 technical replicates for every independent clone.

4.2.2 Sequencing of resistant clones reveals different drug selection mechanism

Once the treated clones showed an increase in proliferation under treatment, indicating acquired resistance, the barcodes were sequenced to investigate the clonal dynamics. Five replicates of the initial DNA collected before the treatment administration were used as controls. The NGS data analysis was performed in collaboration with Dr. Luca Penso Dolfin

(Goncalves group, DKFZ). As expected, since all the samples were sequenced at the same sequencing depth, a similar number of reads was recovered from each of the individual replicate in both MCF7 and T47D (Figure 40 a-b). Since roughly 100,000 cells had been infected, the number of unique barcodes found in the initial population was as expected in MCF7, with 110-115,000 barcodes in the five replicates. A lower number of different barcodes was sequenced in T47D, ranging between 35 and 45,000 individual barcodes in every replicate (Figure 40 c-d). As expected, all treated replicates showed a large decrease in the number of unique barcodes in both cell lines. However an unforeseen consistent reduction was present in the E2 treated clones as well, probably caused by selection of fast growing clones in plastic and loss of complexity during cell passaging (Figure 40 c-d).

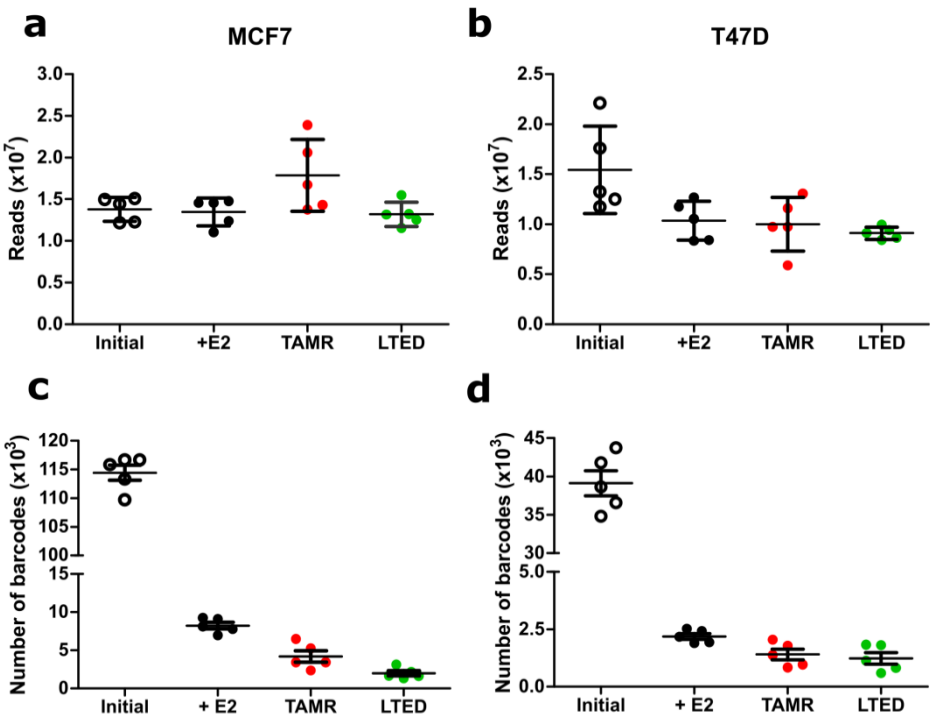

Figure 40: Number of reads and unique barcodes in barcoded cells
(**a**) Absolute number of reads retrieved from sequencing of barcoded MCF7. (**b**) Absolute number of reads retrieved from sequencing of barcoded T47D. (**c**) Number of unique barcodes in barcoded T47D (**d**) Number of unique barcodes in barcoded T47D. Data represented as mean ± SD. Each dot represents an independent replicate

To assess the similarity between replicates, we checked the percentage of shared barcodes in the replicates having been treated in the same conditions. As expected, in the initial population a high number barcodes was shared, with >90% of the barcodes being in common between at least 2 replicates and around 50% shared between 4 or 5 replicates, in both MCF7 and T47D. In the replicates kept in presence of estrogens, the number of shared barcodes decreased, with around 50% being shared by at least 2 replicates. In the treated condition in both cell lines, this loss of shared barcodes was even higher, with only around 25% of the barcodes being shared by at least 2 replicates. When considering only the barcodes shared among all the replicates, the percentages drastically dropped to 1-5% in all the treated conditions. This suggests that the effect of the drug is likely not selecting specific clones but a stochastic enrichment of barcodes is taking place in each replicate.

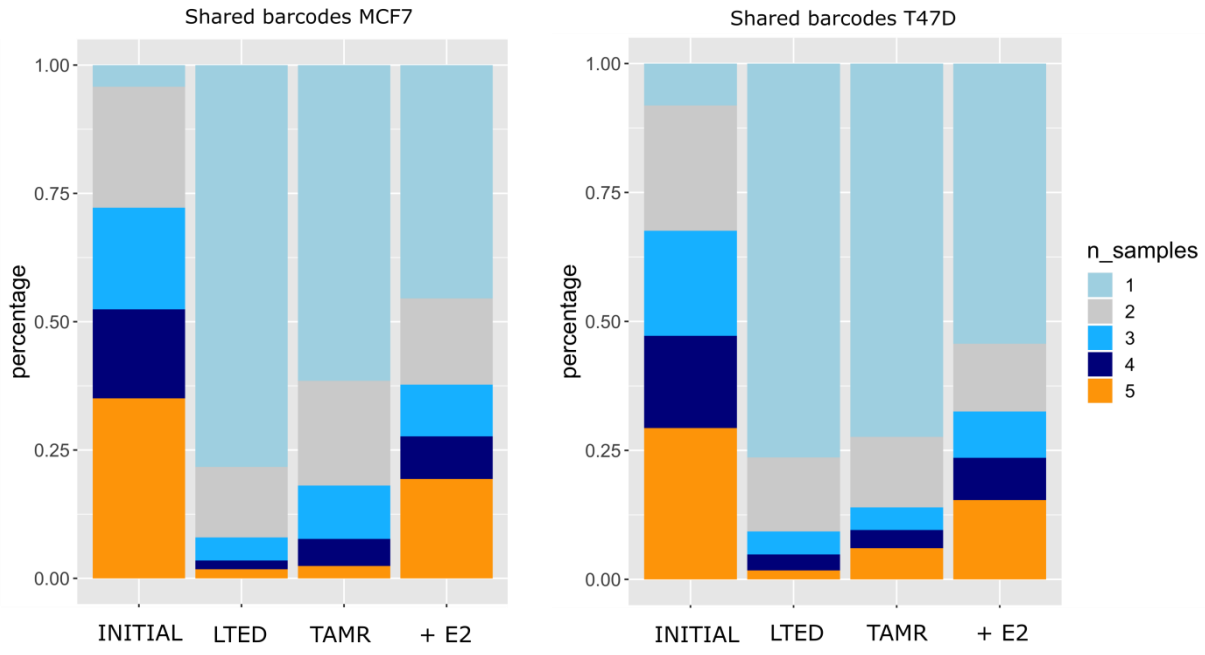

Figure 41: Percentage of shared barcodes between replicates
Percentage of shared barcodes between the five replicates of the initial sample and each treatment group. Left panel represent MCF7, right panel represents T47D.

Since the frequency of specific barcodes in the populations within replicates can have high variations and low frequency barcodes can influence the results, the number of enriched

barcodes compared to the initial population was calculated. A barcode was defined enriched if it was present in the sample in a frequency higher than the most frequent barcode detected in the initial samples. In MCF7 the replicates treated with E2 had around 100 enriched barcodes, on average slightly more than the TAMR clones, that presented with a higher variance. In contrast, the LTED replicates had only few enriched barcodes with one clone even having as little as 2 enriched barcodes (Figure 42 a). In T47D the number of enriched barcodes in the untreated replicates was around 20, while both resistant populations having not more than 10 enriched barcodes (Figure 42 b).

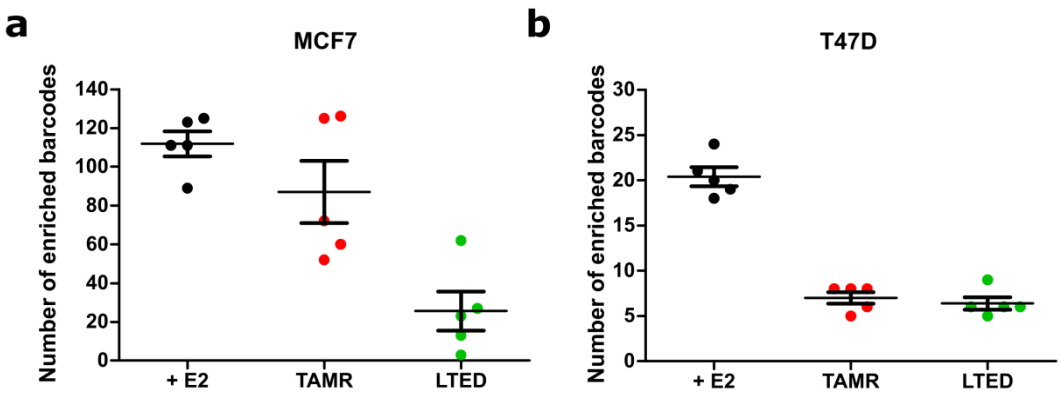

Figure 42: Number of enriched barcodes in barcoded cells
(**a**) Number of enriched barcodes in the MCF7 clones. (**b**) Number of enriched barcodes in the T47D clones. Data represented as mean ± SEM. Each dot represents an independent replicate

The enriched barcodes comprised most of the total cell population. In the control population (cells kept in presence of E2), few barcodes were enriched in all replicates of both cell line systems. This could be expected, as even without treatment some intrinsically more proliferative clones might take over the population over time. The selective pressure caused by endocrine treatments highly affects these numbers in different ways in the two cell lines and with the two distinct treatments. In MCF7 LTED all 5 replicates present different enriched barcodes, with only few shared between 2 replicates. This shows an apparent stochastic enrichment of barcodes in each replicate, with no selection of pre-resistant clones. Also in the

MCF7 TAMR replicates the vast majority of the enriched barcode were not shared, however there were indeed 25 barcodes, accounting for 10% of the total number of enriched barcodes, that were recurrent in 3 or 4 replicates indicating that these indeed had been selected under treatment pressure. In T47D both treatments presented enriched barcodes that were shared among all replicates. In T47D LTED only one barcode was shared, with the rest of the enriched barcodes being present only in 1 or 2 replicates. In T47D TAMR just 2 barcodes were highly enriched and recurrent in all replicates. An additional 4 barcodes were shared between 3 or 4 replicates. These results suggest that in T47D a clear selection of pre-resistant clones had taken place.

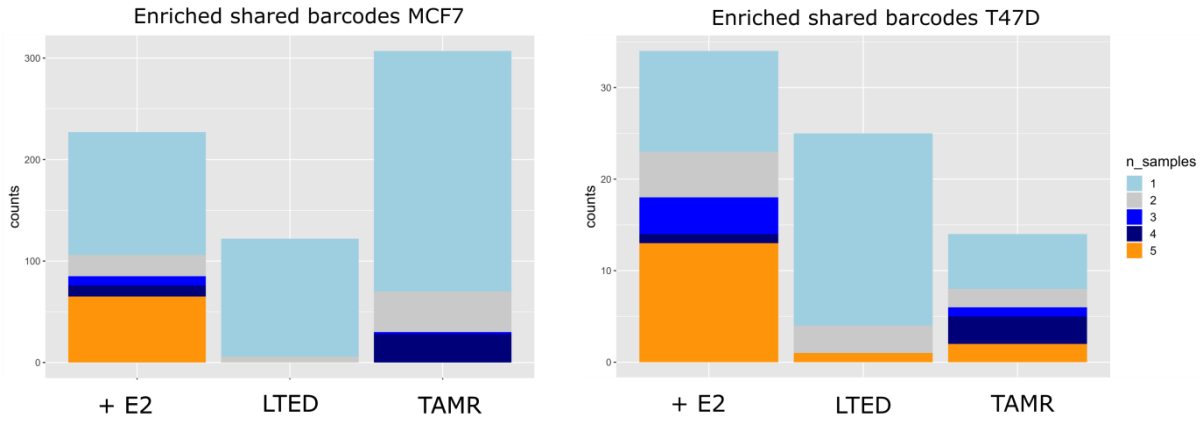

Figure 43: Number of enriched shared barcodes between replicates
Number of enriched barcodes shared between the five replicates of and each treatment group. Left panel represent MCF7, right panel represents T47D.

To investigate deeper the contribution of individual barcodes to the resistant pool and thus the mechanism of resistance development, we next investigated the frequency of the enriched barcodes and the commonalities between treatments. For a meaningful visualization, two different color coding regimes were applied: in MCF7 the top 5 barcodes of each resistant replicate were color-coded, while in T47D the top 25 enriched barcodes in the resistant clones overall.

In MCF7 TAMR several barcodes contributed to the final pool. To our surprise, the top enriched barcodes of each replicate were different compared to the other replicates, indicating that different clones were selected. However no barcode presented a high enrichment and all the enriched barcodes contributed in small percentage to the pool.

As expected from the number of enriched barcodes from Figure 42, in MCF7 LTED the situation was completely different. Here few barcodes contributed to the vast majority of the pool, with replicate 5 being almost completely derived from a single cell. All the enriched barcodes were different among the replicates, confirming the stochasticity of the selection process.

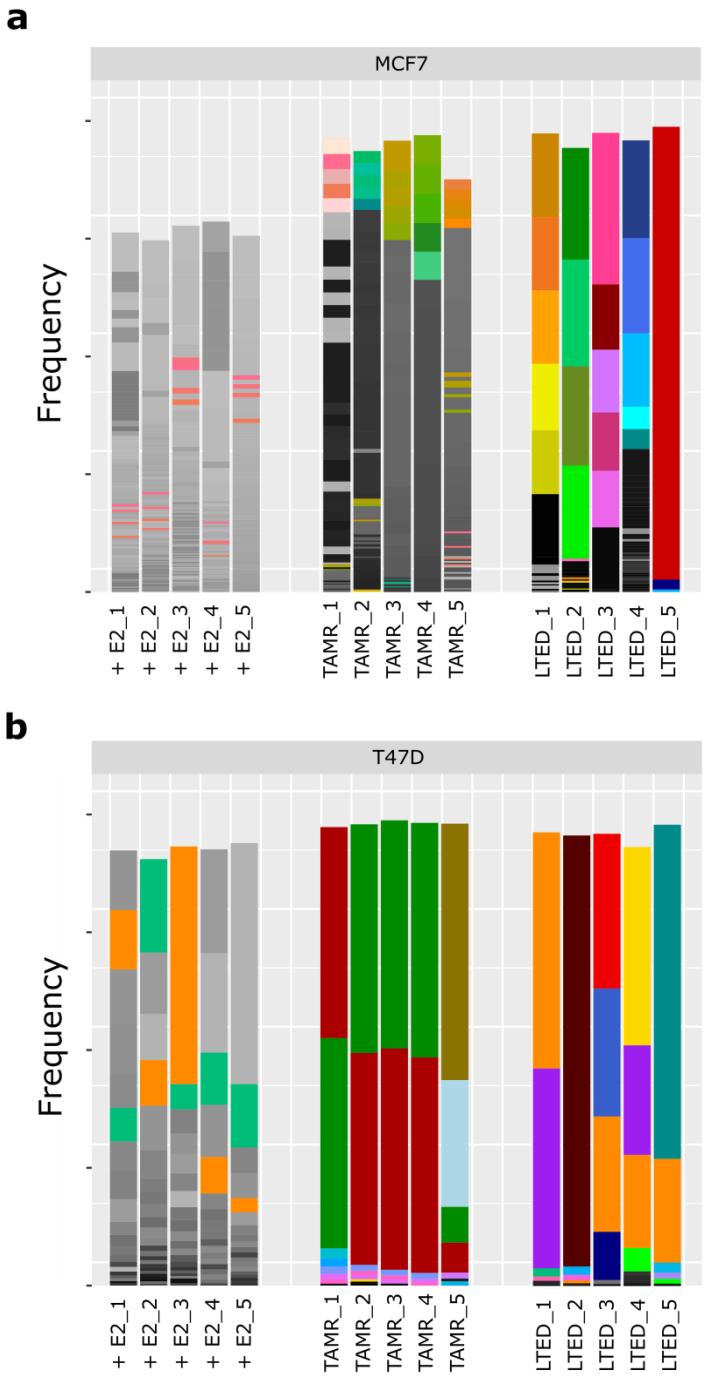

Figure 44: Individual barcodes sharing among treatments and replicates
(**a**) Frequency of individual barcodes in each replicate of MCF7. (**b**) Frequency of individual barcodes in each replicate of T47D. In MCF7 the top 5 barcodes for each replicate in the TAMR and LTED conditions are differentially color-coded. In T47D the overall top 25 barcodes in the TAMR and LTED conditions are differentially color-coded.

Interestingly, in T47D TAMR four replicates were composed mostly of two barcodes, while the TAMR_5 had higher enrichment of 2 other barcodes. This replicate however presented also the same 2 shared barcodes of the other replicates but in much lower frequencies. Notably, also lowly enriched barcodes were shared among 3 or 4 replicates. This data indicates that in T47D TAMR a selection of pre-resistant clones took place as the barcodes are shared among replicates.

Finally, T47D LTED displayed an even different scenario. All of the replicates shared one barcode that contributed differently to the pool proportion (from 50% in replicate 1 to 1% in replicate 2). This barcodes was however enriched also in the E2 treated cells therefore having a proliferating advantage over other clones that was thus not only related to resistance. The other highly enriched barcodes were different in each replicates, with the exception of the violet one, that was shared between clone 1 and 4. As in the MCF7 LTED, one of the replicates was almost completely derived from a single clone. These data indicate that in T47D LTED there is both stochastic selection and enrichment of pre-resistant clones.

Overall the analysis of shared barcodes among replicates and their enrichment revealed different mechanisms of resistance development. Each cell line and each treatment displayed a unique clonal profile that remark the complexity of the clonal selection in the resistance process.

As the enrichment of the same two barcodes in T47D TAMR replicates hinted to a specific selection of clones, I decided to rule out the possibility that this selection was driven by the viral integration and consequent disruprion of a specific gene locus. To address this, we applied S-EPTS/LM-PCR, performed by Genewerk (Schmidt et al. 2001) using one of the T47D TAMR samples (3), one control (+E2_2) and the T47D LTED_2, that was characterized by a dominant clone. The analysis of T47D TAMR_3 identified two insertion sites in chromosomes 6 and 8, with a frequency of 0.58 and 0.34 respectively (Table 10). These frequencies are in contrast with the results from the barcode DNA seq and indicate that the two barcodes integrated in distinct cells. Additionally, the insertion loci are not mapping to coding or regulatory regions therefore making the viral integration sites the driving cause of selection highly unlikely. The

analysis of T47D LTED_2 revealed that the dominant clone had the barcode integrated in chromosome 4 (Table 10). Also in this case, the insertion site was several kilobases away from any coding region or regulatory element.

These data indicate that the viral integration sites did not disrupt any known coding or regulatory region, therefore allowing us to exclude this as a driving force in the clonal selection.

Table 10: Integration site analysis

Integration site	T47D TAMR_3 Freq.	T47D LTED_2 Freq.	T47D +E2_2 Freq.
Chr 6: 120,131,260	0.579	NA	0.000164
Chr 8: 66,103,520	0.342	NA	NA
Chr 4: 112,000,728	NA	0.999	0.000937

4.2.3 Pathway activation profiling of individual replicates

Since the replicates inside a treatment group had different enriched barcodes and were thus derived in most cases from different cells of origin, I wanted to investigate if they had acquired different alterations in pathway activities during the resistance development process. To address this and to identify the differences between replicates and treatments at the functional level, I used RPPA to screen pathways known to be involved in resistance development, as WNT, MAPK and PI3K/AKT. WNT pathway was characterized by probing 12 proteins. The screening of MCF7 cells revealed an upregulation of WNT pathways in all the TAMR replicates, characterized by the high expression of total and phospho β-catenin, CSNK1E, DKK1 and CSNK2B, and the low expression of the negative regulator CTNNBIP1 (Figure 45 a). MCF7 LTED cells, instead, displayed different profiles, with LTED_5 having high upregulation in all the proteins in the WNT pathway, LTED_ 1 and LTED_4 with a partial upregulation, and LTED_2 and LTED_3 showing a downregulation, with low levels of most of the proteins and high levels of

the negative regulator CTNNBIP1 (Figure 45 a). T47D resistant cells showed a lower WNT pathway activity of resistant cells compared to MCF7. Also in T47D, TAMR replicates showed similar profiles, while LTED had higher differences. Of note, LTED_2 showed a distinct profile, with upregulation of activators of the WNT pathway and downregulation of CTNNBIP1 (Figure 45 b).

Another pathway screened was PI3K/AKT/mTOR pathway. While this pathway was not active in MCF7 treated with E2, as indicated by high levels of the negative regulator PTEN, all the TAMR replicates showed activation of the pathway, with upregulation of phosphorylated S6, p90RSK, 4E-BP1, p70, NF-kB and EIF4B. Additionally, TAMR_3 and 4 also presented a specific upregulation of the PRAS40 branch of the AKT pathway (Figure 45 c). Also in this pathway LTED cells showed distinct profiles. Replicate 5 displayed an over-activation of the PI3K/AKT/mTOR pathway with most of the proteins showing high intensities and a parallel inactivation of PTEN. LTED_3 and 4 had no activation in most of the proteins and high levels of the negative regulator PTEN, while LTED_1 and 2 showed intermediate profiles (Figure 45 c). As several clones contribute to these replicates, this intermediate profile could indicate that the individual clones might have different pathway activation profiles. In T47D, E2 treated cells showed a more active PI3K/AKT/mTOR pathway as baseline, but specific changes were detected in the replicates of resistant cells. Of note, the only phospho-protein consistently upregulated the resistant replicates was pPDK1, however downstream effector proteins showed mixed profiles. While in TAM the PI3K/AKT/mTOR pathway was at similar levels compared to the E2 treated cells (or higher for specific branches like PRAS40), LTED replicates displayed a general downregulation, apart from the levels of pAKT. Interestingly LTED_2 showed high levels of total and phospho 4E-BP1, showing a potential dependency on this branch of the AKT pathway (Figure 45 d).

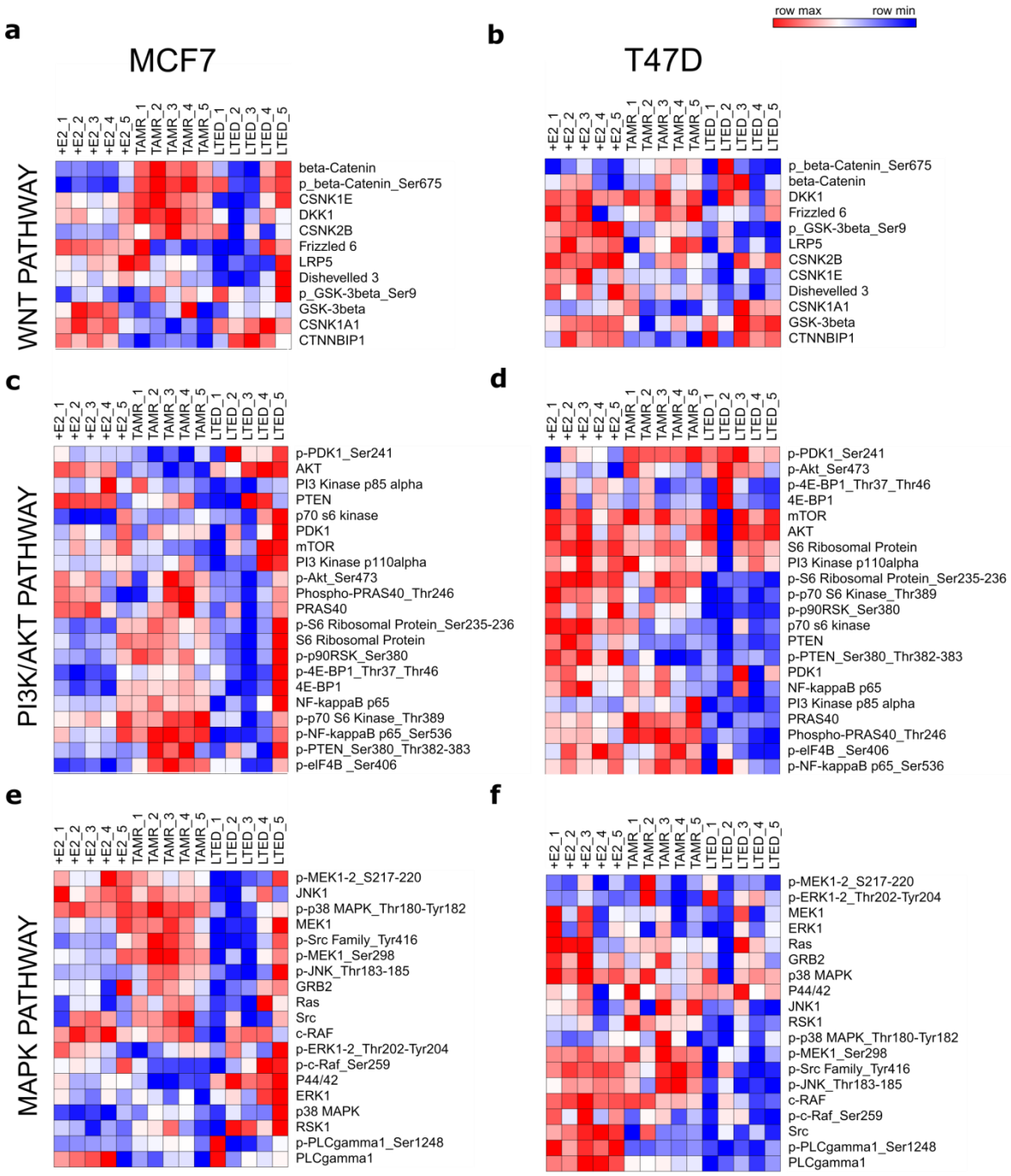

Figure 45: **Heatmaps of RPPA-screened pathways**
(**a-b**) Heatmaps of 12 proteins and phospho-proteins involved in WNT signaling pathway in MCF7 and T47D. (**c-d**) Heatmaps of 21 proteins and phospho-proteins involved in PI3K/AKT signaling pathway in MCF7 and T47D. (**e-f**) Heatmaps of 19 proteins and phospho-proteins involved in MAPK signaling pathway in MCF7 and T47D. Log2 normalized signal intensities for each protein are plotted and color-coding refers to relative intensities in each row independently. Proteins are ordered by hierarchical clustering.

Finally, MAPK pathway analysis revealed an overall upregulation in all replicates of MCF7 TAMR as depicted by high intensities of central kinases (Figure 45 e). As before, in MCF7 LTED cells replicate number 5 (mostly derived from a single cell of origin), showed an upregulation of the pathway, suggesting that this replicate has redundant mechanisms for promoting resistant features. LTED_4 displayed partial upregulation while the other 3 replicates had low levels of most of the proteins in the pathway. Notably, however, LTED_1 showed specific upregulation of PLCγ, indicating a possible peculiar mechanism of resistance in at least one of the 6 highly enriched clones in this replicate (Figure 45 e). T47D, instead, presented a general downregulation of the MAPK pathway, yet with focal upregulation in central kinases. Examples are upregulation of pMEK and ERK in TAMR_2 and LTED_1 or pMEK, pSRC and pJNK in TAMR_3 and 4. While LTED showed a downregulation of MAPK pathway overall, LTED_2 seems to still have higher activities compared to the other replicates as indicated by the high intensities of many phospho-proteins.

Overall the RPPA screening revealed general treatment-specific changes in the resistant replicates as well as replicate-specific ones that might indicate different mechanisms of resistance. The differences in pathway activation are frequently reflecting distinct barcode compositions as for MCF7_LTED5 and T47D_LTED2 (Figure 44) that support the theory of independent mechanisms of resistance development based on the clonal selection.

5. Discussion

Resistance to endocrine therapy in breast cancer is an urgent clinical problem that affects around 40% of the luminal patients. Recent developments allowed the use of new second line treatments that helped improving the prognosis, but the mortality rate for relapsing patients remains extremely high. The limited understanding of the mechanisms underlying resistance development requires greater efforts to identify new targetable genes and pathways involved in the process. In this view, I aimed to identify novel targets through a longitudinal screening during the development of endocrine resistance in ER positive cell lines. This led to the identification of ATF3 as a driver of the resistance process, being involved in the rewiring of MAPK pathway. This study indeed shows that interfering with this gene can increase the sensitivity to endocrine therapies and re-sensitize resistant cells. In addition, in this thesis I also addressed the role of clonality in the resistance process using a barcoding technique. This approach revealed that the resistance mechanism is complex and one general rule cannot be applied to all patients and treatments.

5.1. Longitudinal profiling reveals ATF3 as a potential mediator of resistance

Studies that aim to recapitulate *in vitro* the resistance development commonly focus on resistant cell line models and compare these to their sensitive counterpart. This approach has revealed numerous key alterations involved in resistance development and has led to the development of new therapeutic approaches. However there is a lack of knowledge regarding genes responsible for the survival of the cells to the acute cytotoxic effect of the drugs and the rewiring of their molecular features. From a therapeutic perspective, it is essential to understand the drivers of the resistance phenomena, rather than the downstream alterations, to be able to propose new first-line targets that can help delay the resistance development or

prevent it at all. In this view a deep understanding of the early phases of the treatment may help pinpoint causes and effects, and how they are connected. This approach indeed identified a novel candidate, ATF3, as a central player in this process. Activating Transcription Factor 3 (ATF3) is a transcription factor of the ATF/cAMP responsive element binding (CREB) family and is involved in several cellular responses. ATF3 is expressed at low levels in baseline conditions, but has been shown to be rapidly induced by stress signals to alter several cellular processes relevant to cancer progression (Hai et al. 1999; Gokulnath, Partridge, and Selvamurugan 2015; Ameri et al. 2007). Two different isoforms of ATF3 have been reported in the literature. The long and most abundant isoform, commonly referred to as ATF3, has been shown to homo- or hetero-dimerize with other proteins, as reported in Table 11.

Table 11: Binding partners of ATF3 and dimers' role in physiology

Jun	Th1 differentiation
mP53	Suppressed oncogenic function
p53	Repressed MMP2
	MDM2 mediated degradation
c-FOS	Osteoclast differentiation
c-Jun	Neurite sprouting
	Breast cancer progression
Smad3	Enhanced TGF-β mediated EMT and metastasis
Runx2	Breast cancer metastasis
HDAC	Transcription repression
Stat1	Enhanced hepatocyte apoptosis and pancreatic β-cell apoptosis
FHL2	Regulation of liver cell proliferation and regeneration
Tip 60	Increased HAT activity
ATF4	Stimulated NOXA activation
C/EBPβ	Induced apoptosis via NAG-1 in colorectal cancer
Nrf2	Transcriptional repression
CHOP10	Transcriptional activation

The role of ATF3 in the regulation of transcriptional activity depends on the binding partner and the promoter context. As an example, binding of ATF3 to JUN or JUND usually represses transcription, while its dimerization with JUNB can have both active and repressive roles (Thompson, Xu, and Williams 2009). The shorter isoform (ATF3ΔZip) has been reported to not bind to DNA, therefore suggested to mostly act by sequestration of co-factors and subsequent stimulation of transcriptional activity (B. P. Chen et al. 1994; Hashimoto et al. 2002).

Due to its potential dual role, ATF3 has been found to have different effects on cancer progression. In prostate cancer ATF3 expression has been correlated with worst prognosis and its overexpression has been associated with increased proliferation and metastasis formation (Pelzer et al. 2006). Similarly, ATF3 was reported to promote cell invasion and contribute to tumor spreading in colon cancer (Ishiguro et al. 2000). Additionally, ATF3 knockdown has been proved to impairs Hodgkin Lymphoma as well as glioblastoma and lung cancer cells growth and viability (Janz et al. 2006; MA et al. 2015; Xuebing Li et al. 2017). On the other hand, several studies reported and oncosuppressive roles of ATF3. Its overexpression in liver cancer and hepatocellular carcinoma cells reduced proliferation and motility, while increasing induced apoptosis (Chen *et al.*, 2018; Li *et al.*, 2018). Other reports showed ATF3 as inhibitor of invasion and migration both in colorectal cancer and ovarian cancer cells (Inoue et al. 2018; Bottone 2005; Syed et al. 2005). It thus seems that the role of ATF3 in cancer progression is highly context dependent and tumor-type specific.

In breast cancer ATF3 has been mostly characterized as an oncogene. The ATF3 gene maps to chromosome 1q32.3 in the q1 amplicon. The q1 amplicon is amplified in around 53% of all breast cancers being the most amplified region in breast cancer (Middleton et al. 2018). Overexpression of ATF3 was able to induce spontaneous lesion in the mammary glands via upregulation of the WNT/β-catenin pathway and to promote cancer-initiating features in immortalized mammary epithelial MCF10A cells via the TGFβ pathway (Wang et al. 2008; Yan et al. 2011; Yin et al. 2010). Additionally higher expression of ATF3 has been correlated with worst overall survival in breast cancer (Cao, Yang, and Jiang 2013). ATF3 has been investigated also in the context of chemotherapy and radiotherapy, with surprisingly opposite roles. While being

upregulated upon both treatments, in chemotherapy it has been described as a mediator of cytotoxicity, whereas regulating resistance to treatment with radiotherapy (W. Zhao et al. 2018; Hasim et al. 2018).

Considering this, it was not surprising to find ATF3 among the upregulated genes in response to endocrine therapy treatment. Of particular relevance was the fact that ATF3 was not just increased in the resistance cells, but throughout the process of resistance development as well. Indeed the time-resolved profiling allowed us to discriminate between gene clusters with different behaviors during the resistance process. Notably ATF3 was also a predicted regulator of several genes that shared with ATF3 the peculiar profile of being upregulated after short-time therapy administration. Several of these genes have been reported to be induced by endocrine therapy administration and resistance, as *SOX2*, *DUSP10* and *TGFB2* (Hrstka et al. 2016; Piva et al. 2014; Brandt et al. 2003). Another striking example is the AP-1 complex which is well characterized as a mediator of endocrine resistance development (Malorni et al. 2016; He et al. 2018). Indeed both immediate early stress-response genes *FOS* and *JUN* were upregulated early in my TAMR and LTED systems. The encoded proteins are not only binding partners of ATF3, but are also ATF3 target genes, as predicted by TF binding site analysis based on the MSigDB database. Additionally, it has been shown by ChIP-seq that ATF3 not only localizes to ATF3 TF/CRE motifs (5'-TGACGTCA-3') but also the AP-1 sequence (5'-TGASTCA-3', S = C/G) therefore indicating that that AP-1 and ATF3 could act together in promoting resistance development (J. Zhao et al. 2016).

5.2. ATF3 mediates resistance to therapy through regulation of the MAPK signaling pathway

The findings that ATF3 was upregulated upon treatment stress and might mediate the expression of several other genes involved in the MAPK pathway let to the hypothesis that this gene is a central player in resistance development. To test this I applied different approaches to modulate ATF3 expression as siRNA induced RNA interference, shRNA downregulation,

CRISPR/Cas9 knockout, and lentiviral overexpression. Indeed ATF3 knockdown with siRNA highly affected cell viability and proliferation in MCF7 and T47D, but the effect was not limited to the treated condition. The physiological role of ATF3 varies in different cells, but it is a central protein in the regulation of the stress caused by DNA-damage repair and cell cycle progression (Rohini, Haritha Menon, and Selvamurugan 2018). Additionally upon environmental stress, ATF3 expression increases to mediate the transcription of downstream genes and allow the cell to cope with harming stimuli. This could be the reason of the high toxicity of the RNAi approach, in which the stress caused by the method itself and the knockdown of ATF3 can cooperate towards the fatal phenotype detected.

Due to the difficulty to interpret RNAi results I moved to a stable knockout approach using CRISPR/Cas9. CRISPR/Cas9-induced double strand breaks can be repaired by non-homologous end joining (NHEJ) or by homology directed repair (HDR) if a template is present (Mao et al. 2008; Ran et al. 2013). While NHEJ is the preferred method for non-dividing cells, after one of the allele is repaired with this method, this could be used as a template for the HDR if Cas9 is still present and actively cutting while the cells divide. This mechanism allows obtaining homozygous mutations and indeed single-clone-derived homozygous biallelic ATF3 knockout, carrying the same mutation in both the alleles, were successfully obtained from MCF7. In contrast, no viable knockout clones were retrieved from T47D even after several attempts performed by me as well as by a collaborator at the Weizmann Institute of Science. T47D express higher levels of ATF3 compared to MCF7 cell line (The Human Protein Atlas) and might be dependent on this transcription factor for survival. Therefore, I decided to proceed with the validation of the role of ATF3 kncokout using MCF7. While the ATF3 knockout clones had similar proliferation, cell cycle and apoptotic rate compared to the WT in normal growth conditions, under stress all these processes were drastically affected. Indeed ATF3 knockout caused a strong decrease in proliferation as well as in the number of actively cycling cells under TAM and E2 deprivation, thus increasing the phenotypic effects of treatments in the cells. At the same time the apoptosis rate increased, further supporting the role of ATF3 in regulating stress response. These results are in line with recently published data on the role ATF3 in radioresistance in MCF cells, therefore reinforcing the understanding of ATF3 in treatment

response in breast cancer (W. Zhao et al. 2018). Additionally ATF3 knockout was able to reduce aggressive features, like invasion, commonly associated to the resistant phenotype.

Next I tested if the overexpression of ATF3 could induce the opposite effect and confer resistance to endocrine therapy. Indeed high levels of ATF3 were able to reduce the cytotoxic effects of TAM and, to a lesser extent, also of E2 deprivation in terms of proliferation, cell cycle progression and apoptosis rate. Moreover ATF3 overexpression induced a more invasive phenotype upon TGFβ1 stimulation in MCF7, suggesting a putative role of ATF3 in the metastatic spreading.

ATF3 has been described as a downstream effector of the MAPK pathway through several distinct branches and mechanisms in different contexts. First, *ATF3* promoter has been shown to be activated by the binding of ATF2 and c-jun, two downstream effectors of MAPK signaling (Liang et al. 1996). ATF3 upregulation under stress was proven to be mediated exclusively by the p38 signaling pathway in HeLa cells, while through ERK, SAPK and p38 in colorectal cancer (Lu, Chen, and Hai 2007; Hackl et al. 2010). Other reports showed that its activation is mediated through ERK and p38α in myocytes or by ERK/JNK but not by p38 in rat brains (Guo et al. 2015; Koivisto et al. 2014). Again, these findings demonstrate that the regulation of ATF3 is highly cell and context specific. In breast cancer and particularly in resistance to treatments, ATF3 expression has been described as mediated by pAKT in radioresistance, while mostly by JNK pathway in chemoresistance (Hasim et al. 2018; W. Zhao et al. 2018). Therefore, while the mechanisms of ATF3 induction through MAPK and AKT have been extensively described, the downstream activity of ATF3 to propagate the signal is not well studied.

As RNA-seq results provided insights into the regulation of downstream effectors of MAPK signaling pathway by ATF3, I further explored this through a phospho-proteomic screening with RPPA. This approach revealed a drastic difference in pathway activation profiles in WT cells and ATF3 knockout cells. While in the WT cells endocrine treatments induced activation in several central phospho-proteins as AKT, p38, MEK1, PDK1 and JNK, as well as downstream effectors like phospho c-jun and eIF4B, the two knockout clones displayed a generally less active MAPK and PI3K/AKT pathways. This indicates a central role of ATF3 in regulating MAPK and PI3K/AKT

signaling pathways under therapy and that the lack of ATF3 prevents activation of these pathways as well as of resistance processes. Even if in lower intensity, ATF3 overexpression adjuvated activation of these pathways in both MCF7 and T47D, corroborating the phenotypic findings that ATF3 overexpression confers resistance in sensitive cells.

Stable knockdown of ATF3 was also tested in resistant cells, using an shRNA approach to downregulate ATF3 expression. This was used because lentiviral delivery of shRNA allows for a rapid selection with antibiotics of resistant cells that carry the shRNA, while a CRISPR/Cas9 approach requires single clone selection and expansion. This would select for clones that eventually adapted to survive without ATF3 in the presence of the drug, therefore obtaining ATF3-deficient and potentially yet resistant clones. ShRNA knockdown in resistant cells, however, did not induce a re-sensitization of the cells to therapy in terms of effect on proliferation, cell cycle and apoptosis. This indicates that ATF3 is an essential gene in the gene rewiring processes in the early phase of resistance to cope with the stress induced by the therapy, but once the cells have become fully resistant, ATF3 is not needed for the maintenance of the resistant phenotype. This is an important indication for the clinical aspect of endocrine therapy resistance treatments. The efficiency of combinatorial treatments is highly time-dependent, and the interference with specific pathways after resistance development might not be successful. In this way, ATF3 is a perfect example of a driver of the resistance process that should be tackled in early phases of treatment administration to obtain the desired effects.

5.3. ATF3 regulates TGFB2 to induce MAPK pathway activation

The overall rewiring of MAPK and AKT pathways in ATF3 knockdown and overexpression indicated that ATF3 likely does not directly regulate each individual proteins in the pathways but might act through the upregulation of an upstream mediator. The screening of ATF3 targets suggested *TGFB2* as a possible candidate. TGFβ isoforms are known inducers of MAPK and AKT, especially in pathological conditions (Chapnick et al. 2011; Zhang 2009; Hamidi et al. 2017).

Additionally the crosstalk between TGFβ and ATF3 has been extensively documented in literature. TGFβ1 has been shown to induce ATF3, that in turn enhances TGFβ signaling and promotes cancer initiating feature in normal breast cell lines (Yin et al. 2010). Moreover TGFβ1 was proven to induce ATF3 expression and its interaction with AP-1 proteins in TNBC cell lines (Gokulnath et al. 2017; Kwok et al. 2009). Additionally, TGFβ1 was reported to induce ATF3 in a promoter-specific manner, inducing only transcripts derived by the P2 promoter (Figure 46 a) (Miyazaki et al. 2009; Kha et al. 2019). While all these reports focus on TGFβ1, TGFβ2 has a similar structure and acts on the same receptor, transducing the signal through the same pathways (Hachim et al. 2018). Additionally, binding of ATF3 and AP-1 both in the promoter and enhancers of the TGFβ2 gene has been experimentally proven, suggesting a potential regulation through these transcription factors (Figure 46 b).

Indeed RPPA profiling revealed that TGFβ2 stimulation was able to induce MAPK and AKT pathway activation both in MCF7 and T47D (sensitive and resistant), therefore having a similar role to TGFβ1. Additionally TGFβ2 stimulation induced the expression of ATF3 after 1 week, while no effect was detected in T47D. In RNAi experiments, however, *TGFB2* knockdown did not influence the levels of ATF3. TGFβ2 is therefore able to induce ATF3 expression, but it is not essential for the maintenance of ATF3 expression.

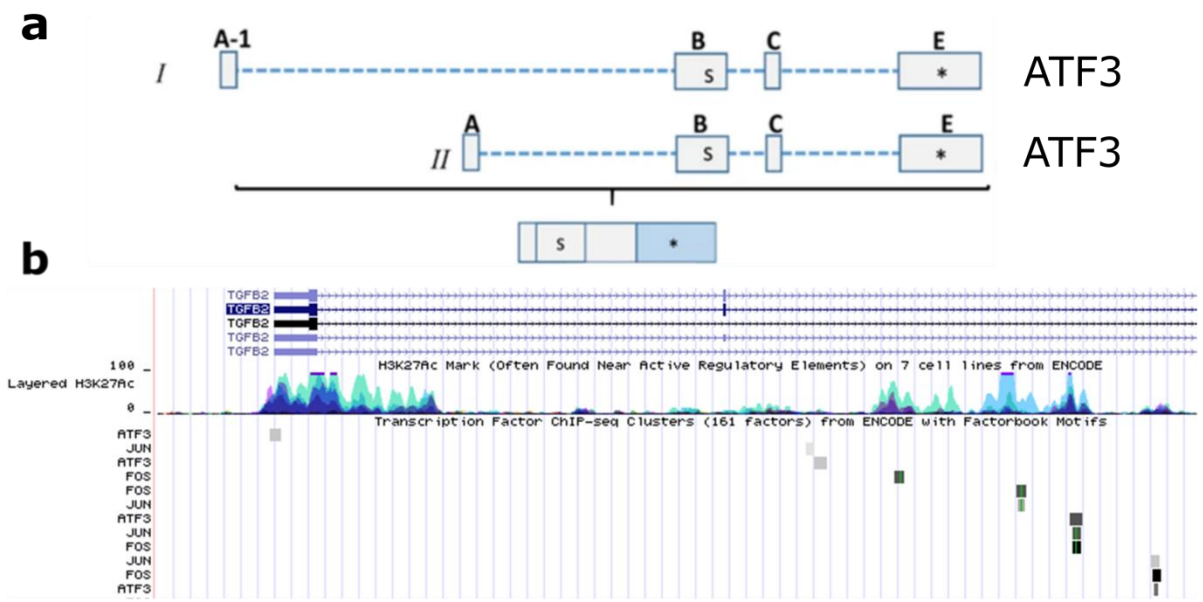

Figure 46: ATF3 and TGFB2 gene layouts
(**a**) Graphical representation of ATF3 promoters (A-I, A-II). Both the isoforms derived from the two distinct promoters code for the same protein (modified from Kha et al. 2019). (**b**) USCS genome browser snapshot of TGFB2 gene with ATF3, JUN and FOS binding sites.

On the other hand, ATF3 knockdown reduced TGFB2 expression in MCF7, while it surprisingly increased it in T47D. This opposite effect on the two cell lines remarks the context-dependency of ATF3. One major difference between MCF7 and T47D is the p53 status, with MCF7 having the WT protein while T47D carrying a mutated version (L194F) (Polotskaia et al. 2015). ATF3 is a known binging partner of p53, and it has been shown to co-localize with it in specific genomic sites and increasing its stability (C. Yan and Boyd 2006; J. Zhao et al. 2016). ATF3 is also able to bind mutated p53 in cells carrying hot-spot mutations conferring oncogenic activity, suppressing its oncogenic function. (Wei et al. 2014). However, no data is available on the specific binding of ATF3 to L194F mutated p53. The binding of ATF3 to WT and mutated p53 could therefore affect several downstream targets of these transcription factors in different ways in the 2 cell lines.

5.4. ATF3 knockout impairs *in vivo* tumor growth under endocrine therapy

Following the promising *in vitro* data on the role of ATF3 in proliferation, cell cycle, apoptosis rate and invasion, the knockout clones were tested *in vivo* in a xenograft mouse model. ATF3 knockouts displayed slower growth *in vivo* under both TAM and LET treatment, confirming the *in vitro* results. Differently from their behavior *in vitro*, the knockouts also showed a slower growth without any treatment administration, indicating a possible role of ATF3 in controlling the baseline proliferation rate of the cells. One unexpected result was the lack of growth inhibition of WT cells in the LET treated group. This could be explained by the adverse effects LET has on pre-menopausal women: the reduction in the peripheral E2 levels activates the hypothalamic-pituitary axis; this increases gonadotropin secretion, which stimulates the ovaries, resulting in even increased E2 production (Scharl and Salterberg 2016). Therefore LET might have stimulated E2 production to levels sufficient to sustain the growth of MCF7 WT. The E2 levels, however, might still not be high enough to support the growth of the ATF3 knockout clones that show a delayed tumor growth.

5.5. Patients data validate ATF3 role in the early response to endocrine therapy

Cell lines are often considered artificial and non-representative of the complexity of tumors. To validate the clinical relevance of ATF3 and to exclude the possibility that my data could be cell culture artifact, several publicly available dataset were analyzed. Indeed ATF3 was induced upon treatment administration in patients' biopsies in all dataset analyzed. Strikingly, in one of them, ATF3 was detected as the most significantly changing gene upon endocrine therapy treatment, strongly validating the results obtained in the cell line models. Other publicly available datasets with information on treatment and survival (TCGA and Metabric) were investigated to correlate ATF3 expression with disease-free survival and overall survival. No

difference was detected using the level of ATF3 in the primary tumors as a prognostic factor (data not shown). This is in agreement with the concept of ATF3 being induced upon stress/treatment: the levels in the untreated primary tumors are not relevant in evaluating the patients' response to therapy and predicting treatment outcome. For this, datasets with biopsies after treatment administration, coupled with long-term follow-up are needed to fully investigate ATF3 association with resistance *in vivo*, but unfortunately no such data is available.

5.6. Barcoding approach uncovers distinct mechanisms of clonal selection in endocrine resistance

Therapy resistance could arise following different mechanisms. One option is the expansion of pre-existing resistant cell populations that get selected under treatment due to clear growth advantage (Shaw et al. 2016; Yu et al. 2014). Alternatively selection could be mediated by a stochastic adaptation and selection of specific clones induced by the treatment itself or that have a favorable state, for example, in the expression levels of relevant genes at the time of treatment (Shaffer et al. 2017; Sharma et al. 2010; Hata et al. 2016).

To address this in the context of endocrine therapy resistance in breast cancer I used a cellular barcoding approach to track single clones during treatment (Bhang et al. 2015). Two luminal A cell lines, MCF7 and T47D, and two treatment, TAM and E2 deprivation, were used. This approach allowed the investigation of several questions: I) Role of clonality in endocrine therapy resistance; II) Identification of the mechanisms of clonal selection (pre-resistant clones' selection or adaptation); III) Identification of treatment-specific mechanisms IV) Identification of cell lines specific mechanism.

The two different cell line displayed striking differences both in terms of the number of barcodes enriched and the types of selection. In absence of selective pressure no robust selection was detected. However few barcodes displayed a consistent enrichment among replicates, particularly in T47D. It is not unexpected that even without the presence of external

stimuli a selection of clones with a proliferative advantage took place, as it has been describe in other contexts. A notable example in *E. coli* showed that, over the time of 60.000 generation kept in the same media without stimuli, different strains were enriched in the population due to their better fitness (Good et al. 2017). Upon treatment pressure however, diverse scenarios were identified. Under TAM treatment, MCF7 did not displayed a strong selection of specific clones, with more than 100 barcodes having similar enrichment within one replicate, while the individual barcodes were mostly not recurrent in the different replicates. In T47D, however, few specific barcodes were selected. These barcodes were common among all the samples, even having the same frequency in four of them. This is of particular interest because, since they were detected in all the clones independently, it represents a selection of pre-resistant clones and not a random adaptation.

One point to consider is that the relative frequency of the two enriched barcodes was strikingly similar in all the replicates. This is unexpected as physiological fluctuation should have resulted in distinct frequencies in the independent replicates. A possible explanation of this observation is that two barcodes had integrated into the same initial cell that therefore has been labeled with two barcodes instead of one. However, independently from being one or two separate clones, a clear selection of resistant clone/s took place. The high frequency of these two barcodes, that potentially hints to just one clone having been selected in four replicates, might also be related to the genomic integration site. Viral integration might have disrupted the genetic locus as a result of integration of the viral sequences thus positively regulating nearby genes providing a selective advantage to the clone. The non-occurrence of these barcodes in E2 treated or LTED cells hints that this had not provided the cells with a general growth advantage, but that this would be directly associate with growth in presence of TAM. To rule out a possible lucus disruption effect, analysis of the integration sites was performed. The viral integration analysis indicated that the two barcodes inserted in genomic regions not annotated as coding regions or regulatory elements, therefore not directly affecting the expression of any gene in their proximity. Additionally, the frequency of the two integration sites was not similar, indicating that the barcodes represent two distinct cell clones.

In LTED treatment, the mechanisms of resistance development were apparently more similar in the two cell lines. Indeed, a selection of one to six clones gave rise to the resistant population in both of the cell lines. Surprisingly enough, apart from one barcode enriched also in the WT that therefore can be considered not only resistance-related, all the resistant replicates presented different enriched barcodes, indicating a stochastic selection in each of the single replicates.

A barcoding approached has recently been applied also by the Polyak group where MCF7 were treated with TAM and fulvestrant (FULV). With >90% of all barcodes shared among four MCF7 TAMR replicates and >70% shared between the two different treatments (Hinohara et al. 2018), their data is in high contrast with that described in this thesis. Indeed, I did not see more than 10% barcodes overlap between four or five replicates in MCF7 TAMR and really few barcodes were shared among treatments (and not consistently in the different replicates). Therefore their conclusion that resistance in MCF7 is mediated by selection of pre-resistant, genetically distinct cells does not fit with the results described above. Additionally, there might be doubts about their claims, as the genetic analysis they use as proof is performed on a different set of cells, not fitting to the overall design of the study. However, such selection might still have occurred in T47D TAMR, but a deeper characterization of the resistant clones and the initial population is needed to define if a genetically or epigenetically driven selection had taken place.

Mechanisms of stochastic adaptation that appear to be the clonal selection method in both LTED treated cell lines has been described in other contexts. For examples, Gefitinib treatment in lung cancer revealed the existence of a subpopulation of cells in a reversible resistant state that was selected due to their stochastic phenotype at the moment of drug treatment (Sharma et al. 2010). A similar selection mechanism has been reported in vemurafenib treatment of melanoma, where transient pre-resistant cells were selected by the drug because they were stochastically expressing defined gene sets at the start of the treatment (Shaffer et al. 2017). These cells are then described to stabilize this transient state to a stable resistant phenotype, eventually with additional genetic or epigenetic alterations. This could explain the selection of

distinct barcodes in the long term estrogen deprived replicates, as different cells might have been in a transient resistant state at the beginning of the treatment and being selected.

5.7. Resistant replicates have different pathway alterations and putative druggabilities

The differences in clonal composition opened the question of phenotypic similarities among the independent resistant replicates. To investigate this, RPPA was used to assess their activation profiles for pathways involved in resistance. It has to be noted that the RPPA approach used here considers the pooled replicates, where specific pathways' alterations of individual subclonal populations might be masked. Replicates with peculiar clonal composition had drastic differences in profiles compared to other replicates that comprised a larger number of individual clones. For example, replicates MCF7 LTED_5 and T47D LTED_2 had one predominant barcode each, indicative of clonal selection. In MCF7 LTED, replicate 5 showed high activation of all pathways screened, while other clones had more pathway specific activation profiles, like replicates 1 and 4 for the WNT pathway and replicate 1 for PLCγ. In T47D LTED the distinct profile of replicate 2 is even more obvious, as all the other replicates displayed highly similar pathway activation profiles. For MCF7 TAMR cells the profiles were almost identical, despite having completely different enriched barcodes. This hints to the fact that the mechanism of resistance development in this cells is acquired, and that the resistance is not acting through selection but rather a convergent adaptation of surviving cells.

Interestingly T47D TAMR replicates, characterized by the same barcode composition, were also similar in terms of pathways activation, but presented replicate-specific features as well. Clear examples are replicate 1, that displayed high AKT/mTOR pathway activation, and replicate 2 that showed a rather active MAPK pathway, with high levels of phosphorylated MEK and ERK. These findings indicate that, even though deriving from the same initial cells, these replicates acquired new molecular features during the resistance process that made them different from one another. This mechanism of diverse alterations arising during treatment from the same

persister cell has been described in other cancer entities and can be applied to endocrine therapy as well (Ramirez et al. 2016). This alterations can be either stochastic or drug-induced in a replicate-specific manner thereby conferring different final resistant profiles (Shaffer et al. 2017). Also in tamoxifen resistance, a previous study had shown differential sensitivity of specific resistant clones to a panel of cytotoxic drugs, therefore demonstrating different paths to resistance (Kangaspeska et al. 2016).

The fact that resistance to endocrine therapy is not only cell line and treatment specific, but also individual replicates arising from the same starting pool could have developed different resistance mechanisms, makes this a really challenging phenomenon to study. In addition the ever-changing features of cancer cells in culture make it even harder to establish unique mechanisms in cancer research. MCF7 themselves, when compared across 27 strains obtained from different labs, showed drastic differences both at the genomic and transcriptomic levels, as well as in drug sensitivity (Ben-David et al. 2018). It is therefore not surprising to see differences between the mechanisms of tamoxifen in MCF7 described in this thesis and the ones described by Polyak and colleagues, as even the cell line of origin in the two labs might have had distinct features (Hinohara et al. 2018).

6. Conclusions and Outlook

In this thesis I addressed the issue of resistance development in breast cancer with two approaches aimed to investigate novel mediators of resistance and identify mechanism underlying clonal selection under treatment.

In the first part of this study I analyzed the early events in resistance development and found ATF3 as a putative driver of this phenomenon through a rewiring of MAPK pathway. Indeed the interference with ATF3 expression caused an increase in drug sensitivity, while its overexpression induced a more resistant-like phenotype in sensitive cells. This was supported by changes in the MAPK pathway and in downstream effectors. Interference with ATF3 in resistance cells did not result in increased sensitivity, proving the role of this gene in the regulation of resistance acquisition process rather than the maintenance of the final resistant state. The role of ATF3 was also confirmed in an *in vivo* xenograft model and its upregulation was detected also in patient datasets, therefore demonstrating clinical relevance of the findings.

While the role of ATF3 was established through these results, the mechanism by which it mediates resistance needs to be further investigated. Particularly it needs to be clarified if its rewiring of the MAPK pathway is direct or mediated by any of its target genes (e.g., *TGFB2*, *JUN*, *FOS*). Additionally, as ATF3 trascripional activity is also mediated by its binding to other co-factor, it needs to be tested if particular binding partners are preferred in the resistance process. Several experiments are on-going to elucidate these points:

- IP-MS (Immunoprecipitation coupled to Mass Spectrometry) to identify specific binding parners of ATF3 at different stages of resistance development.
- ChIP-qPCR of ATF3 at the regulatory elements (promoter and enhancers) of ATF3 target genese, to test if the regulation is mediated by ATF3 direct binding

Due to the observed differences between MCF7 and T47D and the impossibility to obtaining knockout cells for ATF3 in the latter cell line, more efforts are also needed to demonstrate if ATF3 might be relevant only for a subset of luminal A tumors.

The second part of this thesis addressed the mechanisms underlying resistance development in terms of clonal selection. Using a barcoding approach I identified differential mechanism of clonal selection based on the cell line and treatment used. These different mechanisms and clonal enrichments are reflected on distinct pathway profiles and putative drug sensitivities.

I am currently performing a screening with several inhibitors for specific proteins of the pathways tested in RPPA to investigate the differential sensitivity of single replicates to particular drugs.

A series of next generation techniques might be used to investigate the causes of the different barcodes selection and to explore if these genetic/epigenetic features are present in the initial population or are drug induced. Deconvolution to single clones might allow analyzing and interfering with specific alterations in a pure population derived from a single initial cell and further identify specific resistance mechanisms and pathways sensitivities.

References

Abdel-Hafiz, Hany. 2017. “Epigenetic Mechanisms of Tamoxifen Resistance in Luminal Breast Cancer.” *Diseases* 5 (3): 16. https://doi.org/10.3390/diseases5030016.

Ades, Felipe, Dimitrios Zardavas, Ivana Bozovic-Spasojevic, Lina Pugliano, Debora Fumagalli, Evandro de Azambuja, Giuseppe Viale, Christos Sotiriou, and Martine Piccart. 2014. “Luminal B Breast Cancer: Molecular Characterization, Clinical Management, and Future Perspectives.” *Journal of Clinical Oncology : Official Journal of the American Society of Clinical Oncology* 32 (25): 2794–2803. https://doi.org/10.1200/JCO.2013.54.1870.

AlFakeeh, A, and C Brezden-Masley. 2018. “Overcoming Endocrine Resistance in Hormone Receptor-Positive Breast Cancer.” *Current Oncology (Toronto, Ont.)* 25 (Suppl 1): S18–27. https://doi.org/10.3747/co.25.3752.

Ameri, K, E M Hammond, C Culmsee, M Raida, D M Katschinski, R H Wenger, E Wagner, et al. 2007. “Induction of Activating Transcription Factor 3 by Anoxia Is Independent of P53 and the Hypoxic HIF Signalling Pathway.” *Oncogene* 26 (2): 284–89. https://doi.org/10.1038/sj.onc.1209781.

Arnott, John, Stephen Martinkovich, Sonia Lobo Planey, and Darshan Shah. 2014. “Selective Estrogen Receptor Modulators: Tissue Specificity and Clinical Utility.” *Clinical Interventions in Aging* 9 (August): 1437. https://doi.org/10.2147/CIA.S66690.

Bartsch, Rupert, and Elisabeth Bergen. 2018. “ASCO 2018: Highlights in HER2-Positive Metastatic Breast Cancer.” *Memo* 11 (4): 280–83. https://doi.org/10.1007/s12254-018-0441-x.

Ben-David, Uri, Benjamin Siranosian, Gavin Ha, Helen Tang, Yaara Oren, Kunihiko Hinohara, Craig A. Strathdee, et al. 2018. “Genetic and Transcriptional Evolution Alters Cancer Cell Line Drug Response.” *Nature* 560 (7718): 325–30. https://doi.org/10.1038/s41586-018-0409-3.

Bhang, Hyo-eun C, David A Ruddy, Viveksagar Krishnamurthy Radhakrishna, Justina X Caushi, Rui Zhao, Matthew M Hims, Angad P Singh, et al. 2015. “Studying Clonal Dynamics in Response to Cancer Therapy Using High-Complexity Barcoding.” *Nature Medicine* 21 (5): 440–48. https://doi.org/10.1038/nm.3841.

Boér, Katalin. 2017. “Fulvestrant in Advanced Breast Cancer: Evidence to Date and Place in Therapy.” *Therapeutic Advances in Medical Oncology* 9 (7): 465. https://doi.org/10.1177/1758834017711097.

Bottone, F. G. 2005. “The Anti-Invasive Activity of Cyclooxygenase Inhibitors Is Regulated by the Transcription Factor ATF3 (Activating Transcription Factor 3).” *Molecular Cancer Therapeutics* 4 (5): 693–703. https://doi.org/10.1158/1535-7163.MCT-04-0337.

Brandt, Sebastian, Andreas Kopp, Birgit Grage, and Cornelius Knabbe. 2003. “Effects of Tamoxifen on Transcriptional Level of Transforming Growth Factor Beta (TGF-Beta) Isoforms 1 and 2 in Tumor Tissue during Primary Treatment of Patients with Breast Cancer.” *Anticancer Research* 23 (1A): 223–29.

Bray, Freddie, Jacques Ferlay, Isabelle Soerjomataram, Rebecca L. Siegel, Lindsey A. Torre, and Ahmedin Jemal. 2018. "Global Cancer Statistics 2018: GLOBOCAN Estimates of Incidence and Mortality Worldwide for 36 Cancers in 185 Countries." *CA: A Cancer Journal for Clinicians* 68 (6): 394–424. https://doi.org/10.3322/caac.21492.

Cancer Genome Atlas Network, The. 2012. "Comprehensive Molecular Portraits of Human Breast Tumours." https://doi.org/10.1038/nature11412.

Cao, Hua, Zhi-Xue Yang, and Guo-Qin Jiang. 2013. "Expression and Clinical Significance of Activating Transcription Factor 3 in Human Breast Cancer." *Iranian Journal of Basic Medical Sciences* 16 (11): 1151–54. http://www.ncbi.nlm.nih.gov/pubmed/24494067.

Cardoso, F, E Senkus, A Costa, E Papadopoulos, M Aapro, F André, N Harbeck, et al. 2018. "4th ESO–ESMO International Consensus Guidelines for Advanced Breast Cancer (ABC 4)†." *Annals of Oncology* 29 (8): 1634–57. https://doi.org/10.1093/annonc/mdy192.

Chan, Hei Jason, Karineh Petrossian, and Shiuan Chen. 2016. "Structural and Functional Characterization of Aromatase, Estrogen Receptor, and Their Genes in Endocrine-Responsive and –Resistant Breast Cancer Cells." *The Journal of Steroid Biochemistry and Molecular Biology* 161 (July): 73–83. https://doi.org/10.1016/j.jsbmb.2015.07.018.

Chandarlapaty, Sarat, David Chen, Wei He, Patricia Sung, Aliaksandra Samoila, Daoqi You, Trusha Bhatt, et al. 2016. "Prevalence of *ESR1* Mutations in Cell-Free DNA and Outcomes in Metastatic Breast Cancer." *JAMA Oncology* 2 (10): 1310. https://doi.org/10.1001/jamaoncol.2016.1279.

Chapnick, Douglas A, Lisa Warner, Jennifer Bernet, Timsi Rao, and Xuedong Liu. 2011. "Partners in Crime: The TGFβ and MAPK Pathways in Cancer Progression." *Cell & Bioscience* 1 (December): 42. https://doi.org/10.1186/2045-3701-1-42.

Chen, B P, G Liang, J Whelan, and T Hai. 1994. "ATF3 and ATF3 Delta Zip. Transcriptional Repression versus Activation by Alternatively Spliced Isoforms." *The Journal of Biological Chemistry* 269 (22): 15819–26. http://www.ncbi.nlm.nih.gov/pubmed/7515060.

Chen, Cong, Chao Ge, Zheng Liu, Liangyu Li, Fangyu Zhao, Hua Tian, Taoyang Chen, Hong Li, Ming Yao, and Jinjun Li. 2018. "ATF3 Inhibits the Tumorigenesis and Progression of Hepatocellular Carcinoma Cells via Upregulation of CYR61 Expression." *Journal of Experimental & Clinical Cancer Research* 37 (1): 263. https://doi.org/10.1186/s13046-018-0919-8.

Cortés, Javier, Seock-Ah Im, Esther Holgado, Jose M Perez-Garcia, Peter Schmid, and Mariana Chavez-Macgregor. 2017. "Anti-Tumour Treatment The next Era of Treatment for Hormone Receptor-Positive, HER2-Negative Advanced Breast Cancer: Triplet Combination-Based Endocrine Therapies." https://doi.org/10.1016/j.ctrv.2017.09.011.

Creyghton, Menno P, Albert W Cheng, G Grant Welstead, Tristan Kooistra, Bryce W Carey, Eveline J Steine, Jacob Hanna, et al. 2010. "Histone H3K27ac Separates Active from Poised Enhancers and Predicts Developmental State." *Proceedings of the National Academy of Sciences of the United States of America* 107 (50): 21931–36. https://doi.org/10.1073/pnas.1016071107.

Cristofanilli, Massimo, Nicholas C Turner, Igor Bondarenko, Jungsil Ro, Seock-Ah Im, Norikazu Masuda, Marco Colleoni, et al. 2016. "Fulvestrant plus Palbociclib versus

Fulvestrant plus Placebo for Treatment of Hormone-Receptor-Positive, HER2-Negative Metastatic Breast Cancer That Progressed on Previous Endocrine Therapy (PALOMA-3): Final Analysis of the Multicentre, Double-Blind, Phase 3 Randomised Controlled Trial." *The Lancet Oncology* 17 (4): 425–39. https://doi.org/10.1016/S1470-2045(15)00613-0.

Curtis, Christina, Sohrab P Shah, Suet-Feung Chin, Gulisa Turashvili, Oscar M Rueda, Mark J Dunning, Doug Speed, et al. 2012. "The Genomic and Transcriptomic Architecture of 2,000 Breast Tumours Reveals Novel Subgroups." *Nature* 486. https://doi.org/10.1038/nature10983.

Cynthia X. Ma, MD, PhD, Cesar G. Sanchez, MD, Matthew J. Ellis, MD, PhD, FRCP. 2009. "Predicting Endocrine Therapy Responsiveness in Breast Cancer." https://www.cancernetwork.com/breast-cancer/predicting-endocrine-therapy-responsiveness-breast-cancer/page/0/1.

D'Souza, Anishka, Darcy Spicer, and Janice Lu. 2018. "Overcoming Endocrine Resistance in Metastatic Hormone Receptor-Positive Breast Cancer." *Journal of Hematology & Oncology* 11 (1): 80. https://doi.org/10.1186/s13045-018-0620-6.

Dagogo-Jack, Ibiayi, and Alice T. Shaw. 2018. "Tumour Heterogeneity and Resistance to Cancer Therapies." *Nature Reviews Clinical Oncology* 15 (2): 81–94. https://doi.org/10.1038/nrclinonc.2017.166.

Dai, Xiaofeng, Ting Li, Zhonghu Bai, Yankun Yang, Xiuxia Liu, Jinling Zhan, and Bozhi Shi. 2015. "Breast Cancer Intrinsic Subtype Classification, Clinical Use and Future Trends." *Am J Cancer Res* 5 (10): 2929–43.

Davies, Christina, Hongchao Pan, Jon Godwin, Richard Gray, Rodrigo Arriagada, Vinod Raina, Mirta Abraham, et al. 2013. "Long-Term Effects of Continuing Adjuvant Tamoxifen to 10 Years versus Stopping at 5 Years after Diagnosis of Oestrogen Receptor-Positive Breast Cancer: ATLAS, a Randomised Trial." *The Lancet* 381 (9869): 805–16. https://doi.org/10.1016/S0140-6736(12)61963-1.

Díaz Flaqué, María C, Natalia M Galigniana, Wendy Béguelin, Rocío Vicario, Cecilia J Proietti, Rosalía Cordo Russo, Martín A Rivas, et al. 2013. "Progesterone Receptor Assembly of a Transcriptional Complex along with Activator Protein 1, Signal Transducer and Activator of Transcription 3 and ErbB-2 Governs Breast Cancer Growth and Predicts Response to Endocrine Therapy." *Breast Cancer Research* 15 (6): R118. https://doi.org/10.1186/bcr3587.

Dixon, J. M. 2014. "Endocrine Resistance in Breast Cancer." *New Journal of Science* 2014: 1–27. https://doi.org/10.1155/2014/390618.

Dowsett, Mitch, Jack Cuzick, Jim Ingle, Alan Coates, John Forbes, Judith Bliss, Marc Buyse, et al. 2010. "Meta-Analysis of Breast Cancer Outcomes in Adjuvant Trials of Aromatase Inhibitors Versus Tamoxifen." *Journal of Clinical Oncology* 28 (3): 509–18. https://doi.org/10.1200/JCO.2009.23.1274.

EBCTCG. 2005. "Effects of Chemotherapy and Hormonal Therapy for Early Breast Cancer on Recurrence and 15-Year Survival: An Overview of the Randomised Trials." *The Lancet* 365 (9472): 1687–1717. https://doi.org/10.1016/S0140-6736(05)66544-0.

Elston, C W, and I O Ellis. 1991. "Pathological Prognostic Factors in Breast Cancer. I. The

Value of Histological Grade in Breast Cancer: Experience from a Large Study with Long-Term Follow-Up." *Histopathology* 19 (5): 403–10. http://www.ncbi.nlm.nih.gov/pubmed/1757079.

Flaum, Lisa E., and William J. Gradishar. 2018. "Advances in Endocrine Therapy for Postmenopausal Metastatic Breast Cancer." In , 141–54. Springer, Cham. https://doi.org/10.1007/978-3-319-70197-4_9.

Foulkes, William D., Ian E. Smith, and Jorge S. Reis-Filho. 2010. "Triple-Negative Breast Cancer." *New England Journal of Medicine* 363 (20): 1938–48. https://doi.org/10.1056/NEJMra1001389.

Fu, Xiaoyong, C Kent Osborne, and Rachel Schiff. 2013. "Biology and Therapeutic Potential of PI3K Signaling in ER+/HER2-Negative Breast Cancer." *Breast (Edinburgh, Scotland)* 22 Suppl 2 (0 2): S12-8. https://doi.org/10.1016/j.breast.2013.08.001.

Garraway, Levi A., and Pasi A. Jänne. 2012. "Circumventing Cancer Drug Resistance in the Era of Personalized Medicine." *Cancer Discovery* 2 (3): 214–26. https://doi.org/10.1158/2159-8290.CD-12-0012.

Ghayad, Sandra E., Julie A. Vendrell, Sabrina Ben Larbi, Charles Dumontet, Ivan Bieche, and Pascale A. Cohen. 2010. "Endocrine Resistance Associated with Activated ErbB System in Breast Cancer Cells Is Reversed by Inhibiting MAPK or PI3K/Akt Signaling Pathways." *International Journal of Cancer* 126 (2): 545–62. https://doi.org/10.1002/ijc.24750.

Giuliano, Armando E., Stephen B. Edge, and Gabriel N. Hortobagyi. 2018. "Eighth Edition of the AJCC Cancer Staging Manual: Breast Cancer." *Annals of Surgical Oncology* 25 (7): 1783–85. https://doi.org/10.1245/s10434-018-6486-6.

Gokulnath, M., N. C. Partridge, and N. Selvamurugan. 2015. "Runx2, a Target Gene for Activating Transcription Factor-3 in Human Breast Cancer Cells." *Tumor Biology* 36 (3): 1923–31. https://doi.org/10.1007/s13277-014-2796-x.

Gokulnath, M., R. Swetha, G. Thejaswini, P. Shilpa, and N. Selvamurugan. 2017. "Transforming Growth Factor-B1 Regulation of ATF-3, c-Jun and JunB Proteins for Activation of Matrix Metalloproteinase-13 Gene in Human Breast Cancer Cells." *International Journal of Biological Macromolecules* 94 (January): 370–77. https://doi.org/10.1016/J.IJBIOMAC.2016.10.026.

Goldhirsch, A., E. P. Winer, A. S. Coates, R. D. Gelber, M. Piccart-Gebhart, B. Thürlimann, H.-J. Senn, et al. 2013. "Personalizing the Treatment of Women with Early Breast Cancer: Highlights of the St Gallen International Expert Consensus on the Primary Therapy of Early Breast Cancer 2013." *Annals of Oncology* 24 (9): 2206–23. https://doi.org/10.1093/annonc/mdt303.

Good, Benjamin H., Michael J. McDonald, Jeffrey E. Barrick, Richard E. Lenski, and Michael M. Desai. 2017. "The Dynamics of Molecular Evolution over 60,000 Generations." *Nature* 551 (7678): 45–50. https://doi.org/10.1038/nature24287.

Groenendijk, Floris H., Tina Treece, Erin Yoder, Paul Baron, Peter Beitsch, William Audeh, Winand N. M. Dinjens, Rene Bernards, and Pat Whitworth. 2019. "Estrogen Receptor Variants in ER-Positive Basal-Type Breast Cancers Responding to Therapy like ER-Negative Breast Cancers." *Npj Breast Cancer* 5 (1): 15. https://doi.org/10.1038/s41523-

019-0109-7.

Guo, Nannan, Chenling Meng, Wujiao Bai, Quanwei Wei, Fangxiong Shi, John S. Davis, and Dagan Mao. 2015. “Prostaglandin F2α Induces Expression of Activating Transcription Factor 3 (ATF3) and Activates MAPK Signaling in the Rat Corpus Luteum.” *Acta Histochemica* 117 (2): 211–18. https://doi.org/10.1016/J.ACTHIS.2014.12.008.

Hachim, Mahmood Y, Ibrahim Y Hachim, Meiou Dai, Suhad Ali, and Jean-Jacques Lebrun. 2018. “Differential Expression of TGFβ Isoforms in Breast Cancer Highlights Different Roles during Breast Cancer Progression.” *Tumor Biology* 40 (1): 101042831774825. https://doi.org/10.1177/1010428317748254.

Hackl, Christina, Sven A Lang, Christian Moser, Akira Mori, Stefan Fichtner-Feigl, Claus Hellerbrand, Wolfgang Dietmeier, Hans J Schlitt, Edward K Geissler, and Oliver Stoeltzing. 2010. “Activating Transcription Factor-3 (ATF3) Functions as a Tumor Suppressor in Colon Cancer and Is up-Regulated upon Heat-Shock Protein 90 (Hsp90) Inhibition.” *BMC Cancer* 10 (December): 668. https://doi.org/10.1186/1471-2407-10-668.

Hai, T, and M G Hartman. 2001. “The Molecular Biology and Nomenclature of the Activating Transcription Factor/CAMP Responsive Element Binding Family of Transcription Factors: Activating Transcription Factor Proteins and Homeostasis.” *Gene* 273 (1): 1–11. http://www.ncbi.nlm.nih.gov/pubmed/11483355.

Hai, T, C D Wolfgang, D K Marsee, A E Allen, and U Sivaprasad. 1999. “ATF3 and Stress Responses.” *Gene Expression* 7 (4–6): 321–35. http://www.ncbi.nlm.nih.gov/pubmed/10440233.

Hamidi, Anahita, Jie Song, Noopur Thakur, Susumu Itoh, Anders Marcusson, Anders Bergh, Carl-Henrik Heldin, and Maréne Landström. 2017. “TGF-β Promotes PI3K-AKT Signaling and Prostate Cancer Cell Migration through the TRAF6-Mediated Ubiquitylation of P85α.” *Science Signaling* 10 (486): eaal4186. https://doi.org/10.1126/scisignal.aal4186.

Harbeck, Nadia, and Achim Rody. 2012. “Lost in Translation? Estrogen Receptor Status and Endocrine Responsiveness in Breast Cancer.” *Journal of Clinical Oncology* 30 (7): 686–89. https://doi.org/10.1200/JCO.2011.38.9619.

Hashimoto, Yoshinori, Chun Zhang, Junya Kawauchi, Issei Imoto, Mimi T Adachi, Johji Inazawa, Teruo Amagasa, Tsonwin Hai, and Shigetaka Kitajima. 2002. “An Alternatively Spliced Isoform of Transcriptional Repressor ATF3 and Its Induction by Stress Stimuli.” *Nucleic Acids Research* 30 (11): 2398–2406. https://doi.org/10.1093/nar/30.11.2398.

Hasim, Mohamed S., Carolyn Nessim, Patrick J. Villeneuve, Barbara C. Vanderhyden, and Jim Dimitroulakos. 2018. “Activating Transcription Factor 3 as a Novel Regulator of Chemotherapy Response in Breast Cancer.” *Translational Oncology* 11 (4): 988–98. https://doi.org/10.1016/J.TRANON.2018.06.001.

Hata, Aaron N, Matthew J Niederst, Hannah L Archibald, Maria Gomez-Caraballo, Faria M Siddiqui, Hillary E Mulvey, Yosef E Maruvka, et al. 2016. “Tumor Cells Can Follow Distinct Evolutionary Paths to Become Resistant to Epidermal Growth Factor Receptor Inhibition.” *Nature Medicine* 22 (3): 262–69. https://doi.org/10.1038/nm.4040.

Hazzalin, C A, R Le Panse, E Cano, and L C Mahadevan. 1998. “Anisomycin Selectively Desensitizes Signalling Components Involved in Stress Kinase Activation and Fos and Jun

Induction." *Molecular and Cellular Biology* 18 (4): 1844–54. https://doi.org/10.1128/mcb.18.4.1844.

He, Huan, Indranil Sinha, Rongrong Fan, Lars-Arne Haldosen, Feifei Yan, Chunyan Zhao, and Karin Dahlman-Wright. 2018. "C-Jun/AP-1 Overexpression Reprograms ERα Signaling Related to Tamoxifen Response in ERα-Positive Breast Cancer." *Oncogene* 37 (19): 2586–2600. https://doi.org/10.1038/s41388-018-0165-8.

Heckler, Mary M., Hemang Thakor, Cara C. Schafer, and Rebecca B. Riggins. 2014. "ERK/MAPK Regulates ERRγ Expression, Transcriptional Activity and Receptor-Mediated Tamoxifen Resistance in ER+ Breast Cancer." *FEBS Journal* 281 (10): 2431–42. https://doi.org/10.1111/febs.12797.

Heo, Kyung-Sun. 2019. "Regulation of Post-Translational Modification in Breast Cancer Treatment." *BMB Reports* 52 (2): 113–18. https://doi.org/10.5483/BMBREP.2019.52.2.017.

Hinohara, Kunihiko, Hua-Jun Wu, Sébastien Vigneau, Thomas O. McDonald, Kyomi J. Igarashi, Kimiyo N. Yamamoto, Thomas Madsen, et al. 2018. "KDM5 Histone Demethylase Activity Links Cellular Transcriptomic Heterogeneity to Therapeutic Resistance." *Cancer Cell* 34 (6): 939-953.e9. https://doi.org/10.1016/j.ccell.2018.10.014.

Hiscox, Stephen, Wen Go Jiang, Kathrin Obermeier, Kathryn Taylor, Liam Morgan, Raj Burmi, Denise Barrow, and Robert I. Nicholson. 2006. "Tamoxifen Resistance in MCF7 Cells Promotes EMT-like Behaviour and Involves Modulation of β-Catenin Phosphorylation." *International Journal of Cancer* 118 (2): 290–301. https://doi.org/10.1002/ijc.21355.

Hoskins, Janelle M., Lisa A. Carey, and Howard L. McLeod. 2009. "CYP2D6 and Tamoxifen: DNA Matters in Breast Cancer." *Nature Reviews Cancer* 9 (8): 576–86. https://doi.org/10.1038/nrc2683.

Hrstka, Roman, Pavla Bouchalova, Eva Michalova, Eva Matoulkova, Petr Muller, Philip J Coates, and Borivoj Vojtesek. 2016. "AGR2 Oncoprotein Inhibits P38 MAPK and P53 Activation through a DUSP10-Mediated Regulatory Pathway." *Molecular Oncology* 10 (5): 652–62. https://doi.org/10.1016/j.molonc.2015.12.003.

Hu, Zhiyuan, Cheng Fan, Daniel S Oh, JS Marron, Xiaping He, Bahjat F Qaqish, Chad Livasy, et al. 2006. "The Molecular Portraits of Breast Tumors Are Conserved across Microarray Platforms." *BMC Genomics* 7 (1): 96. https://doi.org/10.1186/1471-2164-7-96.

Inoue, Makoto, Yohei Uchida, Makoto Edagawa, Manabu Hirata, Jun Mitamura, Daiki Miyamoto, Kenji Taketani, Shigeki Sekine, Junya Kawauchi, and Shigetaka Kitajima. 2018. "The Stress Response Gene ATF3 Is a Direct Target of the Wnt/β-Catenin Pathway and Inhibits the Invasion and Migration of HCT116 Human Colorectal Cancer Cells." Edited by Chunming Liu. *PLOS ONE* 13 (7): e0194160. https://doi.org/10.1371/journal.pone.0194160.

Inwald, Elisabeth Christine, M. Koller, M. Klinkhammer-Schalke, F. Zeman, F. Hofstädter, M. Gerstenhauer, G. Brockhoff, and O. Ortmann. 2015. "4-IHC Classification of Breast Cancer Subtypes in a Large Cohort of a Clinical Cancer Registry: Use in Clinical Routine for Therapeutic Decisions and Its Effect on Survival." *Breast Cancer Research and Treatment* 153 (3): 647–58. https://doi.org/10.1007/s10549-015-3572-3.

Ishiguro, Tatsuaki, Hirokazu Nagawa, Mikihiko Naito, and Takashi Tsuruo. 2000. "Inhibitory

Effect of ATF3 Antisense Oligonucleotide on Ectopic Growth of HT29 Human Colon Cancer Cells." *Japanese Journal of Cancer Research* 91 (8): 833–36. https://doi.org/10.1111/j.1349-7006.2000.tb01021.x.

Iwamoto, Takayuki, Daniel Booser, Vicente Valero, James L. Murray, Kimberly Koenig, Francisco J. Esteva, Naoto T. Ueno, et al. 2012. "Estrogen Receptor (ER) MRNA and ER-Related Gene Expression in Breast Cancers That Are 1% to 10% ER-Positive by Immunohistochemistry." *Journal of Clinical Oncology* 30 (7): 729–34. https://doi.org/10.1200/JCO.2011.36.2574.

Janz, M., Michael Hummel, Matthias Truss, Brigitte Wollert-Wulf, Stephan Mathas, Korinna Jöhrens, Christian Hagemeier, et al. 2006. "Classical Hodgkin Lymphoma Is Characterized by High Constitutive Expression of Activating Transcription Factor 3 (ATF3), Which Promotes Viability of Hodgkin/Reed-Sternberg Cells." *Blood* 107 (6): 2536–39. https://doi.org/10.1182/blood-2005-07-2694.

Jiang, Xiaojing, Kui-Jin Kim, Taekyu Ha, and Seong-Ho Lee. 2016. "Potential Dual Role of Activating Transcription Factor 3 in Colorectal Cancer." *Anticancer Research* 36 (2): 509–16. http://www.ncbi.nlm.nih.gov/pubmed/26851004.

Kangaspeska, Sara, Susanne Hultsch, Alok Jaiswal, Henrik Edgren, John-Patrick Mpindi, Samuli Eldfors, Oscar Brück, Tero Aittokallio, and Olli Kallioniemi. 2016. "Systematic Drug Screening Reveals Specific Vulnerabilities and Co-Resistance Patterns in Endocrine-Resistant Breast Cancer." *BMC Cancer* 16: 378. https://doi.org/10.1186/s12885-016-2452-5.

Kha, My-Lan, Lisa Hesse, Florian Deisinger, Bence Sipos, Christoph Röcken, Alexander Arlt, Susanne Sebens, Ole Helm, and Heiner Schäfer. 2019. "The Antioxidant Transcription Factor Nrf2 Modulates the Stress Response and Phenotype of Malignant as Well as Premalignant Pancreatic Ductal Epithelial Cells by Inducing Expression of the ATF3 Splicing Variant ΔZip2." *Oncogene* 38 (9): 1461–76. https://doi.org/10.1038/s41388-018-0518-3.

Kim, Charissa, Ruli Gao, Emi Sei, Rachel Brandt, Johan Hartman, Thomas Hatschek, Nicola Crosetto, Theodoros Foukakis, and Nicholas E. Navin. 2018. "Chemoresistance Evolution in Triple-Negative Breast Cancer Delineated by Single-Cell Sequencing." *Cell* 173 (4): 879-893.e13. https://doi.org/10.1016/j.cell.2018.03.041.

Koivisto, Elina, Alicia Jurado Acosta, Anne-Mari Moilanen, Heikki Tokola, Jani Aro, Harri Pennanen, Hanna Säkkinen, Leena Kaikkonen, Heikki Ruskoaho, and Jaana Rysä. 2014. "Characterization of the Regulatory Mechanisms of Activating Transcription Factor 3 by Hypertrophic Stimuli in Rat Cardiomyocytes." Edited by Michael Bader. *PLoS ONE* 9 (8): e105168. https://doi.org/10.1371/journal.pone.0105168.

Kwok, Sukyee, Susan R. Rittling, Nicola C. Partridge, Chellakkan S. Benson, Mayuranathan Thiyagaraj, Narasimhan Srinivasan, and Nagarajan Selvamurugan. 2009. "Transforming Growth Factor-B1 Regulation of ATF-3 and Identification of ATF-3 Target Genes in Breast Cancer Cells." *Journal of Cellular Biochemistry* 108 (2): 408–14. https://doi.org/10.1002/jcb.22267.

Lapidot, Tsvee, Christian Sirard, Josef Vormoor, Barbara Murdoch, Trang Hoang, Julio Caceres-Cortes, Mark Minden, Bruce Paterson, Michael A. Caligiuri, and John E. Dick. 1994. "A

Cell Initiating Human Acute Myeloid Leukaemia after Transplantation into SCID Mice." *Nature* 367 (6464): 645–48. https://doi.org/10.1038/367645a0.

Lehmann, Brian D., Bojana Jovanovi?, Xi Chen, Monica V. Estrada, Kimberly N. Johnson, Yu Shyr, Harold L. Moses, Melinda E. Sanders, and Jennifer A. Pietenpol. 2016. "Refinement of Triple-Negative Breast Cancer Molecular Subtypes: Implications for Neoadjuvant Chemotherapy Selection." Edited by Anna Sapino. *PLOS ONE* 11 (6): e0157368. https://doi.org/10.1371/journal.pone.0157368.

Lehmann, Brian D, Joshua A Bauer, Xi Chen, Melinda E Sanders, A Bapsi Chakravarthy, Yu Shyr, and Jennifer A Pietenpol. 2011. "Identification of Human Triple-Negative Breast Cancer Subtypes and Preclinical Models for Selection of Targeted Therapies." *The Journal of Clinical Investigation* 121 (7): 2750–67. https://doi.org/10.1172/JCI45014.

Leo, Angelo Di, Stephen Johnston, Keun Seok Lee, Eva Ciruelos, Per E Lønning, Wolfgang Janni, Ruth O'Regan, et al. 2018. "Buparlisib plus Fulvestrant in Postmenopausal Women with Hormone-Receptor-Positive, HER2-Negative, Advanced Breast Cancer Progressing on or after MTOR Inhibition (BELLE-3): A Randomised, Double-Blind, Placebo-Controlled, Phase 3 Trial." *The Lancet Oncology* 19 (1): 87–100. https://doi.org/10.1016/S1470-2045(17)30688-5.

Li, Xiaoyan, Shengbing Zang, Haili Cheng, Jiasi Li, and Aimin Huang. 2018. "Overexpression of Activating Transcription Factor 3 Exerts Suppressive Effects in HepG2 Cells." *Molecular Medicine Reports* 19 (2): 869–76. https://doi.org/10.3892/mmr.2018.9707.

Li, Xuebing, Xuexia Zhou, Yongwen Li, Lingling Zu, Hongli Pan, Boning Liu, Wang Shen, Yaguang Fan, and Qinghua Zhou. 2017. "Activating Transcription Factor 3 Promotes Malignance of Lung Cancer Cells in Vitro." *Thoracic Cancer* 8 (3): 181–91. https://doi.org/10.1111/1759-7714.12421.

Liang, G, C D Wolfgang, B P Chen, T H Chen, and T Hai. 1996. "ATF3 Gene. Genomic Organization, Promoter, and Regulation." *The Journal of Biological Chemistry* 271 (3): 1695–1701. https://doi.org/10.1074/jbc.271.3.1695.

Liedtke, Cornelia, and Hans-Christian Kolberg. 2016. "Systemic Therapy of Advanced/Metastatic Breast Cancer - Current Evidence and Future Concepts." *Breast Care (Basel, Switzerland)* 11 (4): 275–81. https://doi.org/10.1159/000447549.

Liu, Guangbo, Ling Su, Xuexi Hao, Ning Zhong, Diansheng Zhong, Sunil Singhal, and Xiangguo Liu. 2012. "Salermide Up-Regulates Death Receptor 5 Expression through the ATF4-ATF3-CHOP Axis and Leads to Apoptosis in Human Cancer Cells." *Journal of Cellular and Molecular Medicine* 16 (7): 1618–28. https://doi.org/10.1111/j.1582-4934.2011.01401.x.

Lombardo, Ylenia, Monica Faronato, Aleksandra Filipovic, Valentina Vircillo, Luca Magnani, and R Charles Coombes. 2014. "Nicastrin and Notch4 Drive Endocrine Therapy Resistance and Epithelial to Mesenchymal Transition in MCF7 Breast Cancer Cells." *Breast Cancer Research* 16 (3): R62. https://doi.org/10.1186/bcr3675.

Lu, Dan, Jingchun Chen, and Tsonwin Hai. 2007. "The Regulation of ATF3 Gene Expression by Mitogen-Activated Protein Kinases." *The Biochemical Journal* 401 (2): 559–67. https://doi.org/10.1042/BJ20061081.

Ma, Cynthia X., Robert J. Crowder, and Matthew J. Ellis. 2011. “Importance of PI3-Kinase Pathway in Response/Resistance to Aromatase Inhibitors.” *Steroids* 76 (8): 750–52. https://doi.org/10.1016/j.steroids.2011.02.023.

MA, SIQI, CHANGHE PANG, LAIJUN SONG, FUYOU GUO, and HONGWEI SUN. 2015. “Activating Transcription Factor 3 Is Overexpressed in Human Glioma and Its Knockdown in Glioblastoma Cells Causes Growth Inhibition Both in Vitro and in Vivo.” *International Journal of Molecular Medicine* 35 (6): 1561–73. https://doi.org/10.3892/ijmm.2015.2173.

Malorni, L., M. Giuliano, I. Migliaccio, T. Wang, C. J. Creighton, M. Lupien, X. Fu, et al. 2016. “Blockade of AP-1 Potentiates Endocrine Therapy and Overcomes Resistance.” *Molecular Cancer Research* 14 (5): 470–81. https://doi.org/10.1158/1541-7786.MCR-15-0423.

Mannsperger, Heiko A., Stephan Gade, Frauke Henjes, Tim Beissbarth, and Ulrike Korf. 2010. “RPPanalyzer: Analysis of Reverse-Phase Protein Array Data.” *Bioinformatics (Oxford, England)* 26 (17): 2202–3. https://doi.org/10.1093/bioinformatics/btq347.

Mantas, D, J D Kostakis, C Markopoulos, and Dimitrios Mantas. 2016. “Hellenic Journal of Surgery 88 Aromatase Inhibitors: A Comprehensive Review in Mechanisms of Action, Side Effects and Treatment in Postmenopausal Early Breast Cancer Patients.” *Hellenic Journal of Surgery*. Vol. 88. https://link.springer.com/content/pdf/10.1007%2Fs13126-016-0326-6.pdf.

Mao, Zhiyong, Michael Bozzella, Andrei Seluanov, and Vera Gorbunova. 2008. “Comparison of Nonhomologous End Joining and Homologous Recombination in Human Cells.” *DNA Repair* 7 (10): 1765–71. https://doi.org/10.1016/J.DNAREP.2008.06.018.

Martínez-Galán, Joaquina, Blanca Torres-Torres, María Isabel Núñez, Jesús López-Peñalver, Rosario Del Moral, José Mariano Ruiz De Almodóvar, Salomón Menjón, et al. 2014. “ESR1gene Promoter Region Methylation in Free Circulating DNA and Its Correlation with Estrogen Receptor Protein Expression in Tumor Tissue in Breast Cancer Patients.” *BMC Cancer* 14 (1): 59. https://doi.org/10.1186/1471-2407-14-59.

McDowell, Ian C., Dinesh Manandhar, Christopher M. Vockley, Amy K. Schmid, Timothy E. Reddy, and Barbara E. Engelhardt. 2018. “Clustering Gene Expression Time Series Data Using an Infinite Gaussian Process Mixture Model.” Edited by Qing Nie. *PLOS Computational Biology* 14 (1): e1005896. https://doi.org/10.1371/journal.pcbi.1005896.

Merenbakh-Lamin, K., N. Ben-Baruch, A. Yeheskel, A. Dvir, L. Soussan-Gutman, R. Jeselsohn, R. Yelensky, et al. 2013. “D538G Mutation in Estrogen Receptor- : A Novel Mechanism for Acquired Endocrine Resistance in Breast Cancer.” *Cancer Research* 73 (23): 6856–64. https://doi.org/10.1158/0008-5472.CAN-13-1197.

Middleton, Justin, Daniel Stover, Tsonwin Hai, Justin D. Middleton, Daniel G. Stover, and Tsonwin Hai. 2018. “Chemotherapy-Exacerbated Breast Cancer Metastasis: A Paradox Explainable by Dysregulated Adaptive-Response.” *International Journal of Molecular Sciences* 19 (11): 3333. https://doi.org/10.3390/ijms19113333.

Milioli, Heloisa H., Renato Vimieiro, Inna Tishchenko, Carlos Riveros, Regina Berretta, and Pablo Moscato. 2016. “Iteratively Refining Breast Cancer Intrinsic Subtypes in the METABRIC Dataset.” *BioData Mining* 9 (1): 2. https://doi.org/10.1186/s13040-015-0078-9.

Miller, Todd W, Justin M Balko, and Carlos L Arteaga. 2011. "Phosphatidylinositol 3-Kinase and Antiestrogen Resistance in Breast Cancer." *Journal of Clinical Oncology : Official Journal of the American Society of Clinical Oncology* 29 (33): 4452–61. https://doi.org/10.1200/JCO.2010.34.4879.

Miyazaki, Keisuke, Shoko Inoue, Kazuhiko Yamada, Masashi Watanabe, Qin Liu, Toshiki Watanabe, Mimi Tamamori Adachi, Yujiro Tanaka, and Shigetaka Kitajima. 2009. "Differential Usage of Alternate Promoters of the Human Stress Response Gene ATF3 in Stress Response and Cancer Cells." *Nucleic Acids Research* 37 (5): 1438–51. https://doi.org/10.1093/nar/gkn1082.

Murphy, Conleth G, and Maura N Dickler. 2016. "Endocrine Resistance in Hormone-Responsive Breast Cancer: Mechanisms and Therapeutic Strategies." *Endocrine-Related Cancer* 23 (8): R337–52. https://doi.org/10.1530/ERC-16-0121.

Murugaesu, N., G. A. Wilson, N. J. Birkbak, T. B. K. Watkins, N. McGranahan, S. Kumar, N. Abbassi-Ghadi, et al. 2015. "Tracking the Genomic Evolution of Esophageal Adenocarcinoma through Neoadjuvant Chemotherapy." *Cancer Discovery* 5 (8): 821–31. https://doi.org/10.1158/2159-8290.CD-15-0412.

Nettles, Kendall W., German Gil, Jason Nowak, Raphaël Métivier, Vandana B. Sharma, and Geoffrey L. Greene. 2008. "CBP Is a Dosage-Dependent Regulator of Nuclear Factor-KB Suppression by the Estrogen Receptor." *Molecular Endocrinology* 22 (2): 263–72. https://doi.org/10.1210/me.2007-0324.

Nguyen, Van T. M., Iros Barozzi, Monica Faronato, Ylenia Lombardo, Jennifer H. Steel, Naina Patel, Philippa Darbre, et al. 2015. "Differential Epigenetic Reprogramming in Response to Specific Endocrine Therapies Promotes Cholesterol Biosynthesis and Cellular Invasion." *Nature Communications* 6 (1): 10044. https://doi.org/10.1038/ncomms10044.

Nowell, P C. 1976. "The Clonal Evolution of Tumor Cell Populations." *Science (New York, N.Y.)* 194 (4260): 23–28.

Parker, Joel S, Michael Mullins, Maggie C U Cheang, Samuel Leung, David Voduc, Tammi Vickery, Sherri Davies, et al. 2009. "Supervised Risk Predictor of Breast Cancer Based on Intrinsic Subtypes." *Journal of Clinical Oncology : Official Journal of the American Society of Clinical Oncology* 27 (8): 1160–67. https://doi.org/10.1200/JCO.2008.18.1370.

Patten, Darren K., Giacomo Corleone, Balázs Győrffy, Ylenia Perone, Neil Slaven, Iros Barozzi, Edina Erdős, et al. 2018. "Enhancer Mapping Uncovers Phenotypic Heterogeneity and Evolution in Patients with Luminal Breast Cancer." *Nature Medicine* 24 (9): 1469–80. https://doi.org/10.1038/s41591-018-0091-x.

Pelzer, Alexandre E., Jasmin Bektic, Petra Haag, Andreas P. Berger, Armin Pycha, Georg Schäfer, Hermann Rogatsch, Wolfgang Horninger, Georg Bartsch, and Helmut Klocker. 2006. "The Expression of Transcription Factor Activating Transcription Factor 3 in the Human Prostate and Its Regulation by Androgen in Prostate Cancer." *Journal of Urology* 175 (4): 1517–22. https://doi.org/10.1016/S0022-5347(05)00651-8.

Peng, Wan-xin, Jian-guo Huang, Liu Yang, Ai-hua Gong, and Yin-Yuan Mo. 2017. "Linc-RoR Promotes MAPK/ERK Signaling and Confers Estrogen-Independent Growth of Breast Cancer." *Molecular Cancer* 16 (1): 161. https://doi.org/10.1186/s12943-017-0727-3.

Pernas, Sonia, Sara M Tolaney, Eric P Winer, and Shom Goel. 2018. "CDK4/6 Inhibition in Breast Cancer: Current Practice and Future Directions." *Therapeutic Advances in Medical Oncology* 10: 1758835918786451. https://doi.org/10.1177/1758835918786451.

Perou, Charles M., Therese Sørlie, Michael B. Eisen, Matt van de Rijn, Stefanie S. Jeffrey, Christian A. Rees, Jonathan R. Pollack, et al. 2000. "Molecular Portraits of Human Breast Tumours." *Nature* 406 (6797): 747–52. https://doi.org/10.1038/35021093.

Perry, RR, Y Kang, and BR Greaves. 1995. "Relationship between Tamoxifen-Induced Transforming Growth Factor Beta 1 Expression, Cytostasis and Apoptosis in Human Breast Cancer Cells." *British Journal of Cancer* 72 (6): 1441–46. https://doi.org/10.1038/bjc.1995.527.

Piva, Marco, Giacomo Domenici, Oihana Iriondo, Miriam Rábano, Bruno M Simões, Valentine Comaills, Inmaculada Barredo, et al. 2014. "Sox2 Promotes Tamoxifen Resistance in Breast Cancer Cells." *EMBO Molecular Medicine* 6 (1): 66–79. https://doi.org/10.1002/emmm.201303411.

Polotskaia, Alla, Gu Xiao, Katherine Reynoso, Che Martin, Wei-Gang Qiu, Ronald C Hendrickson, and Jill Bargonetti. 2015. "Proteome-Wide Analysis of Mutant P53 Targets in Breast Cancer Identifies New Levels of Gain-of-Function That Influence PARP, PCNA, and MCM4." *Proceedings of the National Academy of Sciences of the United States of America* 112 (11): E1220-9. https://doi.org/10.1073/pnas.1416318112.

Pradhan, Madhumita, Leslie A Bembinster, Sarah C Baumgarten, and Jonna Frasor. 2010. "Proinflammatory Cytokines Enhance Estrogen-Dependent Expression of the Multidrug Transporter Gene ABCG2 through Estrogen Receptor and NF{kappa}B Cooperativity at Adjacent Response Elements." *The Journal of Biological Chemistry* 285 (41): 31100–106. https://doi.org/10.1074/jbc.M110.155309.

Prieto-Vila, Marta, Wataru Usuba, Ryou-U Takahashi, Iwao Shimomura, Hideo Sasaki, Takahiro Ochiya, and Yusuke Yamamoto. 2019. "Single-Cell Analysis Reveals a Preexisting Drug-Resistant Subpopulation in the Luminal Breast Cancer Subtype." *Cancer Research*, July, canres.0122.2019. https://doi.org/10.1158/0008-5472.CAN-19-0122.

Raj-Kumar, Praveen-Kumar, Jianfang Liu, Jeffrey A. Hooke, Albert J. Kovatich, Leonid Kvecher, Craig D. Shriver, and Hai Hu. 2019. "PCA-PAM50 Improves Consistency between Breast Cancer Intrinsic and Clinical Subtyping Reclassifying a Subset of Luminal A Tumors as Luminal B." *Scientific Reports* 9 (1): 7956. https://doi.org/10.1038/s41598-019-44339-4.

Ramirez, Michael, Satwik Rajaram, Robert J. Steininger, Daria Osipchuk, Maike A. Roth, Leanna S. Morinishi, Louise Evans, et al. 2016. "Diverse Drug-Resistance Mechanisms Can Emerge from Drug-Tolerant Cancer Persister Cells." *Nature Communications* 7 (1): 10690. https://doi.org/10.1038/ncomms10690.

Ran, F Ann, Patrick D Hsu, Jason Wright, Vineeta Agarwala, David A Scott, and Feng Zhang. 2013. "Genome Engineering Using the CRISPR-Cas9 System." *Nature Protocols* 8 (11): 2281–2308. https://doi.org/10.1038/nprot.2013.143.

Reinert, Tomas, Everardo D Saad, Carlos H Barrios, and José Bines. 2017. "Clinical Implications of ESR1 Mutations in Hormone Receptor-Positive Advanced Breast Cancer."

Frontiers in Oncology 7: 26. https://doi.org/10.3389/fonc.2017.00026.

Reya, Tannishtha, Sean J. Morrison, Michael F. Clarke, and Irving L. Weissman. 2001. "Stem Cells, Cancer, and Cancer Stem Cells." *Nature* 414 (6859): 105–11. https://doi.org/10.1038/35102167.

Riggins, Rebecca B., Randy S. Schrecengost, Michael S. Guerrero, and Amy H. Bouton. 2007. "Pathways to Tamoxifen Resistance." *Cancer Letters* 256 (1): 1–24. https://doi.org/10.1016/j.canlet.2007.03.016.

Robertson, John F R, Igor M Bondarenko, Ekaterina Trishkina, Mikhail Dvorkin, Lawrence Panasci, Alexey Manikhas, Yaroslav Shparyk, et al. 2016. "Fulvestrant 500 Mg versus Anastrozole 1 Mg for Hormone Receptor-Positive Advanced Breast Cancer (FALCON): An International, Randomised, Double-Blind, Phase 3 Trial." *The Lancet* 388 (10063): 2997–3005. https://doi.org/10.1016/S0140-6736(16)32389-3.

Rohini, M., A. Haritha Menon, and N. Selvamurugan. 2018. "Role of Activating Transcription Factor 3 and Its Interacting Proteins under Physiological and Pathological Conditions." *International Journal of Biological Macromolecules* 120 (Pt A): 310–17. https://doi.org/10.1016/j.ijbiomac.2018.08.107.

Ross-Innes, Caryn S., Rory Stark, Andrew E. Teschendorff, Kelly A. Holmes, H. Raza Ali, Mark J. Dunning, Gordon D. Brown, et al. 2012. "Differential Oestrogen Receptor Binding Is Associated with Clinical Outcome in Breast Cancer." *Nature* 481 (7381): 389–93. https://doi.org/10.1038/nature10730.

Rotundo, Maria Saveria, Teresa Galeano, Pierfrancesco Tassone, and Pierosandro Tagliaferri. 2016. "MTOR Inhibitors, a New Era for Metastatic Luminal HER2-Negative Breast Cancer? A Systematic Review and a Meta-Analysis of Randomized Trials." *Oncotarget* 7 (19): 27055–66. https://doi.org/10.18632/oncotarget.7446.

Rugo, Hope S, R Bryan Rumble, Erin Macrae, Debra L Barton, Hannah Klein Connolly, Maura N Dickler, Lesley Fallowfield, et al. 2016. "Endocrine Therapy for Hormone Receptor-Positive Metastatic Breast Cancer: American Society of Clinical Oncology Guideline." *Journal of Clinical Oncology : Official Journal of the American Society of Clinical Oncology* 34 (25): 3069–3103. https://doi.org/10.1200/JCO.2016.67.1487.

Samaddar, J. S., V. T. Gaddy, J. Duplantier, S. P. Thandavan, M. Shah, M. J. Smith, D. Browning, et al. 2008. "A Role for Macroautophagy in Protection against 4-Hydroxytamoxifen-Induced Cell Death and the Development of Antiestrogen Resistance." *Molecular Cancer Therapeutics* 7 (9): 2977–87. https://doi.org/10.1158/1535-7163.MCT-08-0447.

Sammons, Sarah, Noah S. Kornblum, and Kimberly L. Blackwell. 2019. "Fulvestrant-Based Combination Therapy for Second-Line Treatment of Hormone Receptor-Positive Advanced Breast Cancer." *Targeted Oncology* 14 (1): 1–12. https://doi.org/10.1007/s11523-018-0587-9.

Scharl, A, and A Salterberg. 2016. "Significance of Ovarian Function Suppression in Endocrine Therapy for Breast Cancer in Pre-Menopausal Women." *Geburtshilfe Und Frauenheilkunde* 76 (5): 516–24. https://doi.org/10.1055/s-0042-106389.

Schiff, Rachel, Suleiman A Massarweh, Jiang Shou, Lavina Bharwani, Syed K Mohsin, and C

Kent Osborne. 2004. “Cross-Talk between Estrogen Receptor and Growth Factor Pathways as a Molecular Target for Overcoming Endocrine Resistance.” *Clinical Cancer Research : An Official Journal of the American Association for Cancer Research* 10 (1 Pt 2): 331S-6S. http://www.ncbi.nlm.nih.gov/pubmed/14734488.

Schmid, P, M Zaiss, C Harper-Wynne, M Ferreira, S Dubey, S Chan, A Makris, et al. 2018. “Abstract GS2-07: MANTA - A Randomized Phase II Study of Fulvestrant in Combination with the Dual MTOR Inhibitor AZD2014 or Everolimus or Fulvestrant Alone in Estrogen Receptor-Positive Advanced or Metastatic Breast Cancer.” In *General Session Abstracts*, 78:GS2-07-GS2-07. American Association for Cancer Research. https://doi.org/10.1158/1538-7445.SABCS17-GS2-07.

Schmidt, Manfred, Gesa Hoffmann, Manuela Wissler, Nina Lemke, Arne Müßig, Hanno Glimm, David A. Williams, Susanne Ragg, Claus-Ulrich Hesemann, and Christof von Kalle. 2001. “Detection and Direct Genomic Sequencing of Multiple Rare Unknown Flanking DNA in Highly Complex Samples.” *Human Gene Therapy* 12 (7): 743–49. https://doi.org/10.1089/104303401750148649.

Shaffer, Sydney M., Margaret C. Dunagin, Stefan R. Torborg, Eduardo A. Torre, Benjamin Emert, Clemens Krepler, Marilda Beqiri, et al. 2017. “Rare Cell Variability and Drug-Induced Reprogramming as a Mode of Cancer Drug Resistance.” *Nature* 546 (7658): 431–35. https://doi.org/10.1038/nature22794.

Sharma, Sreenath V., Diana Y. Lee, Bihua Li, Margaret P. Quinlan, Fumiyuki Takahashi, Shyamala Maheswaran, Ultan McDermott, et al. 2010. “A Chromatin-Mediated Reversible Drug-Tolerant State in Cancer Cell Subpopulations.” *Cell* 141 (1): 69–80. https://doi.org/10.1016/j.cell.2010.02.027.

Shaw, Alice T., Luc Friboulet, Ignaty Leshchiner, Justin F. Gainor, Simon Bergqvist, Alexei Brooun, Benjamin J. Burke, et al. 2016. “Resensitization to Crizotinib by the Lorlatinib *ALK* Resistance Mutation L1198F.” *New England Journal of Medicine* 374 (1): 54–61. https://doi.org/10.1056/NEJMoa1508887.

Siegel, Rebecca L., Kimberly D. Miller, and Ahmedin Jemal. 2019. “Cancer Statistics, 2019.” *CA: A Cancer Journal for Clinicians* 69 (1): 7–34. https://doi.org/10.3322/caac.21551.

Sikora, Matthew J., Viktoriya Strumba, Marc E. Lippman, Michael D. Johnson, and James M. Rae. 2012. “Mechanisms of Estrogen-Independent Breast Cancer Growth Driven by Low Estrogen Concentrations Are Unique versus Complete Estrogen Deprivation.” *Breast Cancer Research and Treatment* 134 (3): 1027–39. https://doi.org/10.1007/s10549-012-2032-6.

Smith, G Lita. 2014. “The Long and Short of Tamoxifen Therapy: A Review of the ATLAS Trial.” *Journal of the Advanced Practitioner in Oncology* 5 (1): 57–60. http://www.ncbi.nlm.nih.gov/pubmed/25032035.

Sørlie, T, C M Perou, R Tibshirani, T Aas, S Geisler, H Johnsen, T Hastie, et al. 2001. “Gene Expression Patterns of Breast Carcinomas Distinguish Tumor Subclasses with Clinical Implications.” *Proceedings of the National Academy of Sciences of the United States of America* 98 (19): 10869–74. https://doi.org/10.1073/pnas.191367098.

Speirs, V, C Malone, D S Walton, M J Kerin, and S L Atkin. 1999. “Increased Expression of

Estrogen Receptor Beta MRNA in Tamoxifen-Resistant Breast Cancer Patients." *Cancer Research* 59 (21): 5421–24. http://www.ncbi.nlm.nih.gov/pubmed/10554009.

Stanta, Giorgio, and Serena Bonin. 2018. "Overview on Clinical Relevance of Intra-Tumor Heterogeneity." *Frontiers in Medicine* 5 (April): 85. https://doi.org/10.3389/fmed.2018.00085.

Steelman, Linda S., Alberto M. Martelli, Lucio Cocco, Massimo Libra, Ferdinando Nicoletti, Stephen L. Abrams, and James A. McCubrey. 2016. "The Therapeutic Potential of MTOR Inhibitors in Breast Cancer." *British Journal of Clinical Pharmacology* 82 (5): 1189. https://doi.org/10.1111/BCP.12958.

Stone, Andrew, Elena Zotenko, Warwick J. Locke, Darren Korbie, Ewan K. A. Millar, Ruth Pidsley, Clare Stirzaker, et al. 2015. "DNA Methylation of Oestrogen-Regulated Enhancers Defines Endocrine Sensitivity in Breast Cancer." *Nature Communications* 6 (1): 7758. https://doi.org/10.1038/ncomms8758.

Swain, Sandra M., José Baselga, Sung-Bae Kim, Jungsil Ro, Vladimir Semiglazov, Mario Campone, Eva Ciruelos, et al. 2015. "Pertuzumab, Trastuzumab, and Docetaxel in HER2-Positive Metastatic Breast Cancer." *New England Journal of Medicine* 372 (8): 724–34. https://doi.org/10.1056/NEJMoa1413513.

Syed, Viqar, Kasturi Mukherjee, James Lyons-Weiler, Kin-Mang Lau, Tetsuo Mashima, Takashi Tsuruo, and Shuk-mei Ho. 2005. "Identification of ATF-3, Caveolin-1, DLC-1, and NM23-H2 as Putative Antitumorigenic, Progesterone-Regulated Genes for Ovarian Cancer Cells by Gene Profiling." *Oncogene* 24 (10): 1774–87. https://doi.org/10.1038/sj.onc.1207991.

TCGA, The Cancer Genome Atlas. 2008. "Comprehensive Genomic Characterization Defines Human Glioblastoma Genes and Core Pathways." *Nature* 455 (7216): 1061–68. https://doi.org/10.1038/nature07385.

The Human Protein Atlas. n.d. "Cell Atlas - ATF3." Accessed August 22, 2019. https://www.proteinatlas.org/ENSG00000162772-ATF3/cell.

Thompson, Matthew R., Dakang Xu, and Bryan R. G. Williams. 2009. "ATF3 Transcription Factor and Its Emerging Roles in Immunity and Cancer." *Journal of Molecular Medicine* 87 (11): 1053–60. https://doi.org/10.1007/s00109-009-0520-x.

Tokunaga, Eriko, Yasue Kimura, Kojiro Mashino, Eiji Oki, Akemi Kataoka, Shinji Ohno, Masaru Morita, Yoshihiro Kakeji, Hideo Baba, and Yoshihiko Maehara. 2006. "Activation of PI3K/Akt Signaling and Hormone Resistance in Breast Cancer." *Breast Cancer (Tokyo, Japan)* 13 (2): 137–44. http://www.ncbi.nlm.nih.gov/pubmed/16755107.

Traboulsi, T, M El Ezzy, J L Gleason, and S Mader. 2017. "Antiestrogens: Structure-Activity Relationships and Use in Breast Cancer Treatment." *Journal of Molecular Endocrinology* 58 (1): R15–31. https://doi.org/10.1530/JME-16-0024.

Vidula, Neelima, and Hope S. Rugo. 2016. "Cyclin-Dependent Kinase 4/6 Inhibitors for the Treatment of Breast Cancer: A Review of Preclinical and Clinical Data." *Clinical Breast Cancer* 16 (1): 8–17. https://doi.org/10.1016/j.clbc.2015.07.005.

Vies, Peter Da, Joy S. Syne, and Robert I. Nicholson. 1979. "Effects of Estradiol and the Antiestrogen Tamoxifen on Steroid Hormone Receptor Concentration and Nuclear

Ribonucleic Acid Polymerase Activities in Rat Uteri*." *Endocrinology* 105 (6): 1336–42. https://doi.org/10.1210/endo-105-6-1336.

Vuong, Darina, Peter T. Simpson, Benjamin Green, Margaret C. Cummings, and Sunil R. Lakhani. 2014. "Molecular Classification of Breast Cancer." *Virchows Archiv* 465 (1): 1–14. https://doi.org/10.1007/s00428-014-1593-7.

Wang, Aijin, Stacey Arantes, Leqin Yan, Kaoru Kiguchi, Mark J McArthur, Aysegul Sahin, Howard D Thames, C Marcelo Aldaz, and Michael C MacLeod. 2008. "The Transcription Factor ATF3 Acts as an Oncogene in Mouse Mammary Tumorigenesis." *BMC Cancer* 8 (1): 268. https://doi.org/10.1186/1471-2407-8-268.

Wang, Jialiang, Yufang Ma, and Michael K. Cooper. 2013. "Cancer Stem Cells in Glioma: Challenges and Opportunities." *Translational Cancer Research* 2 (5): 429–41. https://doi.org/10.21037/1415.

Wei, Saisai, Hongbo Wang, Chunwan Lu, Sarah Malmut, Jianqiao Zhang, Shumei Ren, Guohua Yu, Wei Wang, Dale D. Tang, and Chunhong Yan. 2014. "The Activating Transcription Factor 3 Protein Suppresses the Oncogenic Function of Mutant P53 Proteins." *Journal of Biological Chemistry* 289 (13): 8947–59. https://doi.org/10.1074/jbc.M113.503755.

Weigelt, B, HM Horlings, B Kreike, MM Hayes, M Hauptmann, LFA Wessels, D de Jong, MJ Van de Vijver, LJ Van't Veer, and JL Peterse. 2008. "Refinement of Breast Cancer Classification by Molecular Characterization of Histological Special Types." *The Journal of Pathology* 216 (2): 141–50. https://doi.org/10.1002/path.2407.

Weinberg, Robert A. 1995. "The Retinoblastoma Protein and Cell Cycle Control." *Cell* 81 (3): 323–30. https://doi.org/10.1016/0092-8674(95)90385-2.

"WHO | Cancer." 2019. *WHO*. https://www.who.int/cancer/en/.

Wood, Alastair J.J., Ian E. Smith, and Mitch Dowsett. 2003. "Aromatase Inhibitors in Breast Cancer." *New England Journal of Medicine* 348 (24): 2431–42. https://doi.org/10.1056/NEJMra023246.

Yan, Chunhong, and Douglas D. Boyd. 2006. "ATF3 Regulates the Stability of P53: A Link to Cancer." *Cell Cycle* 5 (9): 926–29. https://doi.org/10.4161/cc.5.9.2714.

Yan, Leqin, Luis Della Coletta, K. Leslie Powell, Jianjun Shen, Howard Thames, C. Marcelo Aldaz, and Michael C. MacLeod. 2011. "Activation of the Canonical Wnt/β-Catenin Pathway in ATF3-Induced Mammary Tumors." Edited by Robert Oshima. *PLoS ONE* 6 (1): e16515. https://doi.org/10.1371/journal.pone.0016515.

Yates, Lucy R, Moritz Gerstung, Stian Knappskog, Christine Desmedt, Gunes Gundem, Peter Van Loo, Turid Aas, et al. 2015. "Subclonal Diversification of Primary Breast Cancer Revealed by Multiregion Sequencing." *Nature Medicine* 21 (7): 751–59. https://doi.org/10.1038/nm.3886.

Yde, Christina W., Kristina B. Emdal, Barbara Guerra, and Anne E. Lykkesfeldt. 2012. "NFκB Signaling Is Important for Growth of Antiestrogen Resistant Breast Cancer Cells." *Breast Cancer Research and Treatment* 135 (1): 67–78. https://doi.org/10.1007/s10549-012-2053-1.

Yin, Xin, Christopher C Wolford, Yi-Seok Chang, Stephen J McConoughey, Stephen A Ramsey,

Alan Aderem, and Tsonwin Hai. 2010. “ATF3, an Adaptive-Response Gene, Enhances TGF{beta} Signaling and Cancer-Initiating Cell Features in Breast Cancer Cells.” *Journal of Cell Science* 123 (Pt 20): 3558–65. https://doi.org/10.1242/jcs.064915.

Yoo, Young A., Yeul Hong Kim, Jun Suk Kim, and Jae Hong Seo. 2008. “The Functional Implications of Akt Activity and TGF-β Signaling in Tamoxifen-Resistant Breast Cancer.” *Biochimica et Biophysica Acta (BBA) - Molecular Cell Research* 1783 (3): 438–47. https://doi.org/10.1016/J.BBAMCR.2007.12.001.

Yu, H. A., M. E. Arcila, M. D. Hellmann, M. G. Kris, M. Ladanyi, and G. J. Riely. 2014. “Poor Response to Erlotinib in Patients with Tumors Containing Baseline EGFR T790M Mutations Found by Routine Clinical Molecular Testing.” *Annals of Oncology* 25 (2): 423–28. https://doi.org/10.1093/annonc/mdt573.

Zhang, Ying E. 2009. “Non-Smad Pathways in TGF-β Signaling.” *Cell Research* 19 (1): 128. https://doi.org/10.1038/CR.2008.328.

Zhao, Jonathan, Xingyao Li, Mingxiong Guo, Jindan Yu, and Chunhong Yan. 2016. “The Common Stress Responsive Transcription Factor ATF3 Binds Genomic Sites Enriched with P300 and H3K27ac for Transcriptional Regulation.” *BMC Genomics* 17 (1): 335. https://doi.org/10.1186/s12864-016-2664-8.

Zhao, Wenyan, Ming Sun, Shuqiang Li, Zhaofu Chen, and Donghua Geng. 2018. “Transcription Factor *ATF3* Mediates the Radioresistance of Breast Cancer.” *Journal of Cellular and Molecular Medicine* 22 (10): 4664–75. https://doi.org/10.1111/jcmm.13688.

Zorita, Eduard, Pol Cuscó, and Guillaume J Filion. 2015. “Starcode: Sequence Clustering Based on All-Pairs Search.” *Bioinformatics (Oxford, England)* 31 (12): 1913–19. https://doi.org/10.1093/bioinformatics/btv053.

Abbreviations

4E-BP1	Eukaryotic translation initiation factor 4E-binding protein 1
ACTB	β-actin
AI	Aromatase inhibitors
AKT	Serine/Threonine Kinase 1
ATF3	Activating transcription factor 3
BAMBI	BMP and activin membrane bound inhibitor
BCA	Bicinchoninic acid protein assay
BSA	Bovine serum albumin
BL	Basal-like
BrdU	Bromodeoxyuridine
Cas9	CRISPR associated protein 9
CDK	Cycling dependent kinase
cDNA	Complementary deoxyribonucleic acid
ChIP	Chromatin immunoprecipitation
CO_2	Carbon dioxide
CRISPR	Clustered Regularly Interspaced Short Palindromic Repeat
CSNK1A1	Casein kinase 1 alpha 1
CSNK1E	Casein kinase 1 epsilon
CTNNBIP1	Beta-catenin-interacting protein 1
CTRL	Control
DCIS	Ductal carcinoma in situ
DKK1	Dickkopf-related protein 1
DNA	Deoxyribonucleic acid
DMEM	Dulbecco's modified eagle's medium
DMSO	Dimethyl sulfoxide
E2	Estrogen
EDTA	Ethylenediaminetetraacetic acid
EGFR	Epidermal growth factor receptor
ER	Estrogen Receptor
ERα	Estrogen Receptor α

ERBB2	Erb-B2 Receptor Tyrosine Kinase 2
ESR1	Estrogen receptor 1
EtOH	Ethanol
FACS	Fl
FC	Fold change
FITC	Fluorescein isothiocyanate
FBS	Fetal bovine serum
GRB2	Growth factor receptor-bound protein 2
GSK-3α	Glycogen synthase kinase 3 alpha
GSK-3ß	Glycogen synthase kinase 3 beta
HDAC	Histone deacetylase
IDC	Invasive ductal carcinoma
IHC	Immunohistochemistry
JNK	c-Jun N-terminal kinase
KO	Knockout
LRP5	Low-density lipoprotein receptor-related protein 5
LTED	Long term estrogen deprivation
MAPK	Mitogen-Activated Protein Kinase
MOI	Multiplicity of infection
MPER	Mammalian Protein Extraction Reagent
mRNA	Messenger ribonucleic acid
MSK	Mitogen and stress activated kinase
mTOR	Mammalian target of rapamycin kinase
NaF	Sodium Fluoride
NFκB	Nuclear factor kappa-light-chain-enhancer of activated B cells
PAM	Protospacer adjacent motif
PBS	Phosphate buffered saline
PDK1	Phosphoinositide-dependent kinase 1
PFA	Paraformaldehyde
PI	Propidium iodide
PI3K	Phosphatidylinositol-4,5-bisphosphate 3-kinase
PI3KCA	Phosphatidylinositol-4,5-Bisphosphate 3-Kinase Catalytic Subunit Alpha
RNA	Ribonucleic acid

RPS6	Ribosomal protein S6
OE	Overexpression
ON	Overnight
p	Phosphorylated
P/S	Penicillin/Streptomycin
PLC	Phospholipase C
PR	Progesterone receptor
PTEN	Phosphatase and Tensin Homolog
PVDF	Polyvinylidene fluoride
qRT-PCR	Quantitative reverse transcriptase polymerase chain reaction
Rb	Retinoblastoma-associated protein
RIPA	Radioimmunoprecipitation
RNA	Ribonucleic acid
RNAi	Ribonucleic acid interference
RPPA	Reverse phase protein array
RT	Room temperature
SEM	Standard error of the mean
SD	Standard deviation
SDS-PAGE	Sodium dodecyl sulfate polyacrylamide gel electrophoresis
SEM	Standard error of the mean
SERD	Selective estrogen receptor degrader
SERM	Selective estrogen receptor modulator
siRNA	Small interfering ribonucleic acid
SOS	Son of sevenless
TAM	Tamoxifen
TAMR	Tamoxifen resistant
TBS-T	Tris buffered saline with 0.1% Tween 20
TCGA	The cancer genome atlas
TGFβ	Transforming growth factor β
TNBC	Triple negative breast cancer
TP53	Tumor protein 53
TSS	Transcription start site

UCSC	University of California, Santa Cruz
Wnt	Wingless-type MMTV integration site family
WT	Wild type

Acknowledgements

This thesis is the result of 4 years of work that has been supported in different ways by several people. First, I want to thank my thesis supervisor Stefan, for accepting me into the Division of Molecular Genome Analysis, allowing me to develop as an independent researcher and constantly supporting me in the decisions along the way.

I would like to thank Prof. Dr. Frank Lyko for the input and help during my TAC meetings and for agreeing to chair my defense. At the same time, thanks to Prof. Dr. Peter Angel and Dr. Karin Müller-Decker for agreeing to be part of my thesis defense committee.

Being a member of the EpiPredict consortium has allowed me to meet and share these 4 years with many exceptional people. Thanks to all the PIs for their guidance and to all the other PhD fellows for the fun moments we shared. A special thank goes to Luca for taking part in my TAC with helpful advises and for hosting me in his lab for three months. Additionally thanks to Perry, Maryam and Giacomo for directly contributing to my project with their bioinformatic analysis.

I would like to thank Dr. Angela Goncalves and Dr. Luca Penso Dolfin for their bioinformatics contribution to the barcoding projects, Dr. Karin Müller-Decker for the *in vivo* experiments and Dr. Rainer Will for the production of stable cell lines.

MGA has been my home for the last 4 years. It is never easy to leave your country and integrate somewhere new; however every one of you warmly welcomed me and always kept a friendly environment that I cherished. It has been a pleasure working with you all. I am particularly grateful to Heike for joining my project and helping me in the last couple of years. Thanks also to Zuzana and Lukas for bearing me as their supervisor and performing excellent work.

A special mention goes to my office mates over the year: thanks to Stephan for introducing me to the magic world of RPPA, Chiara for adding a bit of Italian spices to the cold Germany and Ana for our afternoon chats.

I am particularly grateful to have met Alex and Devina. You two have helped me along the way and I am happy we created a bond that goes over the lab walls.

I couldn´t have asked for a better PhD brother than Emre to go through this experience. Thanks for everything we shared in the lab. But mostly thanks for the friendship we built outside, from our first beer in the guesthouse garden to the movies to which your “special” taste has dragged me to. I am looking forward to showing you in person how cool Torino’s metro is.

A warm thank goes to all my friends in Torino and abroad, who where always there for me every time I came back to share moments as if the time did not pass.

Special thanks go to my parents and my brother for providing me with their love and support through all my life.

Finally I want to thank the person that changed my life. I started my PhD as a naïve young boy; I am finishing it as a happy married man. Neșe, thank you for every single moment we spent together, your constant presence made this journey not only possible, but a wonderful one. I feel so lucky to have you.